

**EGE UNIVERSITY GRADUATE SCHOOL OF
APPLIED AND NATURAL SCIENCES**

(MASTER OF SCIENCE THESIS)

**INVESTIGATION OF
OXYGEN AND CHLORINE EFFECT ON
LIFETIME OF GLASS FIBER REINFORCED PPA
(POLYPHTHALAMIDE) COMPOSITES
UNDER PRESSURIZED AND HOT WATER
CONDITIONS**

Nur KARAŞAHİN

Supervisor : Assoc. Prof. Dr. Serap CESUR

Co-supervisor : Prof. Dr. Mesut YENİGÜL

Chemical Engineering Department

**Department Code : 603.02.00
Presentation Date : 15.11.2013**

Bornova-İZMİR

2013

Nur KARAŞAHİN tarafından yüksek lisans tezi olarak sunulan “Investigation of Oxygen and Chlorine Effect on Lifetime of Glass Fiber Reinforced PPA (Polyphthalamide) Composites under Pressurized and Hot Water Conditions” başlıklı bu çalışma E.Ü. Lisansüstü Eğitim ve Öğretim Yönetmeliği ile E.Ü. Fen Bilimleri Enstitüsü Eğitim ve Öğretim Yönergesi'nin ilgili hükümleri uyarınca tarafımızdan değerlendirilerek savunmaya değer bulunmuş ve 15.11.2013 tarihinde yapılan tez savunma sınavında aday oybirliği/oyçokluğu ile başarılı bulunmuştur.

Jüri Üyeleri:

İmza

Jüri Başkanı : Doç. Dr. Serap CESUR

Raportör Üye : Y.Doç.Dr. Seçkin ERDEN

Üye : Prof.Dr. Mustafa DEMİRCİOĞLU

ÖZET**BASINÇLI VE SICAK SU ŞARTLARINDAKİ OKSİJEN VE KLOR BİLEŞENLERİNİN CAM FİBER KATKILI PPA (POLİFTALAMİD) KOMPOZİTLERİNİN KULLANIM VE YAŞAM SÜRECİ ÜZERİNDEKİ ETKİLERİNİN ARAŞTIRILMASI**

KARAŞAHİN, Nur

Yüksek Lisans Tezi, Kimya Mühendisliği Anabilim Dalı

Tez danışmanı: Doç. Dr. Serap CESUR

İkinci danışmanı: Prof. Dr. Mesut YENİGÜL

Kasım 2013, 112 sayfa

Bu tez çalışmasında, temel olarak %40 cam fiber katkı poliftalamid malzemesinden üretilmiş örneklerin yaşlanma sürecindeki davranış karakteristiği araştırılmıştır. Çeşitli cam fiber oranlarında poliftalamid (PPA), poliamid 66 (PA 66) ve polipropilen (PP) örneklerle de kıyaslama testleri yürütülmüştür. Hem standart örnekler, hem de kombine kullanılan gerçek parçalar üzerinde testler yürütülmüştür. Kombi merkezi ısıtma (CH) ve sıcak kullanım suyu (DHW) örnekleri ayrı ayrı incelenmiştir. Literatür yaşlanma hızı üzerine iki etkin bileşen olarak oksijen ve kloru vurguladığından (Solvay, 2002; Solvay, 2011; Gates, 2003; Martin, 2008; Lampman, 2003), bu moleküllerin etkileri irdelenmiştir.

Malzemenin kristal yapısı ve bu yapının yaşlanma mekanizması üzerindeki etkileri, DSC (diferansiyel taramalı kalorimetre) cihazında izotermal olmayan koşullarda Ozawa modeli ile incelenmiştir. Model PPA GF40 örneklerin izotermal olmayan kristalizasyon davranışına başarılı bir şekilde uyum sağlamıştır. Farklı sıcaklıklarda hesaplanan Ozawa grafiklerinde, genellikle sıcaklık arttıkça Ozawa sabiti m 'in arttığı, fakat Ozawa hız sabiti $K(T)$ 'nin azaldığı görülmüştür. Avrami yaklaşımı üzerinden hesaplanan büyüme hızları ve kristalizasyon yarı zamanları, hem CH, hem de DHW örnekleri özellikle 6061-saate dek sabit kalma veya azalma eğilimindedirler. Kristalizasyon süreci üzerinden Augis-Bennett ve Kissinger grafikleri ile örneklerin aktivasyon enerjileri hesaplanmıştır. Belirleme

(korelasyon) katsayısı (R^2), Augis-Bennett modelinin genel olarak uygulanabilir olmadığını göstermiştir. Bunun yanında, daha yüksek R^2 değerleri sergileyen Kissenger modelinin uygulanabilir olduğu görülmüştür. DSC deneylerinden elde edilen T_m ve T_c değerleri, DHW örneklerin maruz kaldığı, oksijen çözünmüş agresif su ortamını doğrular şekilde, daha yüksek değişimler göstermektedir. Hidrolik parça (HP) örneklerin kristallik dereceleriye (X_c), özellikle 20 °C/dak. soğutma hızıyla yapılan testler, değerlerin düşüşünü net olarak ortaya koymuştur.

Hem CH, hem de DHW örneklerinde yapılan TGA analizlerinde çok farklı sonuçlar elde edilmemiştir. Termal kararlılık açısından, her iki uygulama şartlarında malzemenin benzer performans gösterdiği ve 0-saat örneklere kıyasla termal kararlılığını kaybetmediği açıktır.

FTIR analizleri, hidrofilik amid bağlarının suda çözünmesine bağlı olarak, tüm örneklerdeki karbon bağlarına oranlı amid ve aromatik bağları, yaşlanma zamanıyla orantılı çok belirgin olmayan bir artış eğilimi göstermiştir.

SEM görüntüleri, hem CH, hem de DHW örnekleri için 1700-saat örneklerinden itibaren çatlak oluşumlarını göstermektedir. Bu sebeple bazı bölgelerde, polimer matrisi-cam fiber arayüzeylerinin yeterince iyi olmadığı görülmektedir. Ancak arayüzey çoğunlukla iyi bir görüntü sergilemektedir.

Bağıl viskozite değerleri incelendiğinde, 6061-saatlik DHW örneklerinin, CH örneklere kıyasla 1.5 kat daha fazla düştüğü görülmüştür. Bu sonuç da DHW örneklerinin maruz kaldığı daha saldırgan ortamla örtüşmektedir.

Çeşitli oranlarda cam fiber içeren farklı polimer örneklerinde mekanik özelliklerin değişimleri incelenmiştir. Tüm sonuçlar, cam fiber katkılı PPA malzemesinin, alternatif olarak incelenen PA 66 ve PP malzemelerine kıyasla çok daha yüksek performans gösterdiğini kanıtlamıştır.

Anahtar kelimeler: polimerlerin yaşlanması, cam fiber katkılı kompozit malzeme, izotermal olmayan kristalizasyon kinetikleri, Ozawa, Avrami, Arrhenius, mekanik özellikler.

ABSTRACT**INVESTIGATION OF OXYGEN AND CHLORINE EFFECT ON
LIFETIME OF GLASS FIBER REINFORCED PPA
(POLYPHTHALAMIDE) COMPOSITES UNDER PRESSURIZED
AND HOT WATER CONDITIONS**

KARAŞAHİN, Nur

Master Thesis, Chemical Engineering Department

Supervisor: Assoc. Prof. Dr. Serap CESUR

Co-supervisor: Prof. Dr. Mesut YENİGÜL

November 2013, 112 pages

In this thesis study, parts produced out of polyphthalamide with 40% glass fiber content material was mainly researched to understand ageing behaviour characteristics. Some comparison tests were also conducted with various glass fiber reinforced polyphthalamides (PPA), polyamide 66 (PA 66) and polypropylene (PP) samples. The components in central heating (CH) side and domestic hot water (DHW) side of combi-boilers were studied separately. Since the literature mainly emphasizes two dominant stressors as oxygen and chlorine effects on ageing speed (Solvay, 2002; Solvay, 2011; Gates, 2003; Martin, 2008; Lampman, 2003), the effects of these molecules were studied.

The crystal structure and its effects on ageing mechanism were investigated under nonisothermal conditions with Ozawa model by DSC (differential scanning calorimeter). The Ozawa model successfully fits the nonisothermal crystallization behavior of the PPA GF40 samples. It was generally observed as temperature increases, Ozawa constant m increases, but Ozawa rate constant $K(T)$ decreases. The growth rates calculated over Avrami approach and the crystallization half time values tend to remain stable or decrease especially until 6061-hour for both CH and DHW samples. Related with activation energy calculations of crystallization results, Kissinger and Augis-Bennett plots of the samples were obtained. Coefficient of determination (R^2) results show that Augis-Bennett model

is mostly not valid for this material. However, Kissinger model is mostly applicable as seen with higher R^2 values. DSC experiments showed that, T_m and T_c reductions were higher for DHW parts which are attributable to more aggressive aqueous test media with oxygen dissolution. Degree of crystallinity (X_c) values of hydraulic part (HP) samples gives a noticeable drop especially with tests conducted by a cooling rate of 20 °C/min.

TGA experiments for CH and DHW samples shows that there is not noticeable difference for the these values. So in terms of thermal stability values of the samples, the performances are similar for both application conditions and also they keep their thermal stability when compared with 0-hour samples.

The FTIR analyses conducted for all samples show that amide and aromatic bonds relative to carbon bonds tend to show a small increase due to dissolution of hydrophilic amide bonds in the structure.

The SEM images show that cracks are visible since 1700 hours of aged samples for both CH and DHW samples. It seems like the polymer matrix-glass fiber interaction was not good enough in some regions. However, mostly the interaction at polymer matrix-glass fiber interface is good.

Relative viscosity results show that, in the long term, DHW samples were destructed around 1.5 times more after 6061-hr at inner sides of the parts when compared with CH samples. This result is in line with more aggressive media.

Change of mechanical properties was investigated for various glass fiber containing polymeric materials. All results show that, glass fiber reinforced polyphthalamide materials have much better performance when compared with PA 66 and PP.

Keywords: ageing of polymers, glass fiber reinforced composite material, nonisothermal crystallization kinetics, Ozawa, Avrami, Arrhenius, mechanical properties.

dedicated to

*whom has contribution to crystallization,
polymer degradation and understanding
the mechanisms of these processes...*

ACKNOWLEDGEMENT

I want to express my deep gratitude to my research supervisor, Assoc. Prof. Dr. Serap Cesur and co-supervisor Prof. Dr. Mesut YENİGÜL for their sincere and courageous guidance throughout this master journey. Since due to change of thesis topic because of my career way, I needed to start a new project from the beginning, my supervisor always had been the supporter for all milestones during this journey. Related with research methodologies and engineering approach, she reflected all her knowledge openly. I learned a lot from her systematic approach and very well structured organization of working principle. I also learned a lot of things and had the chance to benefit from many years of experiences of my co-supervisor Prof. Dr. Mesut YENİGÜL. It was reassuring to get answers whenever I had questions on the way.

This thesis had been supported by Bosch Thermotechnology for supplying me the necessary sources and encouraging to complete this study.

My family, for their love, sensibility and creating the wonderful atmosphere to study most efficiently, had been always praise for my living. Thank you mom (Gülizar İSLAM) for your pure love without any expectation, thank you my father (Fikret İSLAM) for always being a guide for your children, thank you my sister (Pelin İSLAM) for being my best friend of my life. Lastly I want to define my deep feelings and respect to my husband Şahin KARAŞAHİN for him being my sharer of my life as my new family.

This master thesis was one of the most valuable journeys of my life with ups and downs together which I had many personal gainings. It would for sure be harder to complete this study without priceless solidarity we built. Solidarity is one of the most important and key philosophies of my life and I want to finalize my words by stressing importance of solidarity with a quotation; “Teamwork makes the dream work”, so we did it quite well.

TABLE OF CONTENTS

	<u>Pages</u>
ÖZET	v
ABSTRACT	vii
ACKNOWLEDGEMENT	xi
TABLE OF CONTENTS	xiii
TABLE OF FIGURES	xvii
LIST OF TABLES	xviiiiv
NOMENCLATURE	xxiv
1. INTRODUCTION	1
2. LITERATURE ON DEGRADATION KINETICS OF POLYMERIC COMPOSITES	4
2.1 Ageing Theory	4
2.1.1 Chemical ageing	5
2.1.2 Physical ageing	5
2.1.3 Mechanical Ageing	6
2.2 Models for Crystallization Kinetics and Activation Energy	7
2.2.1 Avrami model for isothermal crystallization	7

TABLE OF CONTENTS (continued)

	<u>Pages</u>
2.2.2 Nonisothermal crystallization kinetics.....	9
2.2.3 Avrami-Jeziorny model for nonisothermal crystallization	15
2.2.4 Ozawa model for nonisothermal crystallization	16
2.2.5 Liu Mo model for comparison of isothermal and nonisothermal crystallization.....	16
2.2.6 Effective activation energy (E) of crystallization	17
2.2.7 Arrhenius model for activation energy calculation.....	21
2.3 Glass Fiber Effect in Polymeric Materials	23
2.4 Oxygen and Chlorine as Ageing Accelerators	32
2.4.1 Oxygen effect.....	32
2.4.2 Chlorine effect.....	35
2.5 Injection Molding and Its Effects on Crystallinity.....	37
3. EXPERIMENTAL.....	40
3.1 Materials.....	40

TABLE OF CONTENTS (continued)

	<u>Pages</u>
3.2 Methods	41
3.2.1 Tests with hydraulic parts	41
3.2.2 Tests with tensile test specimens (TTS)	51
4. RESULTS AND DISCUSSION.....	55
4.1 DSC Analysis of HP Samples	55
4.1.1 Melting point measurements of HP PPA GF40 samples.....	55
4.1.2 Degree of crystallinity	63
4.1.3 Crystallization kinetics	66
4.1.4 Activation energy of crystallization.....	73
4.2 TGA Analysis of HP Samples	75
4.3 FTIR Analysis of HP Samples.....	79
4.4 SEM Analysis of HP Samples	83
4.5 Relative Viscosity Analysis of HP Samples.....	88
4.6 Tensile Properties of TTS ww and TTS wow	89
4.7 Impact Strength of TTS	95
5. CONCLUSION	98

TABLE OF CONTENTS (continued)

	<u>Pages</u>
6. RECOMMENDATIONS	101
7. REFERENCES.....	102
CURRICULUM VITAE	107
APPENDICES	

TABLE OF FIGURES

<u>Figures</u>	<u>Pages</u>
1.1 General amide structure.....	1
1.2 Polyphthalamide main structure.	1
1.3 Polyphthalamide detailed molecular formula.....	1
2.1 Exothermic and endothermic reaction graphs for formation of products and reactants.....	7
2.2 Evaluation of property data over time by Avrami approach.	9
2.3 T dependencies for the growth rate (dash line) from Eq. 2.17 and the effective activation energy (solid line) from Eq. 2.20. The E value turns negative when crystallization occurs at temperatures above T_{max}	19
2.4 Graph trend for a property change over time.....	23
2.5 Tensile strength at break versus time graph for various glass fiber content filled polymers.....	24
2.6 Impact resistance versus time graph for various glass fiber content filled polymers.	25
2.7 Fracture surface ahead of crack initiation region for PA specimens,.....	27
2.8 Effect of volume fraction on strength (Crawford, 2005).....	28
2.9 O ₂ degradation effect on the structure.	32
2.10 Effects of oxygen content (a) on weight and (b) T _g of a graphite/thermoplastic.....	33
2.11 Time temperature superposed data for Nylon, percent tensile strength remaining versus shifted time. Data are shifted to 109 °C (reference temperature).	34
2.12 Weight change of various polymers after exposure to chlorinated water at 60°C (Solvay, 2002).	36

TABLE OF FIGURES (continued)

<u>Figures</u>	<u>Pages</u>
2.13 Water sorption versus crystallinity degree of polymer.....	37
3.1 Test set-up for ageing of PPA GF40 samples.....	41
3.2 Micracut precision cutting device.....	42
3.3 DSC thermogram, exhibiting a melting transition consistent with a PET resin (Jansen, 2001).....	44
3.4 DSC analysis for nonisothermal testing methodology.....	45
3.5 TGA thermogram showing the weight-loss for a typical plastic resin (Scheirs, 2000).....	46
3.6 FTIR spectrum showing correlation between structure and absorption bands (Jansen, 2001).....	48
3.7 Basic components of a SEM microscope.....	49
3.8 Test set-up and TTS samples.....	52
3.9 Thermoset versus thermoplastic stress-strain behavior.....	53
3.10 Charpy test specimen types and test configuration.....	54
4.1 Thermograms of PPA GF40 HP samples, a) 0-hr. CH with a cooling rate of 5 °C/min, b) 0-hr. CH with a cooling rate of 10 °C/min, c) 0-hr. CH with a cooling rate of 20 °C/min.....	57
4.2 T_{m1} and T_{m2} values for HP samples at various cooling rates (a) CH, (b) DHW.....	59

TABLE OF FIGURES (continued)

<u>Figures</u>	<u>Pages</u>
4.3 $T_{m1} - T_{m2}$ value changes for HP samples at various cooling rates (a) CH, (b) DHW.....	60
4.4 1700-hr. DHW with a cooling rate of 5 °C/min.	61
4.5 Thermograms of HP PPA GF40 samples that show exothermic peak before T_m	63
4.6 X_C changes for HP samples at various cooling rates (a) CH, (b) DHW.	64
4.7 DSC exotherms of 0-hr CH HP samples at various cooling rates (CR).	67
4.8 Time dependent relative crystallinity of 0-hr CH HP samples at various cooling rates (CR).....	67
4.9 Avrami plot of 0-hr CH HP samples at various cooling rates (CR).	68
4.10 Relative crystallinity of 2500-hr HP CH samples vs. T various cooling rates (CR).....	70
4.11 Ozawa plot of 2500-hr HP CH samples.	71
4.12 Kissinger plots of nonisothermally crystallized selected samples.	73
4.13 Augis-Bennett plots of nonisothermally crystallized selected samples.....	74
4.14 TGA graphs for HP PPA GF40 CH samples.....	76
4.15 TGA graphs for HP PPA GF40 DHW samples.....	77
4.16 Functional groups of CH HP PPA GF40 samples by FTIR.	79
4.17 Functional groups of DHW HP PPA GF40 samples by FTIR.	79
4.18 Amide (1286) to carbon bonds (3290 and 2926) ratio for HP CH samples.	81

TABLE OF FIGURES (continued)

<u>Figures</u>	<u>Pages</u>
4.19 Aromatic rings (1536) to carbon bonds (3290 and 2926) ratio for HP CH samples.	81
4.20 Amide (1286) to carbon bonds (3290 and 2926) ratio for HP DHW samples.	82
4.21 Aromatic rings (1536) to carbon bonds (3290 and 2926) ratio for HP DHW samples.	82
4.22 SEM images of HP PPA GF40 components' CH side.....	85
4.23 SEM images of HP PPA GF40 components' DHW side.....	87
4.24 Absolute values of tensile strength for DIN-impact tensile bars (80x15x1 mm ³) related to original conditioned values at 1000 ppm chlorinated 95 °C water after 3000 hr.....	90
4.25 Absolute values of tensile strength for ISO-tensile bars (60x10x3 mm ³) related to original conditioned values at 1000 ppm chlorinated water after 3000 hr at 95 °C.....	91
4.26 Relative decrease of tensile strength for DIN-impact tensile bars (80x15x1 mm ³) related to original conditioned values at 1000 ppm chlorinated water after 3000 hr at 95 °C.	92
4.27 Relative decrease of tensile strength - thick ISO-bars compared to thin DIN-bars at 1000 ppm chlorinated water at 95 °C.	92
4.28 Tensile strength versus time for DIN-impact tensile bars (80x15x1 mm ³) at 1000 ppm chlorinated water at 95 °C.	93
4.29 Absolute values of tensile strength for ISO-tensile bars (60x10x3 mm ³) related to original conditioned values at 1000 ppm chlorinated water after 5000 hr at 95 °C.....	93
4.30 Relative decrease of tensile strength for ISO-tensile bars (60x10x3 mm ³) related to original conditioned values at 1000 ppm chlorinated water after 5000 hr at 95 °C.....	94

TABLE OF FIGURES (continued)

<u>Figures</u>	<u>Pages</u>
4.31 Tensile strength versus time for ISO-tensile bars (60x10x3 mm ³) at 1000 ppm chlorinated water at 95 °C.....	94
4.32 Tensile strength retention mastercurves	95
4.33 Absolute values of impact strength for charpy impact tensile bars (80x10x4 mm ³) related to original conditioned values at 1000 ppm chlorinated water after 5000 hr at 95 °C.....	96
4.34 Relative decrease of impact strength for charpy impact tensile bars (80x10x4 mm ³) related to original conditioned values at 1000 ppm chlorinated water after 5000 hr at 95 °C.....	97
4.35 Impact strength versus time.....	97

LIST OF TABLES

<u>Tables</u>	<u>Pages</u>
1.1 Drinking water regulations in different countries.....	2
1.2 Thermal properties of Grivory HT1V-4 FWA Black 9225.....	3
2.1 Avrami exponents for various types of crystal growth geometries.....	10
2.2 Types of glass fibers (Wallenberger et al, 2001).....	24
2.3 Typical properties of fiber reinforced Nylon 6.6 (Crawford, 2005).....	25
2.4 Properties with various glass fiber contents (Crawford, 2005).....	26
2.5 Compositions of commercial glass fibers.....	29
2.6 Physical and mechanical properties of glass fibers.....	30
2.7 Projected % weight loss after exposure to 2 ppm chlorinated deionized H ₂ O at 60°C.....	36
2.8 HDT of samples under different mold temperatures (Brooks, 1990).....	38
2.9 Crystallization temperature change with different cooling rates.....	39
3.1 Test specimens and conducted tests.....	40
3.2 Dataset for halflife time of PPA GF40.....	42
4.1 T _m values of HP PPA GF40 samples obtained from nonisothermal DSC thermograms.....	58
4.2 T _c values of HP PPA GF40 samples obtained from nonisothermal DSC thermograms.....	58
4.3 ΔH _m , ΔH _c and X _c values of HP PPA GF40 samples.....	65
4.4 Avrami exponent (n), growth rate constant (K), crystallization half time (t _{1/2}) values.....	69
4.5 Ozawa constants and K(T) values of samples.....	72

LIST OF TABLES (continued)

<u>Tables</u>	<u>Pages</u>
4.6 Activation energy values of crystallization obtained from Kissinger and Augis Bennett models for nonisothermally crystallized selected PPA GF40 HP samples.	75
4.7 Half life times and T transitions for HP PPA GF40 samples via TGA experiments.....	78
4.8 Groups of HP PPA samples defined by FTIR (Coates, 2000; Skoog, 1991). .	80
4.9 Relative viscosity changes over time.....	88

NOMENCLATURE

<u>Symbols</u>	<u>Explanations</u>
A	Pre-exponential factor
b	The surface nucleus thickness [mm]
C	Concentration of the solute [mol/L]
E_A	Activation energy [J/mol]
E_N	Activation energy for nucleation [J/mol]
E_G	Activation energy for growth [J/mol]
G	Growth rate [cm/s]
g'	Geometrical factor
H	Heat flow [J/g]
k	Reaction rate constant [1/s]
k_B	Boltzmann constant
k_H	Constant with the dimensions of pressure divided by concentration
K(T)	Cooling crystallization function
L	Number of nuclei
m	Ozawa exponent
n	Avrami exponent
$n=m+1, Iv$	Integer or half integer depending on mechanism of growth and dimensionality of the crystal

N	Nucleation rate [the number of nuclei per unit time per unit volume] [number of nuclei/m ³ .s]
r	The radius of the spherical crystal at time t [mm]
R	Universal gas constant [J/mol.K]
$t_{1/2}$	crystallization half time [min]
T	Temperature [°C]
T_c	Crystallization temperature [°C]
T_g	Glass transition temperature [°C]
T_o	Initial room temperature [°C]
T_∞	Hypothetical temperature at which viscous flow ceases [°C]
U^*	Activation energy of the segmental jump [J/mol]
V_t	Volume of crystallization material
X	Degree of crystallinity [%]
X_r	Relative crystallinity
$X(t)$	Time dependent degree of crystallinity [%]
Z_c	The growth rate under the nonisothermal crystallization
Z_t	Rate parameter in the nonisothermal crystallization process
α	Ratio of Avrami exponent n to the Ozawa exponent m
α_{ex}	Extended transformed fraction
ϕ	Cooling rate [°C/min]
ρ	Partial pressure of the solute in the gas above the solution

σ	Lateral surface free energy [mJ/m ²]
σ_e	Fold surface free energy [mJ/m ²]
σ_{fu}	Ultimate tensile strength for the fiber [MPa]
σ_{mu}	Ultimate tensile strength for the matrix [MPa]
σ'_m	Matrix stress at the fracture strain of the fibers [MPa]
σ_m	Tensile strength for the matrix [MPa]

1. INTRODUCTION

Polyphthalamide (PPA) is a polymer composed from a diacid and a diamine. However, the diacid portion contains at least 55% terephthalic acid (TPA) or isophthalic acid (IPA). TPA or IPA are aromatic components which serve to raise the melting point, glass transition temperature and generally improve chemical resistance of standard aliphatic nylon polymers (Harper, 2002). The melting and glass transition temperatures of Grivory HT1 is 325 °C and 130 °C respectively.

The one that will be studied has the molecular structure as given in Figures-1.2 and 1.3 below;

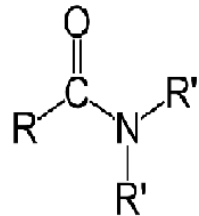


Figure-1.1 General amide structure.

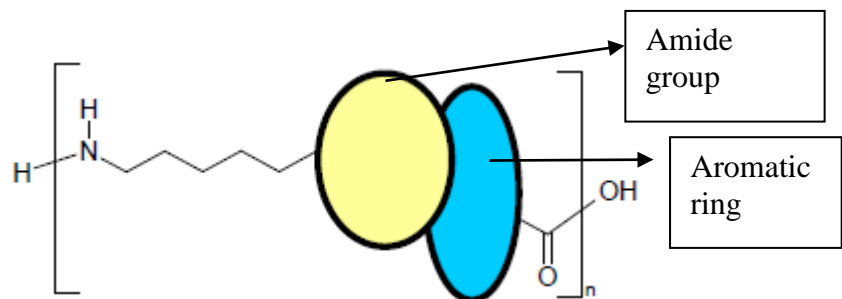


Figure-1.2 Polyphthalamide main structure.

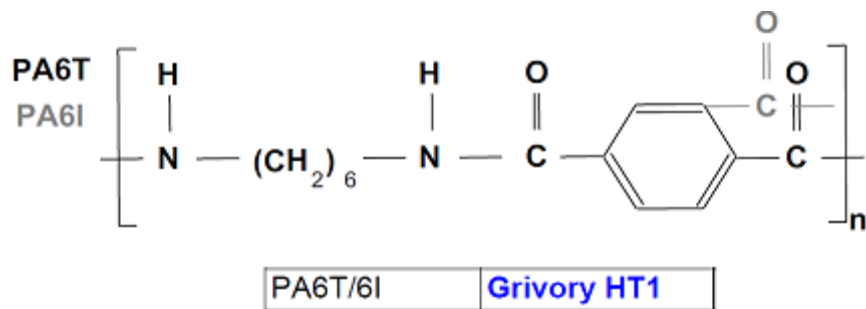


Figure-1.3 Polyphthalamide detailed molecular formula.

Polyamides may be produced by the reaction of a difunctional organic acid with a functional amine, or the self-condensation of either an ω -amino acid or a lactam. A wide variety of acids and amines can be reacted to produce and a number of polyamides are commercially important. The polyamides are named firstly with the number of carbon atoms in the monomers with the diamine component. Thus, a polyamide made from hexamethylene diamine and adipic acid is called polyamide 6,6 or nylon 6,6, and one made from hexamethylene diamine and dodecanedioic acid would be nylon 6,12. When an aromatic diacid is used instead of an aliphatic diacid, the nomenclature is modified to reflect the isomeric form of the aromatic diacid, and the term polyphthalamide may be used to distinguish these polymers from those of solely aliphatic raw materials (AMODEL® Polyphthalamide Design Guide, 2003).

The material used in this thesis study meets regulations related with drinking water contact for Germany, France, UK and USA countries. The standards can be seen in Table-1.1;

Table-1.1 Drinking water regulations in different countries.

Country	Standard Name	Content
Germany	KTW	Applications where they are in contact with cold and hot drinking water (90°C)
France	ACS	Migration levels for direct contact with drinking water
UK	WRAS	Approved for applications where they are in contact with hot drinking water (85°C)
USA	NSF61	Certified for hot-water applications (82°C)

In Turkey, the standard related with drinking water acceptable limits is TSE 266 and this standard is also met by PPA polymer. Some thermal properties regarding PPA can be found in Table-1.2 below.

Table-1.2 Thermal properties of Grivory HT1V-4 FWA Black 9225 (EMS Material Database).

Thermal Properties						
Melting point	DSC	ISO 11357	°C	dry		325
Heat deflection temperature HDT/A	1.8 MPa	ISO 75	°C	dry		280
Heat deflection temperature HDT/C	8.0 MPa	ISO 75	°C	dry		200
Thermal expansion coefficient long.	23-55°C	ISO 11359	10 ⁻⁴ /K	dry		0.15
Thermal expansion coefficient trans.	23-55°C	ISO 11359	10 ⁻⁴ /K	dry		0.50
Maximum usage temperature	long term	ISO 2578	°C	dry		140
Maximum usage temperature	short term	ISO 2578	°C	dry		250

Glass-fiber reinforced grades of polyphthalamide have usages for applications where high durability is necessary.

The crystallization process significantly influences polymer properties through the crystal structure and morphology established during the phase transition from the viscous molten state to the semicrystalline solid state. The final polymeric material properties are dependent on the morphology generated during their processing. So, the knowledge of the parameters affecting crystallization is crucial for the optimization of the processing conditions and the properties of the end product (Durmus et al., 2005; Vyazovkin et al., 2005).

The polymer matrix composite (PMC) materials for the use-environment will eventually result in irreversible change(s) in the original properties of the material and effectively limit operating life. The change in properties over time in polymeric composites is referred to as ‘ageing’.

2. LITERATURE ON DEGRADATION KINETICS OF POLYMERIC COMPOSITES

There are many studies conducted in literature about degradation of polymeric materials. Here, a highlight on effective mechanisms and crystallization kinetics' effect on degradation for polymers will be given.

2.1 Ageing Theory

Ageing may be divided into three primary mechanisms: chemical, physical and mechanical (Martin, 2008). The interaction (if any) between these three areas is highly dependent on two variables: material characteristics and ageing environment. All ageing mechanisms may be additive or subtractive depending on material type, the environment and applied collective loads on it. So it is important to determine environmental stresses during the application and to go deeper for the most critical stress factors that cause the material to pass to significant chemical, physical, and mechanical changes during the application. Heat, moisture, mechanical load, etc. are all environmental degradation factors. The critical degradation mechanism changes in one or more bulk physical properties of the material system.

In general, material testing is a costly process that often involves many materials-related disciplines and a wide variety of laboratory equipment. While long-term, real-time testing is required to assess the durability of materials fully, accelerated ageing reduces the expense and time by being able to consider the long-term effects of the components within the system by the help of more harsh application parameters. This type of information may then lead to changes in the standard practice for materials selection and provide quantitative results for manufacturers and fabricators to follow new and improved specific procedures.

Accelerated ageing is defined as the process or processes required to accelerate a specific critical degradation mechanism and/or mechanisms relative

to a baseline ageing condition; thereby resulting in the material reaching the same aged end-state as a real-time aged material, but in less time.

Validation of ageing methods takes place through a comparison of mechanical properties, damage mechanisms, and physical parameters (e.g. weight loss, changes in glass transition or fracture toughness) determined from accelerated testing with those from real-time ageing tests. Three types of ageing process can be explained as below:

2.1.1 Chemical ageing

Chemical ageing is related to irreversible changes in the polymer chain/network through mechanisms such as cross-linking or chain scission. Chemical degradation mechanisms include thermo-oxidative, thermal, and hydrolytic ageing. At typical operating temperatures, cross-linking and oxidation are the dominant chemical ageing mechanisms. Thermo-oxidative degradation becomes increasingly important as the exposure temperature and time increase. Frequently, chemical ageing results in an increase in cross-linking density that can lead to changes in material densification and increases the T_g which in turn will influence mechanical properties such as strength and stiffness.

2.1.2 Physical ageing

Physical ageing will occur when a polymer is rapidly cooled below its T_g and the material evolves toward thermodynamic equilibrium. This evolution is characterized by changes in the free volume, enthalpy, and entropy of the polymer and will produce measurable changes in the mechanical properties.

Physical ageing is responsible for changes over time of modulus, strength, and ductility for polymers in the glassy range. Since most polymer composite structures are used in the glassy range of the polymeric matrix, physical ageing has an important impact on long-term durability of composites used in applications. Physical ageing is thermoreversible for all amorphous polymers by heating the polymer above its T_g and subsequently rapidly quenching the material.

It is assumed that this thermo-reversible behavior does not occur in thermoset materials due to the tendency for elevated temperature to affect their extent of cross-linking time and/or influence chain scission. Operational mean temperature and lifetime thermal history have a strong influence on the rate of physical ageing.

2.1.3 Mechanical Ageing

Mechanical degradation mechanisms are irreversible processes that are observable on the macroscopic scale. These degradation mechanisms include matrix cracking, delamination, interface degradation, fiber breaks, and thus have a direct effect on more of structure dependent engineering properties such as stiffness and strength.

Plastic and rubber materials lose their mechanical properties over time with respect to chain breakages, loss of additive materials, crack formation in structure, etc... This mechanism is called degradation. The effects that have important role on degradation of the material may be thermal, oxidative, combined effect of temperature and oxidation that is thermo-oxidative and environmental chemical attack where all may be explained in terms of environmental stress factors.

The degradation kinetics of the material will tend to accelerate as temperature rises so the main stressor, that is chosen to accelerate lifetime determination tests, is temperature. All other parameters other than temperature are kept constant and tests are employed at chosen temperatures that are lower than maximum long-term service temperature of the material. The long-term service temperature is defined as the maximum temperature at which a plastic has changed no more than 50% of its initial properties after 20,000 hours of storage in hot (EN 60216-1:2001 Electrical insulating materials -Properties of thermal endurance-, 2001). That's why, this value has been taken into consideration for lifetime estimation of the material. Choosing very high temperature(s) brings misleading results.

The ageing rate of the material is dependent on activation energy that is the characteristic property of the material. The activation energy expresses the

hydrolytic and thermal degradation effects over formation of degradation products from reactants by exceeding activation energy value throughout the reaction. During the reaction, by collision of atoms in the structure, the simpler constituents are formed and generally collision tends to increase by temperature rise. Figure-2.1 shows the exothermic and endothermic reaction graphs for formation of products from reactants. So as in our case, endothermic reaction needs temperature to be increased to accelerate formation of degradation products.

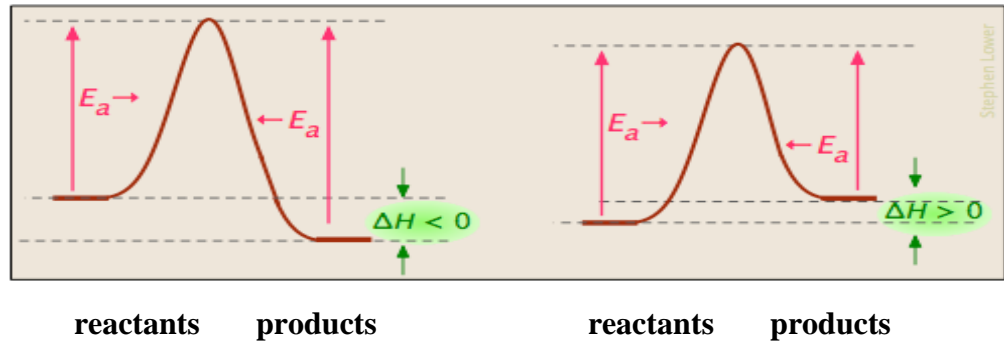


Figure-2.1 Exothermic and endothermic reaction graphs for formation of products from reactants.

2.2 Models for Crystallization Kinetics and Activation Energy

There are various models defined in the literature for evaluation of crystallization kinetics of materials. Starting from most well-known Avrami model, other models as Avrami-Jeziorny, Ozawa, Lui Mo will also be investigated those explain the complexity of crystallization kinetics more in detail.

2.2.1 Avrami model for isothermal crystallization

Bulk crystallization of polymers, the crystallization kinetics can be represented with Eq. 2.1 below (Janeschitz, 2010).

$$1 - X = e^{-V_t} \quad 2.1$$

where X is the degree of crystallinity and V_t is the volume of crystallization material, which should be determined by considering the following two cases: (a) the nuclei are predetermined, that is, they all develop at once on cooling the polymer, and (b) the crystals nucleate sporadically. For a spherical crystal in case (a);

$$dV_t = 4\pi r^2 L dr \quad 2.2$$

where r represents the radius of the spherical crystal at time t and L is the number of nuclei. Assuming the radius r grows linearly with time, and $r = Kt$. Integration of Eq. 2.2 and substitution into Eq. 2.1, one obtains;

$$1 - X = e^{-K t^3} \quad 2.3$$

where K is the growth rate and equal to;

$$K = \left(\frac{4}{3}\right) \pi K^3 L \quad 2.4$$

For sporadic nucleation, case (b), the argument is above followed, but the number of spherical nuclei is allowed to increase linearly with time at rate u . Then nucleation from time t_i to time t will create a volume increase of;

$$dV_t = \left(\frac{4}{3}\right) \pi K^3 (t - t_i)^3 u dt_i \quad 2.5$$

Integration of Eq. 2.5 between $t_i = 0$ and t , and substitution into Eq. 2.1, one obtains;

$$1 - X = e^{-K t^4} \quad 2.6$$

where K is equal to;

$$K = \left(\frac{1}{3}\right) \pi K^3 u \quad 2.7$$

The equations can be generalized by replacing the power of t with the Avrami exponent n ,

$$1 - X = e^{-K t^n}$$

$$\ln(-\ln(1-X(t))) = \ln(K) + n \ln(t) \quad 2.8$$

After experimental studies conducted by DSC, the characteristic Avrami graphs are obtained as in Figure-2.2 (Rattaa, 2000) for 1,3-bis(4-aminophenoxy)

benzene (TPER) and 3,3',4,4'-biphenyltetracarboxylic dianhydride (BPDA), and endcapped with phthalic anhydride.

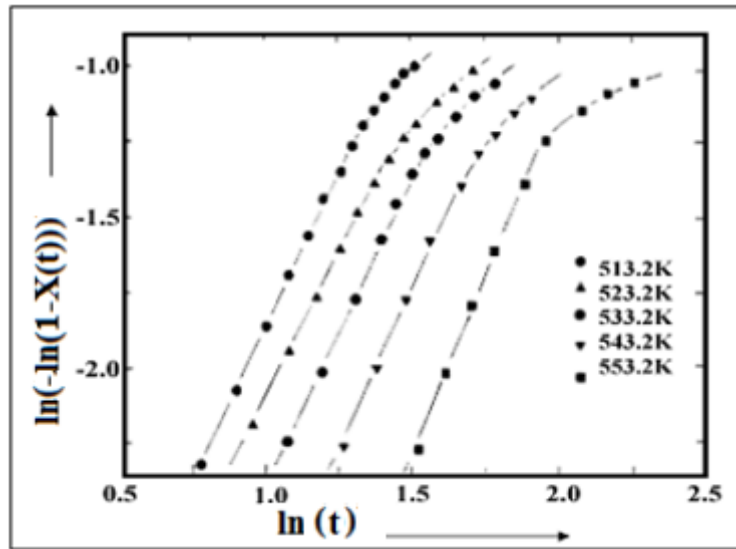


Figure-2.2 Evaluation of property data over time by Avrami approach.

2.2.2 Nonisothermal crystallization kinetics

There are many models in the literature explaining the crystallization kinetics of material. Avrami is one of the most favorable one that is conducted frequently and is applicable for isothermal conditions.

Avrami's model describes the kinetics of phase transformation under the assumption of spatially random nucleation. A quasi-exact analytical solution of Avrami's model when the transformation takes place under continuous heating was studied recently (Farjas and Roura, 2006). Solution has been obtained with different activation energies for both nucleation and growth rates. The relation obtained is also a solution of the so-called Kolmogorov–Johnson–Mehl–Avrami (KJMA) transformation rate equation. The corresponding nonisothermal KJMA transformation rate equation differs from the one obtained under isothermal conditions only by a constant parameter, which depends only on the ratio between nucleation and growth rate activation energies. Consequently, a minor correction allows to extend the KJMA transformation rate equation to continuous heating conditions. KJMA model under isothermal conditions is:

$$\alpha = 1 - \exp[-(kt)^{m+1}]$$

where α is the transformed phase fraction, k is the overall rate constant that generally depends on temperature, $m+1$ is usually known as Avrami's exponent and t is time. Differentiation of the Eq. 2.9 gives:

$$\frac{d\alpha}{dt} = (m + 1)k(1 - \alpha) \cdot [-\ln(1 - \alpha)]^{m/m+1} \quad 2.10$$

Although above equation is obtained for the isothermal conditions, it constitutes the basis for analyzing nonisothermal experiments.

The Avrami constants obtained from Figure-2.2 gives idea about the crystal shape and kinetics of the material. Avrami exponents for various shapes of crystal growth geometries are given in Table-2.1 (Hiemenz, 1984);

Table-2.1 Avrami exponents for various types of crystal growth geometries.

Avrami Exponent	Crystal Geometry	Nucleation Type	Rate Determination
0.5	Rod	Athermal	Diffusion
1	Rod	Athermal	Nucleation
1.5	Rod	Thermal	Diffusion
2	Rod	Thermal	Nucleation
1	Disc	Athermal	Diffusion
2	Disc	Athermal	Nucleation
2	Disc	Thermal	Diffusion
3	Disc	Thermal	Nucleation
1.5	Sphere	Athermal	Diffusion
2.5	Sphere	Thermal	Diffusion
3	Sphere	Athermal	Nucleation
4	Sphere	Thermal	Nucleation

In real case, the conditions are nonisothermal and KJMA equation can be analyzed with respect to either when activation energy of crystal nucleation (E_N) and growth (E_G) are equal (isokinetic case) or when they are not equal.

2.2.2.1 Isokinetic case (energy of crystal nucleation = energy of crystal growth)

For the transformations involving nucleation and growth, and assuming that the nuclei of the new phase are randomly distributed;

$$\alpha = 1 - \exp[-\alpha_{\text{ex}}] \quad 2.11$$

where α_{ex} is the extended transformed fraction, i.e., the resulting transformed fraction if nuclei grow through each other and overlap without mutual interference.

$$\alpha_{\text{ex}}(t) = \int_0^t N(\tau) v(\tau, t) d\tau \quad 2.12$$

N is the nucleation rate and $v(\tau, t)$ is the volume transformed at time t by a single nucleus formed at time τ given by Eq. 2.13:

$$v(\tau, t) = \sigma \left(\int_{\tau}^t G(z) dz \right)^m \quad 2.13$$

Here σ is a shape factor (e.g., $\sigma = 4\pi/3$ for spherical grains), G is the growth rate and m depends on the growth mechanism, e.g., $m = 3$ for three-dimensional growth. Eqs. 2.11-2.13 show the kinetics of the transformation under very general assumptions about the rate constants (any time or temperature dependence) and for any thermal history.

The KJMA relation, Eq. 2.11 is the particular solution for isothermal conditions provided that both G and N do not depend on temperature. The overall rate constant is given by:

$$k = \left(\frac{\sigma N G^m}{m+1} \right)^{1/m+1} \quad 2.14$$

In most practical situations it is possible to assume an Arrhenian temperature dependence for both N and G:

$$N = N_0 \exp(-E_N/k_B T) \quad \text{and} \quad G = G_0 \exp(-E_G/k_B T) \quad 2.15$$

where E_N and E_G are the activation energies for nucleation and growth, respectively, and K_B is the Boltzmann constant. 0 subscripts refers to initial values of these parameters. Substitution of Eq. 2.15 into Eq. 2.14 gives:

$$k = \left(\frac{\sigma N_0 G_0^m}{m+1} \right)^{1/m+1} \exp\left(-\frac{E}{k_B T}\right) \equiv k_0 \exp\left(-\frac{E}{k_B T}\right) \quad 2.16$$

where overall activation energy;

$$E \equiv \frac{E_N + mE_G}{m+1} \quad 2.17$$

Introducing Eq. 2.15 into Eq. 2.16 gives;

$$v(\tau, t) = \sigma \left(\frac{G_0 E_G}{\beta k_B} \right)^m \left[p\left(\frac{E_G}{k_B T}\right) - p\left(\frac{E_G}{k_B T'}\right) \right]^m \quad 2.18$$

Finally the transformed fraction becomes;

$$\alpha = 1 - \exp \left\{ - \left[k_0 \frac{E}{\beta k_B} p \left(\frac{E}{k_B T} \right) \right]^{m+1} \right\} \quad 2.19$$

2.2.2.2 General case ($E_N \neq E_G$)

The transformed fraction here is;

$$\alpha = 1 - \exp \left\{ - \left[k_0 C \frac{E}{\beta k_B} p \left(\frac{E}{k_B T} \right) \right]^{m+1} \right\} \quad 2.20$$

where C is a constant and calculated as;

$$C \equiv \left(\frac{(m+1)! E^{m+1}}{\prod_{i=0}^m (E_N + i E_G)} \right)^{1/m+1} \quad 2.21$$

As a consequence, the approximate solution for the general nonisothermal case is also a solution of the isothermal KJMA rate equation with the overall rate constant k multiplied by the constant (Farjas and Roura, 2006).

2.2.2.3 Nonisothermal KJMA rate equation

The equation of nonisothermal experiments is obtained from the isothermal solution and it constitutes the basis for analysis. Differentiation of Eq. 2.9 gives the transformed phase fraction α as given in Eq. 2.22 below (Farjas and Roura, 2006):

$$\frac{d\alpha}{dt} = (m+1) \cdot C \cdot k \cdot (1-\alpha) \cdot [-\ln(1-\alpha)]^{m/m+1} \quad 2.22$$

In another study conducted, a different methodology was brought (Saxena et al., 1999). As usual, isothermal crystallization with a nucleation rate independent

of time, the fraction X , in terms of nucleation frequency per unit volume I_v and crystal growth rate u is given by;

$$X = 1 - \exp(-g' I_v u^m t^n) \quad 2.23$$

where g' is a geometrical factor, $n=m+1$ and I_v is integer or half integer depending on mechanism of growth and dimensionality of the crystal. When nucleation and growth rate are independent of time, m is assumed to be between 1 and 3 in isothermal crystallization. So Eq. 2.23 can be written as;

$$X = 1 - \exp(-Kt^n) \quad 2.24$$

X : crystallization fraction, n : Avrami exponent and K : rate of both nucleation and growth.

K is given as;

$$K = K_o \exp(-E/RT) \quad 2.25$$

E : apparent activation energy, K_o : pre-exponential factor, R : universal gas constant and T : temperature in Kelvin

The analysis of nonisothermal kinetics has been developed from isothermal case that follows Johnson–Mehl–Avrami (JMA) Law under isothermal conditions.

In another study, the concept of additivity by considering a process of two iso-thermal treatment was explained. For a period of time t_1 , $X= f_1(t)$ and after a jump in temperature, the second treatment starts where $X= f_2(t)$. Since the process is assumed to be additive, transformation at T_2 is exactly the same as if the amount transformed at the end of first treatment is $X_1= f_1(t)$. Since all had been formed at T_2 , so if t_2 the time that would have been required to produce same extent of transformation X_1 as was produced at T_1 ($f_1(t)= f_2(t)$) then entire process is described;

$$X = f_1(t), \quad t < t_1, \quad 2.26$$

$$X = f_2(t + t_2 - t_1), \quad t > t_1 \quad 2.27$$

This a simple basis for transformation to nonisothermal conditions.

2.2.3 Avrami-Jeziorny model for nonisothermal crystallization

The kinetics of nonisothermal crystallization are interpreted using the relative crystallinity as a function of temperature, $X(T)$, defined as;

$$X(T) = \frac{\int_{T_0}^T \left(\frac{dH}{dT} \right) dT}{\int_{T_0}^{T_c} \left(\frac{dH}{dT} \right) dT} \quad 2.28$$

where H is the heat flow, is calculated for the nonisothermal DSC experiments. In the nonisothermal experiments described here the temperature is directly proportional to the cooling time ($t=(T_0-T)/\phi$) and an equivalent time dependent degree of crystallinity, $X(t)$. ϕ is the cooling rate. Based on the assumption that the crystallization temperature, T_c , is constant, the Avrami relation between the degree of crystallinity and the crystallization time was adapted to describe the nonisothermal crystallization by Mandelken;

$$X_c(t) = 1 - (\exp - Z_t \times t^n) \quad 2.29$$

$$(\ln - \ln(1 - X_c(t))) = n \times \ln(t) + Z_t \quad 2.30$$

where $X_c(t)$ is relative crystallinity, Z_t is the rate parameter in the nonisothermal crystallization process. In order to eliminate the effect of the cooling or heating rate $\phi=dT/dt$, the rate parameter characteristic of the kinetics of nonisothermal crystallization was modified by Jeziorny;

$$\log Z_c = \frac{\log Z_t}{\phi} \quad 2.31$$

Plot of $\ln(-\ln(1-X_c(t)))$ versus $\ln t$ gives the values of n and Z_t as the slopes and intercepts, respectively. The parameter of Avrami exponent n describes the

growing mechanism and geometry of crystallization, and the parameter Z_c describes the growth rate under the nonisothermal crystallization process (Kahraman, 2013).

2.2.4 Ozawa model for nonisothermal crystallization

The kinetics approach frequently used for nonisothermal crystallization process of semi crystalline polymers is Ozawa model. The Avrami model requires that crystallization occurs at quench cooling and constant temperature and that the nuclei grow as spherulites. From these assumptions, Ozawa deduced the following expression for the untransformed material fraction. It is based on the extended form of Avrami approximation assuming that the nonisothermal crystallization process could be composed of small isothermal steps. Ozawa equation is as follows;

$$X_c(t) = 1 - \exp\left(\frac{K(T)}{\phi^m}\right) \quad 2.32$$

$$\ln(-\ln(1 - X_c(t))) = \ln(K(T)) - m \times \ln(\phi) \quad 2.33$$

where $X_c(t)$ is the relative crystallinity, $K(T)$ is the cooling crystallization function, which is a complicated function of nucleation and growth rates, ϕ is the absolute value of the cooling rate and m is the Ozawa exponent.

2.2.5 Liu Mo model for comparison of isothermal and nonisothermal crystallization

Liu and coworkers also used to describe the nonisothermal melt-crystallization process (Durmus et al., 2005). Liu and coworkers offered a new method combining the Avrami and Ozawa equations at a given value of $X(t)$ as follows:

$$\ln(K(T)) - m \times \ln(\phi) = \ln(Z_t) - n \times \ln(t) \quad 2.34$$

$$\ln(\phi) = \ln(F(T)) - \alpha \times \ln(t) \quad 2.35$$

where $F(T)=[K(T)/Zt]^{1/m}$ refers to the value of the cooling rate, which has to be chosen at the unit crystallization time when the measured system amounts to a certain relative crystallinity; $K(T)$ is the crystallization rate parameter, and α is the ratio of the Avrami exponent n , to the Ozawa exponent m ; that is, $\alpha = n/m$. It could be seen that $F(T)$ has a definite physical and practical meaning which means that high cooling rate is needed to reach this $X_c(t)$ in a unit time, which also indicates the difficulty in crystallization process. At a given degree of crystallinity, from the plots of $\ln(\phi)$ versus $\ln(t)$, the values of α and $F(T)$ could be obtained by the slopes and intercepts, respectively.

2.2.6 Effective activation energy (E) of crystallization

Related with the studies conducted before, measurement of the overall crystallization kinetics was done over Arrhenius equation. These were not developed for crystallization of polymers and, therefore, does not reflect such key phenomena as incomplete crystallization or chain folding. Similar problem is encountered when the popular Kissinger equation applied for estimating the so-called “activation energy of crystallization”.

While not at all applicable to the melt crystallization, the application of this equation to the glass crystallization yields an “activation energy”, whose meaning is obscure as the temperature dependence of the crystallization rate has a clearly non-Arrhenius character. Meaningful parameters of polymer crystallization are most commonly derived in the frameworks of the Hoffman-Lauritzen theory and are typically based on microscopic measurements of the crystal growth rates. A new approach allows one to obtain the K_g and U^* parameters of the Hoffman-Lauritzen theory by applying an isoconversional method to DSC data on nonisothermal crystallization. The Hoffman-Lauritzen theory suggests that the linear growth rate of a polymer crystal, G depends on temperature, T as follows:

$$G = G_0 \exp\left(\frac{-U^*}{R(T - T_\infty)}\right) \exp\left(\frac{-K_g}{T\Delta Tf}\right) \quad 2.36$$

where G_0 is the preexponential factor, U^* is the activation energy of the segmental jump, $\Delta T = T_m - T$ is the undercooling, $f = 2T/(T_m + T)$ is the correction factor, T_∞ is a hypothetical temperature at which viscous flow ceases (usually taken 30 K below the glass transition temperature, T_g). The kinetic parameter K_g has the following form;

$$K_g = \frac{nb\sigma\sigma_e T_m}{\Delta h_f k_B} \quad 2.37$$

where b is the surface nucleus thickness, σ is the lateral surface free energy, σ_e is the fold surface free energy, T_m is the equilibrium melting temperature, Δh_f is the heat of fusion per unit volume of crystal, k_B is the Boltzmann constant, and n takes the value 4 for crystallization regime I and III, and 2 for regime II. The parameters U^* and K_g are usually determined by measuring microscopically the growth rate in a series of isothermal runs and substituting the measured value in rearranged Eq. 2.36;

$$\ln(G) + \frac{U^*}{R(T - T_\infty)} = \ln(G_0) - \frac{K_g}{T\Delta Tf} \quad 2.38$$

Then K_g can be determined from the linear plot of the lefthand side of Eq. 2.38 plotted against $(T\Delta Tf)^{-1}$. The parameter U^* is either varied to determine the best linearity or, more frequently, is taken as the universal value $1.5 \text{ kcal.mol}^{-1}$ (i.e., 6.3 kJ.mol^{-1}).

The need of determining the growth rates is a major obstacle to applying Eq. 2.38 to DSC data. It had been proposed to replace the growth rate with the reciprocal time to 50% of the relative crystallinity that can be readily measured by DSC for isothermal conditions. However, this modification has a purely empirical character and is not applicable to nonisothermal conditions. Recently an

alternative method was developed that makes use of temperature dependence of the effective activation energy (or the temperature coefficient) defined as:

$$E = -R \frac{d \ln(G)}{dT^{-1}} = U^* \frac{T^2}{(T - T_\infty)^2} + K_g R \frac{T_m^2 - T^2 - T_m T}{(T_m - T)^2 T} \quad 2.39$$

Figure-2.3 shows schematically a theoretical dependence of E on T.

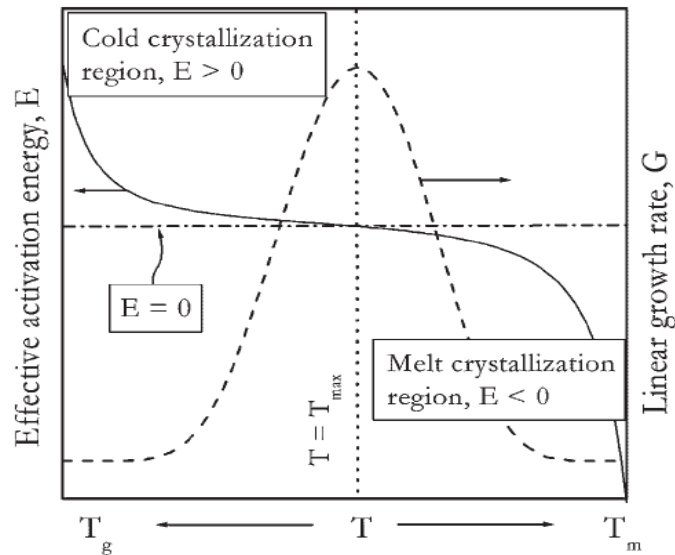


Figure-2.3 T dependencies for the growth rate (dash line) from Eq. 2.36 and the effective activation energy (solid line) from Eq. 2.39. The E value turns negative when crystallization occurs at temperatures above T_{max} .

Effective activation energy represents the energy barriers of mass transport and nucleation. The temperature determines the relative contributions of these processes to the growth rate and, therefore, the value of E. This value is called the effective activation energy to differentiate it from the true activation energy that represents the height of the energy barrier.

There are two major temperature regions in Figure-2.3. In the melt crystallization region, the measurements are performed by cooling a polymer from above T_m . The rate of crystallization decreases with increasing temperature giving rise to negative values of E_A . The growth rate is predominantly determined by the nucleation rate in that region. The cold crystallization region is typically accessed by heating glassy polymers. The respective values of E_A are positive as the rate of

crystallization increases with increasing temperature. In this region the growth rate is mostly determined by mass transport. The two regions are separated by the temperature of the maximum growth rate, T_{\max} at which the value of E_A approaches zero. By performing crystallization in different temperature regions one can obtain practically any value of E from large positive to large negative numbers that clearly suggests that E_A is not an energy barrier of crystallization (Vyazovkin and Dranca, 2006).

Kissinger and Augis–Bennett equations can be seen as follows respectively;

$$\frac{d \left\{ \ln \left(\frac{\phi}{T_c^2} \right) \right\}}{d \left\{ \frac{1}{T_c} \right\}} = -\frac{\Delta E_A}{R} \quad 2.40$$

$$\frac{d \left\{ \ln \left(\frac{\phi}{T_o - T_c} \right) \right\}}{d \left\{ \frac{1}{T_c} \right\}} = -\frac{\Delta E_A}{R} \quad 2.41$$

where ϕ is the cooling rate ($^{\circ}\text{C}/\text{min}$), T_c is the crystallization peak temperature ($^{\circ}\text{C}$), T_o is the initial room temperature, ΔE_A (kJ/mol) is the activation energy of crystallization process, and R is the universal gas constant (8.314 J/mol.K). When the parameter $\ln(\phi/T_c^2)$ or $\ln(\phi/(T_o-T_c))$ is plotted against $1/T_c$, the slope of the curve gives the activation energy of the crystallization process. ΔE_A is negative because of exothermic nature of the transition from melt to crystalline state, and the negative activation energy values also imply that crystallization mechanisms are accelerated by decreasing the temperature.

2.2.7 Arrhenius model for activation energy calculation

The property of a material will go worse over time dependent upon environmental stressors. The change over time will give the chance to understand the degradation rate of material. At least 2 different temperatures are necessary to end up with an activation energy calculation. Eq. 2.23 is the general reaction rate formula for a chemical reaction (Bernstein R. et al., 2010; Celina, M. et al., 2005; Bernstein, R. et al., 2005);

$$k = A \times e^{-E_a/RT} \quad 2.42$$

Where k: reaction rate constant (1/s), A: pre-exponential factor, R: gas constant (J/mol.K), T: temperature (K)

At temperatures T_1 and T_2 , Eq. 2.43 and Eq. 2.44 are obtained;

$$\ln(k_1) = \ln(A) - E_a/RT_1 \quad 2.43$$

$$\ln(k_2) = \ln(A) - E_a/RT_2 \quad 2.44$$

Division of Eq. 2.43 to Eq. 2.44 gives Eq. 2.45;

$$\ln(k_1/k_2) = E_a/R \times ((1/T_2 - 1/T_1)) \quad 2.45$$

The slope of $\ln(k_1/k_2)$ vs. $(1/T_2 - 1/T_1)$ graph from Eq. 2.45 is equal to E_a / R .

The equation can be written also in the form like Eq. 2.46;

$$E_a = \frac{R \times \ln\left(\frac{a_{T_1}}{a_{T_2}}\right)}{\left(\frac{1}{T_2} - \frac{1}{T_1}\right)} \quad 2.46$$

where a_T is acceleration factor at defined temperature.

Theory of Calculations

Under viscoelastic conditions, one method useful for obtaining long-term design data is the time-temperature superposition principle. This principle states

that the mechanical response at long times at some particular temperature is equivalent to the mechanical response at short times but at some higher temperature. By determining shift factors, it is possible to determine which temperature to use in obtaining long-term data from short-term tests. This is essentially true for linear viscoelastic behavior in the absence of a phase change. So for definition of activation energy, change of a mechanical property which can be correlated to real lifetime failure should have been measured.

Steps followed to calculate activation energy can be listed as follows;

1. After defining main influences and ageing media properties, the samples are started to be aged over time at 3 different T's.

Temperature Choice of Ageing Media

- Check maximum long-term operation temperature ($T_{\max, \text{application}}$). This is $T_{\text{test},1}$.
- Look at maximum long-term (at least 2000 hours) use temperature from data-sheet of the material ($T_{\max, \text{material}}$).

According to value of $T_{\max, \text{material}}$, choose option a or b as defined below.

Make sure:

$$|T_{\text{test},1} - T_{\text{test},2}| \geq 10\text{K}, |T_{\text{test},2} - T_{\text{test},3}| \geq 10\text{K} \text{ and } |T_{\text{test},1} - T_{\text{test},3}| \geq 10\text{K}$$

$$\mathbf{a.} \quad T_{\max, \text{material}} \geq T_{\max, \text{application}} + 20 \text{ K}$$

$$T_{\text{test},2} = T_{\text{test},1} + 10 \text{ K to } 20\text{K} \text{ (maximum T limit not to be exceeded)}$$

$$T_{\text{test},3} = T_{\text{test},1} + 20 \text{ K to } 40\text{K} \text{ (maximum T limit not to be exceeded)}$$

$$\mathbf{b.} \quad T_{\max, \text{application}} \leq T_{\max, \text{material}} < T_{\max, \text{application}} + 20 \text{ K}$$

$$T_{\text{test},2} = T_{\text{test},1} + 10 \text{ K to } 20\text{K} \text{ (maximum T limit not to be exceeded)}$$

$$T_{\text{test},3} = T_{\text{test},1} - 10 \text{ K to } 20\text{K} \text{ (maximum T limit not to be exceeded)}$$

2. The samples are taken out with certain time intervals.

3. The samples are tested for relevant failure property and these dataset are recorded for further activation energy calculation steps.
 - The samples are tested for relevant failure property and % property change vs. log time graph is drawn at 3 different temperatures as in Figure-2.4.
 - The parallelism of three lines at three different temperatures on “failure property vs. log ageing time” graph is followed to assure that same degradation mechanism is valid over the chosen temperature. In case of any abnormal trend, the highest temperature should be lowered and new tests for lowered temperature should be started.

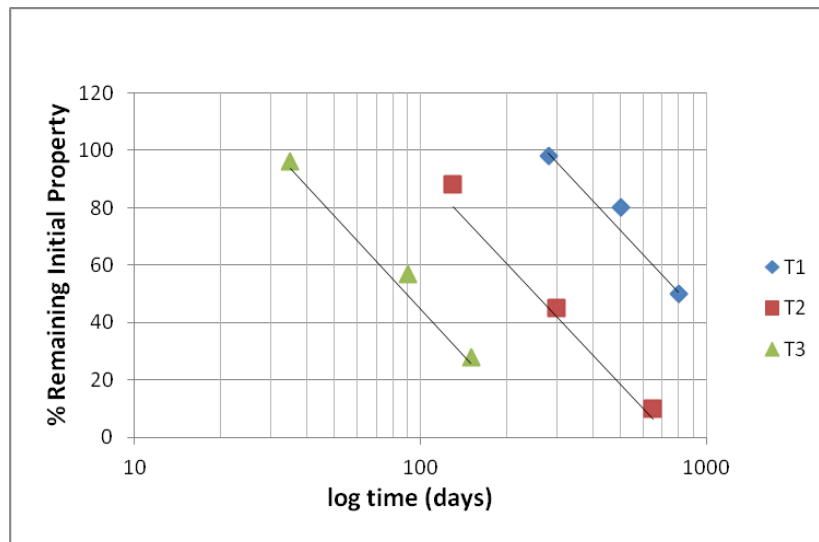


Figure-2.4 Graph trend for a property change over time.

2.3 Glass Fiber Effect in Polymeric Materials

Glass fibers are used in polymeric materials to exhibit useful bulk properties such as hardness, transparency, resistance to chemical attack, stability, and inertness, as well as desirable fiber properties such as strength, flexibility, and stiffness (Wallenberger et al., 2001).

Glass fibers fall into two categories, low-cost general-purpose fibers and premium special-purpose fibers. Over 90% of all glass fibers are general-purpose

products. These fibers are known by the designation E-glass and are subject to ASTM specifications. The letters in front of fiber type can be seen in Table-2.2 below. The type of glass fiber used in studies PPA polymer is E-glass fiber.

Table-2.2 Types of glass fibers (Wallenberger et al., 2001).

Letter designation	Property or characteristic
E, electrical	Low electrical conductivity
S, strength	High strength
C, chemical	High chemical durability
M, modulus	High stiffness
A, alkali	High alkali or soda lime glass
D, dielectric	Low dielectric constant

Polyphthalamide with a glass fiber (GF) content of 40 % was selected because that shows the best stiffness to strength ratio. On the other hand from the results of Figures-2.5 and 2.6 together with price-performance relationship standpoints, PPA GF40 was chosen for the specific application. Other company that needs more stiffness may go to GF50 or even GF60 but this material may show slightly critical weld line strength, higher density and so higher price. When it comes to GF30, it shows some demolding problem and probably longer cycle time if the tool is not ideal. Some parts in GF30 and GF40 show similar shrinkage.

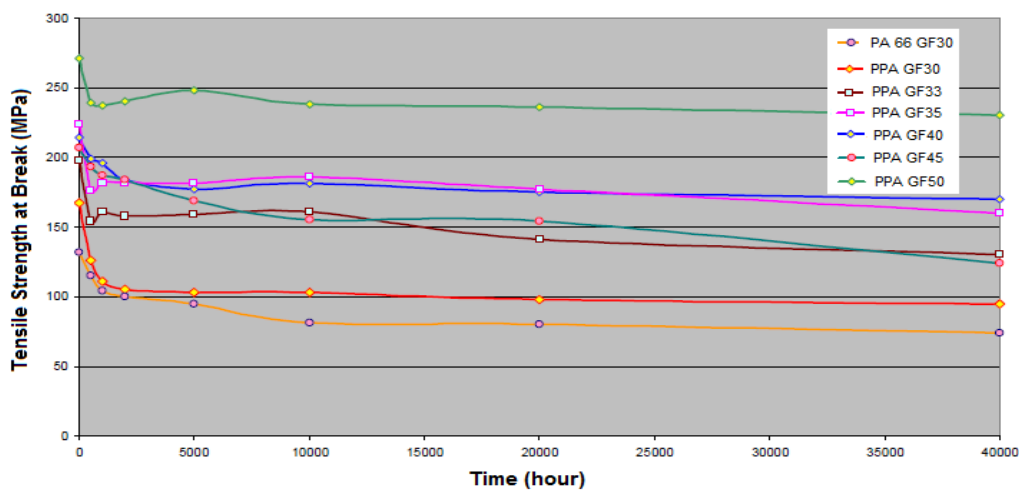


Figure-2.5 Tensile strength at break versus time graph for various glass fiber content filled polymers.

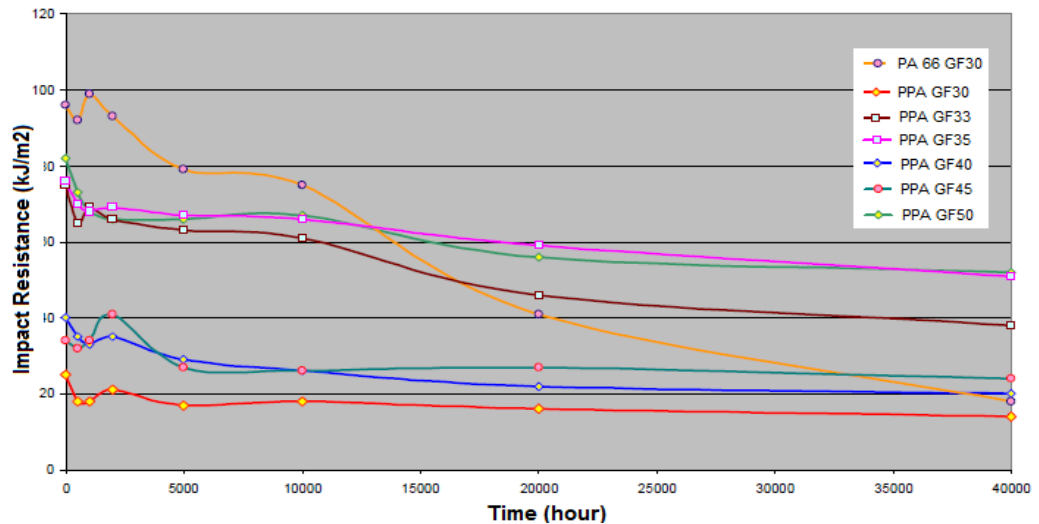


Figure-2.6 Impact resistance versus time graph for various glass fiber content filled polymers.

A wide variety of thermoplastics have been used as the base for reinforced plastics. These include polypropylene, nylon, styrene-based materials, thermoplastic polyesters, acetal, polycarbonate, polysulphone, etc. The choice of a reinforced thermoplastic depends on a wide range of factors which includes the nature of the application, the service environment and costs. Some typical properties of fiber reinforced nylons with respect to fiber fraction are given in Table-2.3.

Property	Weight fraction, W_f						
	0	0.10	0.20	0.30	0.40	0.50	0.60
Density	1140	1210	1280	1370	1460	1570	1700
Tensile strength (GN/m ²)	0.07	0.09	0.13	0.18	0.21	0.23	0.24
% elongation at break	60	3.5	3.5	3.0	2.5	2.5	1.5
Flexural modulus (GN/m ²)	2.8	4.2	6.3	9.1	11.2	15.4	19.6
Thermal expansion $\mu\text{m/m}^\circ\text{C}$	90	37	32	30	29	25	22
Water absorption (24 hr)	1.6	1.1	0.9	0.9	0.6	0.5	0.4

Table-2.3 Typical properties of fiber reinforced Nylon 6.6 (Crawford, 2005).

Reinforcing fibers have diameters varying from 7 μm to 100 μm . They may be continuous or in the form of chopped strands (lengths 3 mm-50 mm). The length to diameter ratio is called the Aspect Ratio. The properties of a short-fiber composite are very dependent on the aspect ratio-the greater the aspect ratio the greater will be the strength and stiffness of the composite.

Effect of fiber type on properties of reinforced Nylon 6.6 can be seen in the Table-2.4 with the given properties;

Table-2.4 Properties with various glass fiber contents (Crawford, 2005).

Material	Weight fraction (W_f)	Density (kg/m^3)	Tensile strength (GN/m^2)	Flexural modulus (GN/m^2)
Nylon 66	–	1140	0.07	2.8
Nylon 66/glass	0.40	1460	0.2	11.2
Nylon 66/carbon	0.40	1340	0.28	24.0
Nylon 66/glass/carbon	0.20C/0.20G	1400	0.24	20.0
Nylon 66/glass beads	0.40	1440	0.09	5.6

The greatest improvement in the strength and stiffness of a plastic is achieved when it is reinforced with uni-directional continuous fibers. The analysis of such systems is relatively straightforward.

Some methods of improving composite toughness were proposed (Akay, 1995): (i) the use of fibers with small diameters ($\sim 10/\mu\text{m}$), which reduce stress concentration at fiber tips due to the closer packing of the fibers; (ii) the use of longer fibers than conventional ones, these have the effect of reducing the number of fiber tips which act as stress concentrators; and (iii) the introduction of interfacial layers between the fiber and matrix. If a soft layer such as rubber could be used, the initiation of the interfacial microfailure would be expected to be reduced due to large deformation of the layer. By contrast, the use of a rigid layer with a modulus intermediate between that of the fiber and matrix, is considered to lower the stress concentration along the fiber sides.

The length of fibers found in the material can be observed via microscope on crack point, see Figure-2.7 (Akay, 1995).

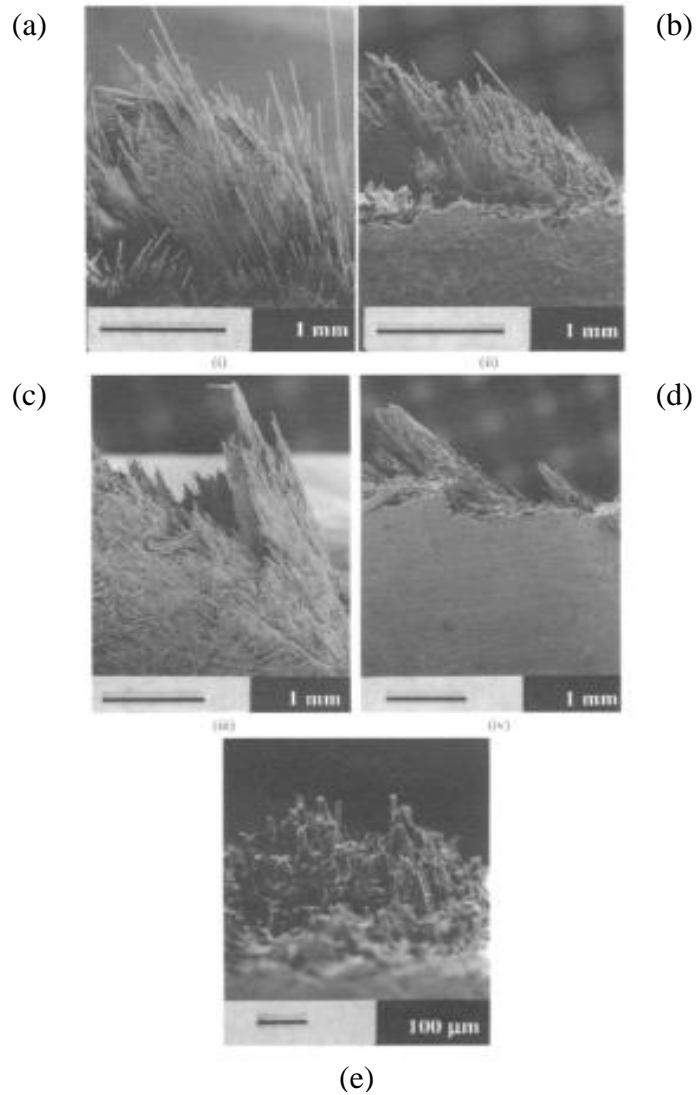


Figure-2.7 Fracture surface ahead of crack initiation region for PA specimens,

- a) 50% w. Long Fiber PA, b) 50% w. Long Fiber PA plaque, c) 60% w. Long Fiber PA, d) 60% w. Long Fiber PA plaque, e) 50% w. Short Fiber PA.

The strengthening effect of the fibers is only observed when the volume fraction is greater than a certain value of V_1 . The value of V_1 seen on Fig-2.8 is obtained by Eq. 2.47.

$$\sigma_{mu} = \sigma_{fu}V_1 + \sigma'_m(1 - V_1)$$

$$V_1 = \frac{\sigma_{mu} - \sigma'_m}{\sigma_{fu} - \sigma_m}$$

2.47

where;

σ_{mu} : ultimate tensile strength for the matrix

σ'_m : matrix stress at the fracture strain of the fibers

σ_{fu} : ultimate tensile strength for the fiber

σ_m : tensile strength for the matrix

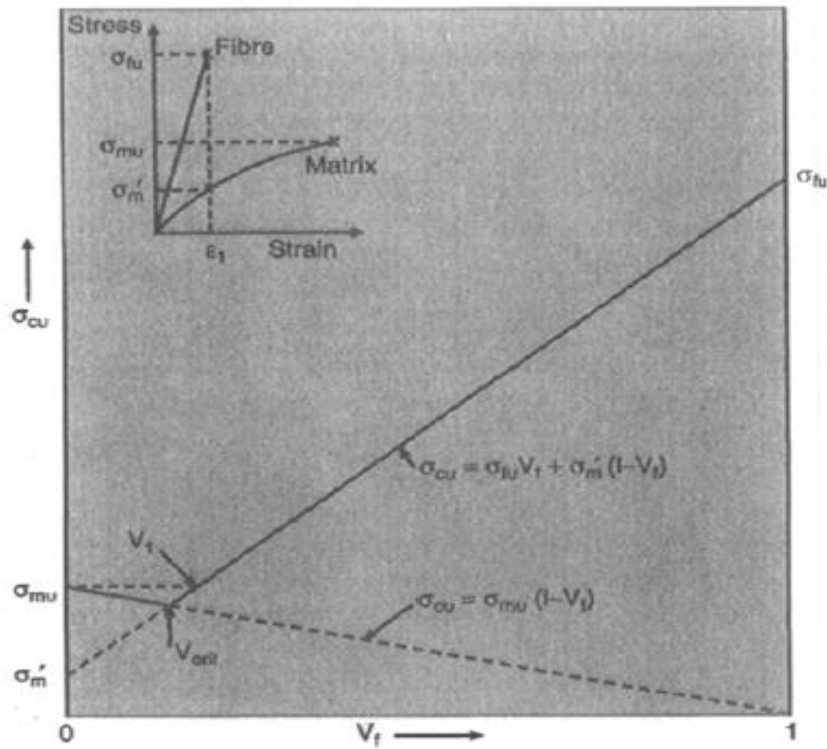


Figure-2.8 Effect of volume fraction on strength (Crawford, 2005)

The “composition” and “physical and mechanical properties” for different types of glass fibers can be seen in Table-2.5 and Table-2.6 respectively (Wallenberger et al., 2001).

Table-2.6 Physical and mechanical properties of glass fibers.

Fiber	Coefficient of linear expansion, $10^{-6}/^{\circ}\text{C}$	Specific heat, $\text{cal/g}^{\circ}\text{C}$	Dielectric constant at room temperature and 1 MHz	Dielectric strength, kV/cm	Volume resistivity at room temperature $\log_{10} (\Omega \text{ cm})$	Refractive index (bulk)	Weight loss in 24 h in 10% H_2SO_4 , %	Tensile strength at 23 °C (73 °F)		Young's modulus		Filament elongation at break, %
								MPa	ksi	GPa	10^6 psi	
General-purpose fibers												
Boron-containing E-glass	4.9–6.0	0.192	5.86–6.6	103	22.7–28.6	1.547	~41	3100–3800	450–551	76–78	11.0–11.3	4.5–4.9
Boron-free E-glass	6.0	...	7.0	102	28.1	1.560	~6	3100–3800	450–551	80–81	11.6–11.7	4.6
Special-purpose fibers												
ECR-glass	5.9	1.576	5	3100–3800	450–551	80–81	11.6–11.7	4.5–4.9
D-glass	3.1	0.175	3.56–3.62	1.47	...	2410	349
S-glass	2.9	0.176	4.53–4.6	130	...	1.523	...	4380–4590	635–666	88–91	12.8–13.2	5.4–5.8
Silica/quartz	0.54	...	3.78	1.4585	...	3400	493	69	10.0	5

(a) The log 3 forming temperature is the temperature of a melt at a reference viscosity of $100 \text{ Pa} \cdot \text{s}$ (1000 P).

In a study conducted before (Akay et al., 1995), it was clearly seen that fracture toughness of injection-moulded long-glass-fiber-reinforced polyamide 6,6 (average fiber aspect ratio in mouldings, $l/d = \sim 55$) was noticeably higher when compared to short-glass-fiber-reinforced polyamide 6,6 ($l/d \sim 20$). It was mainly observed on conditioned samples after they absorb certain amount of moisture. Instrumented drop-weight impact tests indicated brittle fracture for unreinforced polyamide 6,6 causing possible catastrophic shattering into several pieces. Short-fiber and long-fiber materials both remained intact after impact, however again long-fiber material including specimens had smaller dimensions of the damaged area.

It was found before fracture to occur by fiber pull-out rather than breakage, independent of whether brittle or ductile matrices were used. However, later work that is investigating modes of crack propagation in injection moulded short-glass and carbon-fiber-reinforced thermoplastics, it was established that the main crack will grow in a fiber avoidance mode (eg. a path of least resistance). The local mode of crack tip advancement varies with matrix ductility and the interfacial bond strength (Mandell et al., 1981).

Some further methods also were proposed for improving composite toughness (Lampman, 2003):

- (i) the use of fibers with small diameters ($\sim 10/\mu\text{m}$), which reduce stress concentration at fiber tips due to the closer packing of the fibers,
- (ii) the use of longer fibers than conventional ones, these have the effect of reducing the number of fiber tips which act as stress concentrators,
- (iii) the introduction of interfacial layers between the fiber and matrix. If a soft layer such as rubber could be used, the initiation of the interfacial microfailure would be expected to be reduced due to large deformation of the layer. By contrast, the use of a rigid layer with a modulus intermediate between that of the fiber and matrix, is considered to lower the stress concentration along the fiber sides.

2.4 Oxygen and Chlorine as Ageing Accelerators

The polymers age over time in the media they are in contact with. The ageing is accelerated significantly to have predictions within shorter time durations by the addition of oxidizing elements found in the media which are called as accelerators. In this study, mainly chlorine and oxygen are the focused substances since they are well-known with their dominant ageing effects on the material.

2.4.1 Oxygen effect

Oxygen degrades polymers to lower molecular weight (MW) fragments by reacting with polymer free radicals to form peroxy free radicals ($\text{ROO}\cdot$) and hydroperoxides (ROOH). Free radicals have an unshared electron and react in any way they can to restore the atom or molecule to a balanced structure. Often that leads to chain scission. As MW goes down, most polymeric properties suffer. As little as 5-10% reduction in MW may cause failure of the part. Avoiding contact with oxygen and using an antioxidant (AO) as a free radical scavenger are means of preventing degradation (Moalli, 2001).

The destruction mechanism O_2 on polymer structure can be seen in Figure-2.9;

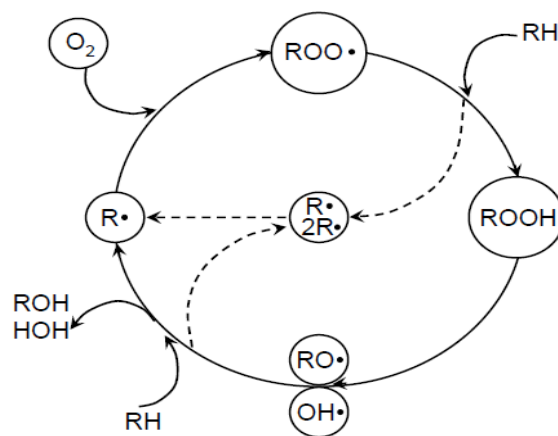


Figure-2.9 O_2 degradation effect on the structure.

The choice of oxygen concentration for polymeric structures was decided with respect to oxygen solubility in water in a temperature range of 0-40 °C that covers the tap water use profile of people and it was seen that 10 ppm is a reasonable value to reflect the average value (Water: Monitoring & Assessment, 2013).

In a previous study conducted (Gates and Grayson, 1998), it is clearly seen that physical properties and glass transition temperatures of polymers tend to change to a noticeable level when compared to the ones that are not exposed to oxygen. So it should be considered as a dominant effective element in the media. In Figure-2.10 below, these effects can be seen.

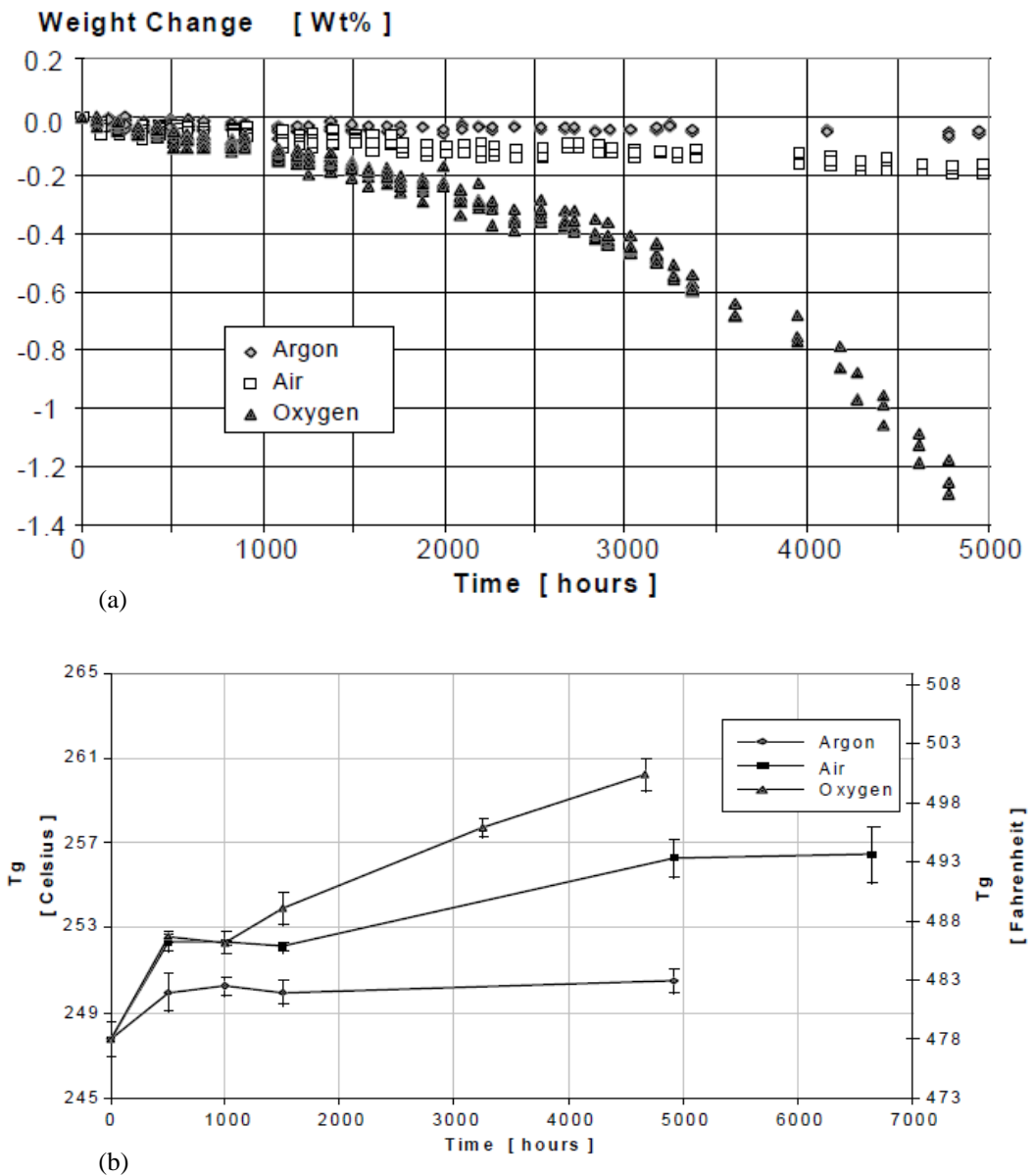


Figure-2.1 Effects of oxygen content (a) on weight and (b) T_g of a graphite/thermoplastic.

Accelerated ageing has been investigated on Nylon 6.6 fibers used in parachutes both in thermal-oxidative and 100% relative humidity conditions (Bernstein et al., 2005). Tensile strength change over time was studied. For the various experiments employed at different temperatures, the tensile strength versus time graphs were obtained and shift factors were calculated in Figure-2.11 below;

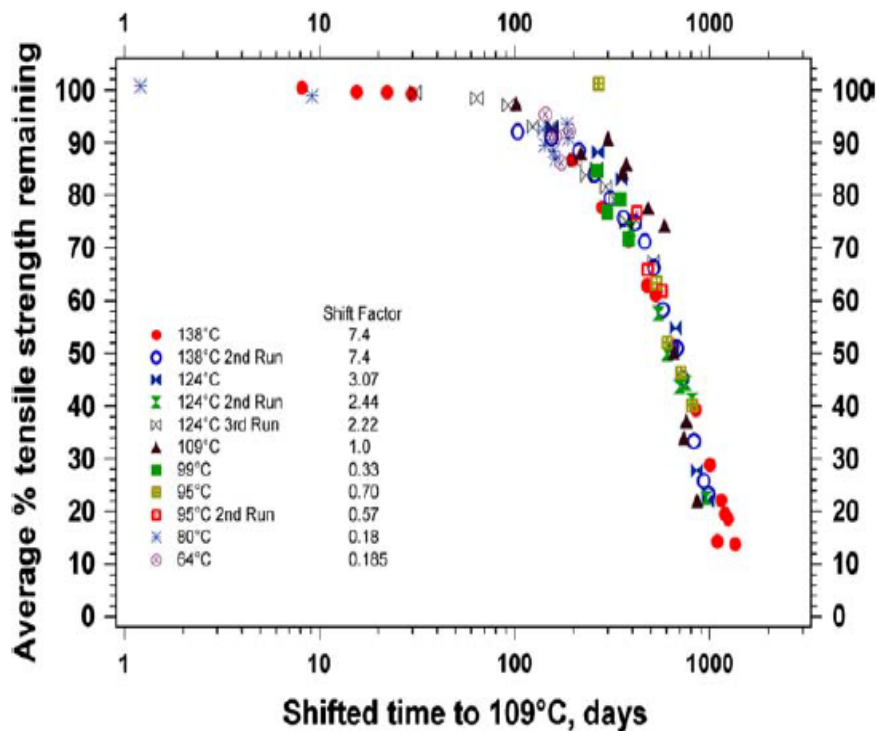


Figure-2.11 Time temperature superposed data for Nylon, percent tensile strength remaining versus shifted time. Data are shifted to 109 °C (reference temperature).

10 ppm dissolved oxygen value in aqueous environment was checked to see if it was achievable to dissolve with defined test conditions over Henry's Law. It was seen with the calculations that at a temperature of 95 °C and a pressure of 6 bar it is far below the maximum achievable dissolution limit. So the system was set up to run with 10 ppm oxygenated aqueous media. The Henry's law can be put into mathematical terms as in Eq. 2.48:

$$p = k_H c \quad 2.48$$

where P is the partial pressure of the solute in the gas above the solution, c is the concentration of the solute and k_H is a constant with the dimensions of pressure divided by concentration. The constant, known as the Henry's law constant, depends on the solute, the solvent and the temperature.

k_H value for oxygen dissolved in water at 298 K is 769.2 L.atm/mol.

As the pressure and temperature values are obtained over Eq. 2.48, it is handy to consult below Table-1 in Appendix-A. Since in fresh water conditions, the water is exposed to very high pressures and also lowered pressures whenever tapping is done by combi-boiler user, 10 ppm O_2 was chosen as average use conditions by the customer side.

2.4.2 Chlorine effect

Chlorine is used in city water supply for disinfection purposes and it transforms to hypochlorous acid in its media. This is a strong oxidizer, which is capable of breaking the carbon-to-carbon bonds of the polymer chain, effectively disintegrating it. The fact that chlorinated water reduces the service life of polyolefin products is well recognized in the United States, where disinfection of the water supply via chlorination is widely used. ASTM F-2023-04 and the NSF P-171 protocol have been utilized to measure the effect of chlorine on these piping systems. For the polyolefins, it was shown that there's a measurable difference with the thickness of virgin and aged samples in circulating water up to 50 % at 7000 hours even with a low water flowrate (~0.1 gpm) (Backman, 2010).

Recently, chlorine effect for 3 types of polymers were studied. ASTM test specimens (both tensile and flex with 1/8-inch wall thicknesses) were placed in chlorinated water baths for six months (Solvay, 2002). Each week bars were removed, weighed, tested for mechanical properties, and measured for thickness. Three different levels of chlorine exposure were used in order to predict reaction rates and temperature was chosen as 60 °C in order to simulate typical residential hot water system. The chlorine level of the baths was maintained by adding chlorine three times per week. The exposure to chlorine affected the physical and mechanical properties of acetal copolymer and 33% glass-filled Nylon 6.6

adversely. The results for 3 materials can be observed in the Figure-2.12 given below.

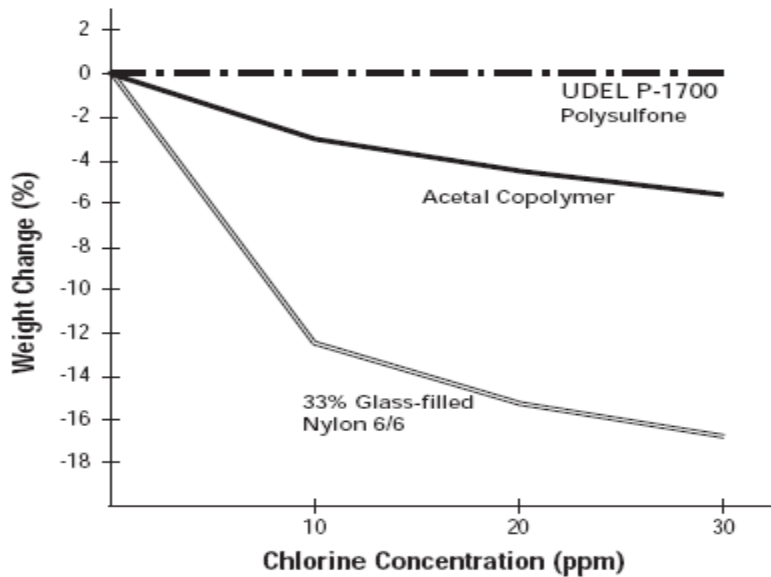


Figure-2.2 Weight change of various polymers after exposure to chlorinated water at 60°C (Solvay, 2002).

The prediction from the results obtained for usual concentration level of 2 ppm chlorine is given in Table-2.6 for all of three materials (Solvay, 2002).

Table-2.7 Projected % weight loss after exposure to 2 ppm chlorinated deionized H₂O at 60°C.

	5 yrs	10 yrs	15 yrs	20 yrs
UDEL P-1700	0	0	0	0
Acetal Copolymer	4.8	9.6	14.3	19.1
33% Glass-Filled Nylon 6/6	42.2	84.4	100	100

As a result of the explained effects above, together with water diffusing through the polymer matrix and its amorphous regions (see Figure-2.13), the media will make the polymer matrix and glass fiber interfaces to separate and cause loss of mechanical properties over time.

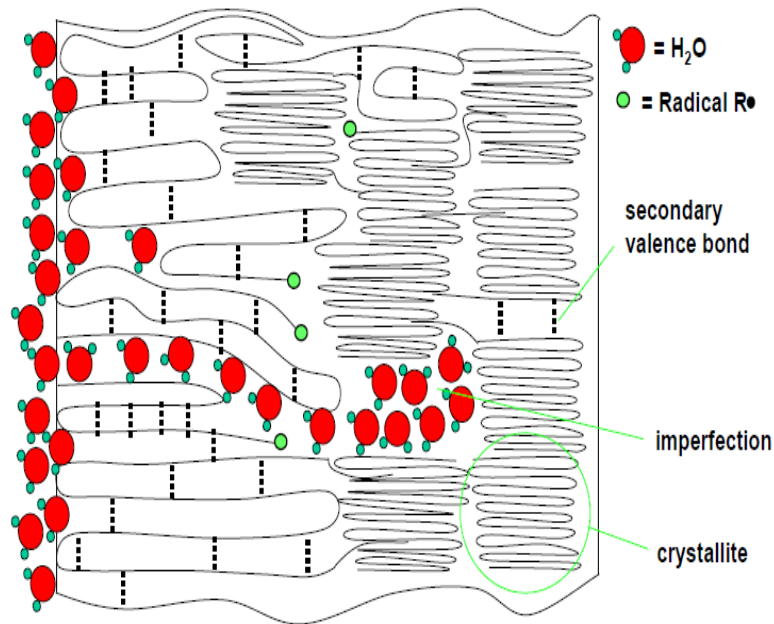


Figure-2.33 Water sorption versus crystallinity degree of polymer.

2.5 Injection Molding and Its Effects on Crystallinity

Molded articles prepared from polyphthalamide compositions exhibit excellent mechanical and thermal properties, including especially high heat deflection temperatures, even when molded using molds heated to temperatures below the glass transition temperature of the polyphthalamide component, often facilitating molding using steam or hot water-heated molds (Brooks, 1990).

Polyphthalamides which, when filled with glass fibers, have heat deflection temperatures at 264 psi, determined according to ASTM D-648, above 240°C. Compositions according a previously published patent are prepared from dicarboxylic acid compounds comprising terephthalic acid and isophthalic acid compounds in a mole ratio of 80:20 to about 99:1 and diamines comprising hexamethylene diamine and trimethylhexamethylene diamine in a mole ratio of about 98:2 to about 60:40 (Poppe et al., 1986).

Attainment of optimum properties in such polyphthalamide molded articles also can be complicated by molding conditions required to develop sufficient crystallinity in the molded polyphthalamides to achieve significant increases in heat deflection temperature and other properties dependent on crystallinity. In

general, the polyphthalamides have glass transition temperatures (T_g) generally ranging up to about 135 °C. However conventional steam or hot water heated molds, which typically can reach temperatures up to about 100 °C, may be inadequate to allow for consistent development of sufficient crystallinity in many of the polyphthalamides to obtain significant property appreciation or may require undesirably long molding cycle times and higher mold temperatures to do so. Of course, higher mold temperatures can be achieved with oil heated molds or annealing of molded articles can be conducted to increase crystallization and to enhance properties dependent thereon; however, both of these alternatives add cost and complexity to a molding operation. Accordingly, it will be appreciated that it would be desirable to modify such polyphthalamides to facilitate consistent attainment of heat deflection temperatures (HDT) and other desirable properties in molding without sacrificing other desirable properties.

Crystallinity of the polyphthalamides and HDT's of glass fiber-filled compositions tend to decrease with greater numbers of substituents per carbon atom and with larger substituent groups.

Table-2.8 HDT of samples under different mold temperatures (Brooks, 1990).

Annealed Properties							
Samples	7	8	9	10	11	C	B
HDT at 1.82 Mpa (264 psi) (°C)							
Mold Temperature							
38 °C	277	280	278	-	-	275	-
66 °C	281	281	282	-	-	278	-
93 °C	281	282	281	278	264	274	232
121 °C	279	285	281	-	-	281	-
Increase in HDT after annealing (°C)							
Mold Temperature							
38 °C	12	10	11	-	-	35	-
66 °C	13	11	15	-	-	35	-
93 °C	13	10	7	3	8	23	9
121 °C	-2	8	4	-	-	12	-

A significant increase was seen in HDT for the control (Example C) sample after annealing bars mold cool in tools set below 100 °C.

The above HDT results indicate the need to mold cool polyphthalamide at temperatures above the boiling point of water to achieve desirable thermal properties without the costly expense of annealing. The results also demonstrate the ability to mold polyphthalamide in tools set below the boiling point of water if small quantities of a thermotropic liquid crystalline polymers (TLCP) are added as a nucleator, without the added expense of annealing to achieve desirable HDT values.

Table-2.9 Crystallization temperature change with different cooling rates.

Cooling Rate (°C/min)	T _c (°C)	Cooling Rate (°C/min)	T _c (°C)
80	215	5	253
40	232	2.5	258
20	243	1.25	261
10	252	-	-

In Table-2.9, the data that illustrates the effect of cooling rate on the crystallization temperature (T_c) of the polyphthalamide.

Note that in the injection molding process, the cooling rate at the skin of the part is significant faster than 80 °C/min resulting in a quenched skin. The core cools at a much slower rate resulting in a cooling rate gradient between skin and core. As shown in Table-2.9, the slower the cooling rate, the higher the temperature at which crystallization begins resulting in a higher level of crystallinity, all else similar.

3. EXPERIMENTAL


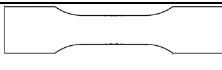
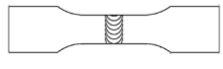
3.1 Materials

Polyphthalamide with the brand name “Grivory HT1V-4 FWA Black 9225” is a type of a 40% glass fiber reinforced engineering thermoplastic material from EMS Grivory company. It is a semi-crystalline, partially aromatic copolyamide polymer that has stiffer, stronger structure when compared to other type of polyamides. It has also better heat distortion stability and chemical resistance when compared to other polyamides. “Introduction” section contains more detailed properties. For comparison of mechanical properties, glass fiber reinforced PA 66 and PP tensile and impact specimens were also used.

There are 3 types of samples used in the study and the ageing effects on samples were observed with different types of experiments as seen in Table-3.1. While some set of tests were employed on standard specimens as tensile bars with and without weldline, other group of experiments were conducted on real parts which are referred to as hydraulic parts. The tensile specimens were produced by injection moulding with below parameters:

Flange 80 - 100°C	Zone-1 330 - 340°C	Zone-2 330 - 345°C	Zone-3 330 - 345°C	Nozzle 330 - 340°C	Melt 340°C
-----------------------------	------------------------------	------------------------------	------------------------------	------------------------------	----------------------

Table-3.1 Test specimens and conducted tests.

Sample Shapes	Types	TESTS				
		DSC	SEM	FT-IR	MECHANICAL TESTS	TGA
	HP	X	X	X	X	X
	TTS wow				X	
	TTS ww				X	

HP: Hydraulic part, TTS wow: Tensile test specimen without weld-line, TTS ww: Tensile test specimen with weld-line

3.2 Methods

3.2.1 Tests with hydraulic parts

Central Heating side parts of the PPA GF40 HP samples were aged under 2.5 bar and 95°C water media without oxygen. The domestic side parts of the PPA GF40 samples were aged under 6 bar and 95 °C water media with 10 ppm oxygen. Figure-3.1 shows the test set-up used for ageing of samples.

Table-3.2 shows a dataset for 4 mm standard test specimens and calculation methodology based on Arrhenius approach explained in Section 2.2.7. The bold font written cells give out the average activation energies at given ageing percentages. However, with tests done on real parts via same Arrhenius approach, the effective activation energy value was given as 46000 J/mol from the supplier. The time necessary to age the material within user temperature conditions which is equivalent to 15 years lifetime was defined as 24000 hours over this given activation energy (E_a) value.



Figure-3.1 Test set-up for ageing of PPA GF40 samples.

Table-3.2 Dataset for halflife time of PPA GF40.

Remaining % for burst strength	Data Point	T (°C)	T (K)	1/T (K)	1000/T (K)	$t_{1/2}$ (hr)	a_T	$\ln(a_T)$	E_a (J/mol)
50%	1	140	413	0.002421	2.4213	80	37.5	3.62434	101771
	2	125	398	0.002513	2.5126	270	11.11	2.40795	97739
	3	110	383	0.002611	2.6110	880	3.41	1.22645	95811
	4	95	368	0.002717	2.7174	3000	1	Average	98440
70%	1	140	413	0.002421	2.4213	50	40	3.68888	103583
	2	125	398	0.002513	2.5126	160	12.5	2.52573	102519
	3	110	383	0.002611	2.6110	550	3.64	1.29098	100852
	4	95	368	0.002717	2.7174	2000	1	Average	102318
90%	1	140	413	0.002421	2.4213	20	55	4.00733	112525
	2	125	398	0.002513	2.5126	70	15.71	2.75457	111808
	3	110	383	0.002611	2.6109	300	3.67	1.29928	101501
	4	95	368	0.002717	2.7174	1100	1	Average	108611

a_t : acceleration factor, T: temperature, $t_{1/2}$: halflife time, E_a : activation energy

The specimens for tests from HP samples were prepared by cutting thin slices from same point of the plastics by Micracut 176 precision cutting device as given in Figure-3.2.

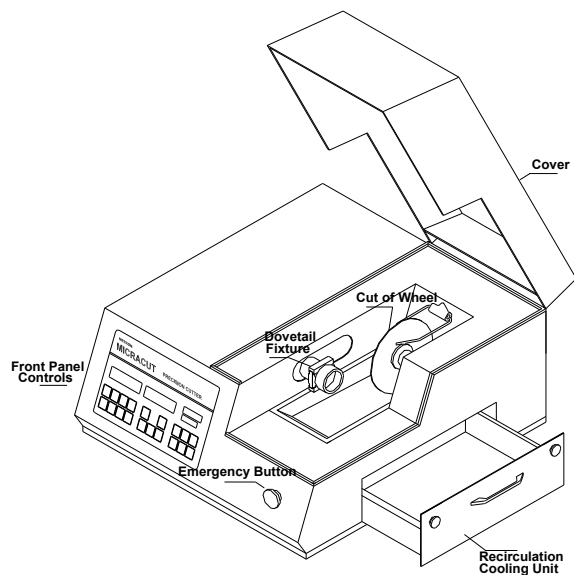


Figure-3.2 Micracut precision cutting device.

3.2.1.1 DSC analysis

Differential scanning calorimetry (DSC) is a thermoanalytical technique in which heat flow is measured as a function of temperature and/or time. The obtained measurements provide quantitative and qualitative information regarding physical and chemical changes involving exothermic and endothermic processes, or changes in the heat capacity in the sample material (Jansen, 2001). The technique is used to evaluate thermal transitions within a material. Such transitions include melting, evaporation, crystallization, solidification, cross linking, chemical reactions, and decomposition.

The heat of fusion represents the energy required to melt the material and is calculated as the area under the melting endotherm. The level of crystallinity is determined by comparing the actual as-molded heat of fusion with that of a 100% crystalline sample. The level of crystallinity that a material has reached during the molding process can be practically assessed by comparing the heat of fusion obtained during an initial analysis of the sample with the results generated during the second run, after slow cooling. The level of crystallinity is important, because it impacts the mechanical, physical, and chemical resistance properties of the molded article. In general, rapid or quench cooling results in a lower crystalline state. This is the result of the formation of frozen amorphous regions within the preferentially crystalline structure.

Recrystallization, or the solidification of the polymer, is represented by the corresponding exothermic transition as the sample cools. The recrystallization temperature (T_c) is taken as the peak of the exotherm, and the heat of recrystallization is the area under the exotherm. Some slow-crystallizing materials, such as poly-(ethylene terephthalate) and polyphthalamide, undergo low-temperature crystallization, representing the spontaneous rearrangement of amorphous segments within the polymer structure into a more orderly crystalline structure. Such exothermic transitions indicate that the as-molded material had been cooled relatively rapidly. Figure-3.3 shows a low temperature crystallization exothermic peak from a DSC experiment.

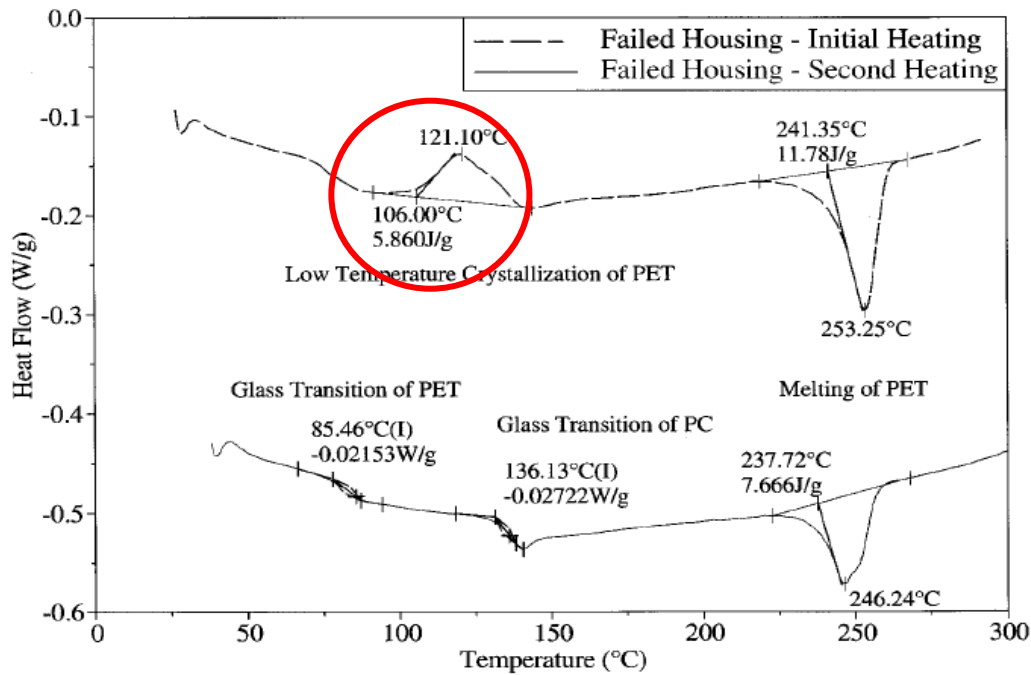


Figure-3.3 DSC thermogram, exhibiting a melting transition consistent with a PET resin (Jansen, 2001).

The tests for 0, 1700, 2500, 6061, 7400 hour samples of both CH and DHW side parts were investigated via DSC experiments for nonisothermal crystallization kinetics. Steps of DSC experiment can be defined as;

- 1) Starting from room temperature, go up to 400 °C with a heating rate of 10 °C/min.
- 2) Remain isothermal at 400 °C for 5 minutes.
- 3) Cool down with a cooling rate (CR) of 5, 10 and 20 °C/min for 3 different sets of experiments.
- 4) Repeat steps 1-3 once more.

The tests were carried out with TA Instruments brand, Q20 model DSC instrument. The method conducted for these set of experiments can be seen in Figure-3.4.

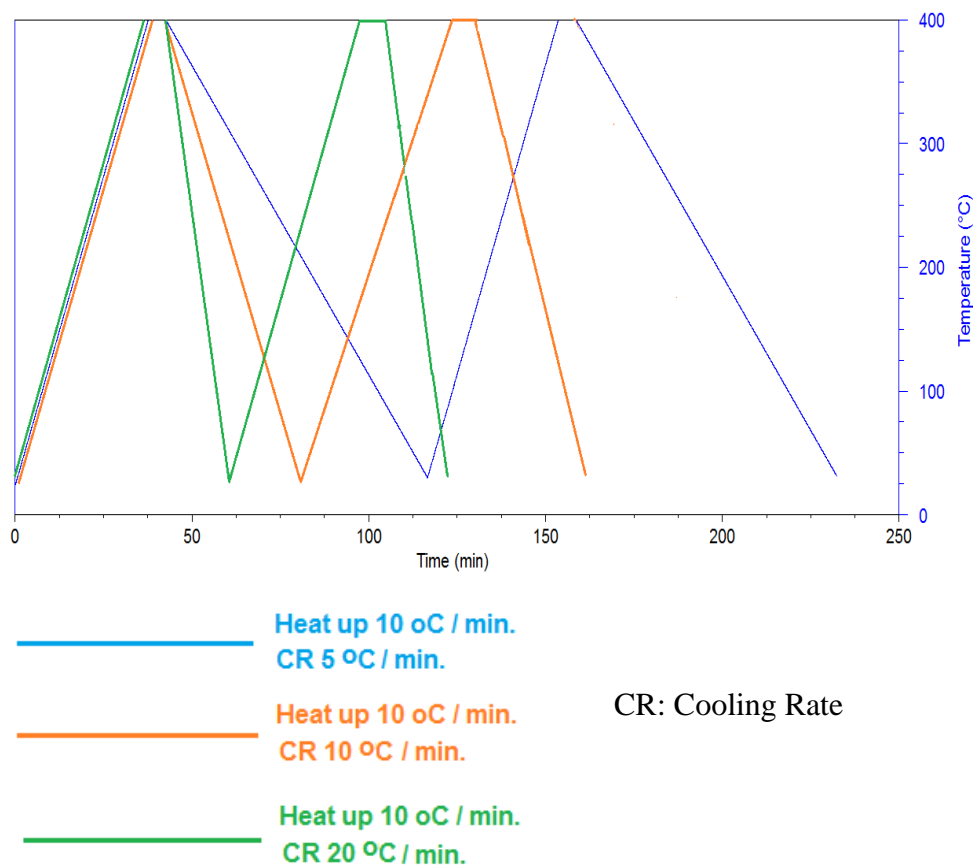


Figure-3.4 DSC analysis for nonisothermal testing methodology.

3.2.1.2 TGA analysis

Thermogravimetric analysis (TGA) is a thermal analysis technique that measures the amount and rate of change in the weight of a material as a function of temperature or time in a controlled atmosphere. The weight of the evaluated material can decrease due to volatilization or decomposition or increase because of gas absorption or chemical reaction. Thermogravimetric analysis can provide valuable information regarding the composition and thermal stability of polymeric materials. The obtained data can include the volatiles content, inorganic filler content, carbon black content, the onset of thermal decomposition, and the volatility of additives such as antioxidants (Scheirs, 2000).

Thermogravimetric analysis instruments consist of two primary components: a microbalance and a furnace. The sample is suspended from the

balance while heated in conjunction with a thermal program. A ceramic or, more often, a platinum sample boat is used for the evaluation. For TGA tests, the sample is usually heated from ambient room temperature to 1000 °C in a dynamic gas purge of nitrogen.

The results obtained as part of TGA evaluation are known as a thermogram. The TGA thermogram illustrates the sample weight, usually in percent of original weight, on the y-axis as a function of time or, more commonly, temperature on the x-axis. The weight-change transitions are often highlighted by plotting the corresponding derivative on an alternate y-axis.

Thermogravimetric analysis is a key analytical technique used in the assessment of the composition of polymeric-based materials. The quantitative results obtained during a TGA evaluation directly complement the qualitative information produced by FTIR analysis. The relative loadings of various constituents within a plastic material, including polymers, plasticizers, additives, carbon black, mineral fillers, and glass reinforcement, can be assessed. Noncombustible material remaining at the conclusion of the TGA evaluation is often associated with inorganic fillers. The assessment of a plastic resin composition is illustrated in Figure-3.5.

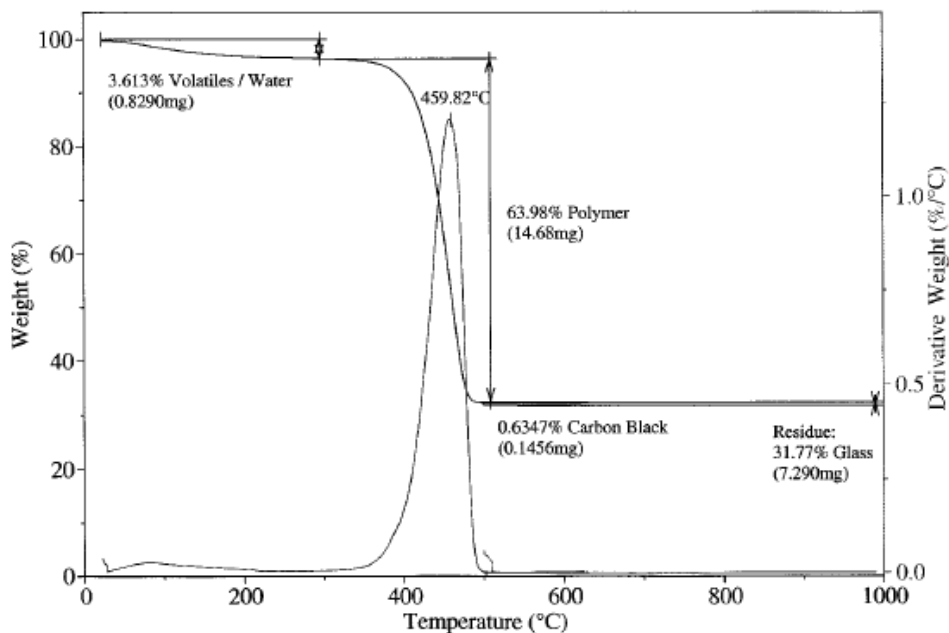


Figure-3.5 TGA thermogram showing the weight-loss for a typical plastic resin (Scheirs, 2000).

Experiments were conducted under nitrogen atmosphere with a flow rate of 50 mL/min for a temperature range between 30 °C and 750 °C with 20 °C/min. heating rates. The instrument used for experiments is Perkin Elmer Diamond TG/DTA.

3.2.1.3 FTIR analysis

Fourier transform infrared spectroscopy (FTIR) is a nondestructive microanalytical spectroscopic technique that involves the study of molecular vibrations (Jansen, 2001). The analysis results provide principally qualitative, but also limited quantitative, information regarding the composition and state of the material evaluated. Fourier transform infrared spectroscopy uses infrared energy to produce vibrations within the molecular bonds that constitute the material evaluated. Vibrational states of varying energy levels exist in molecules. Transition from one vibrational state to another is related to absorption or emission of electromagnetic radiation (Jansen, 2001). These vibrations occur at characteristic frequencies, revealing the structure of the sample. FTIR produces a unique spectrum, which is comparable to the fingerprint of the material. It is the principle analytical technique used to qualitatively identify polymeric materials.

Several different sampling techniques, all involving either transmission or reflection of the infrared energy, can be used to analyze the sample material. This allows the evaluation of materials in all forms, including hard solids, powders, liquids, and gases. Depending on the spectrometer and the corresponding accessories, most samples can be analyzed without significant preparation or alteration. In the analysis of polymeric materials, transmittance, reflectance, and attenuated total reflectance (ATR) are the most common sampling techniques.

Regardless of the sampling technique, the beam of infrared energy is passed through or reflected from the sample and directed to a detector. The obtained spectrum shows those frequencies that the material has absorbed and those that have been transmitted, as illustrated in Figure-3.6. The spectrum can be interpreted manually, or more commonly, compared with voluminous library references with the aid of a computer.

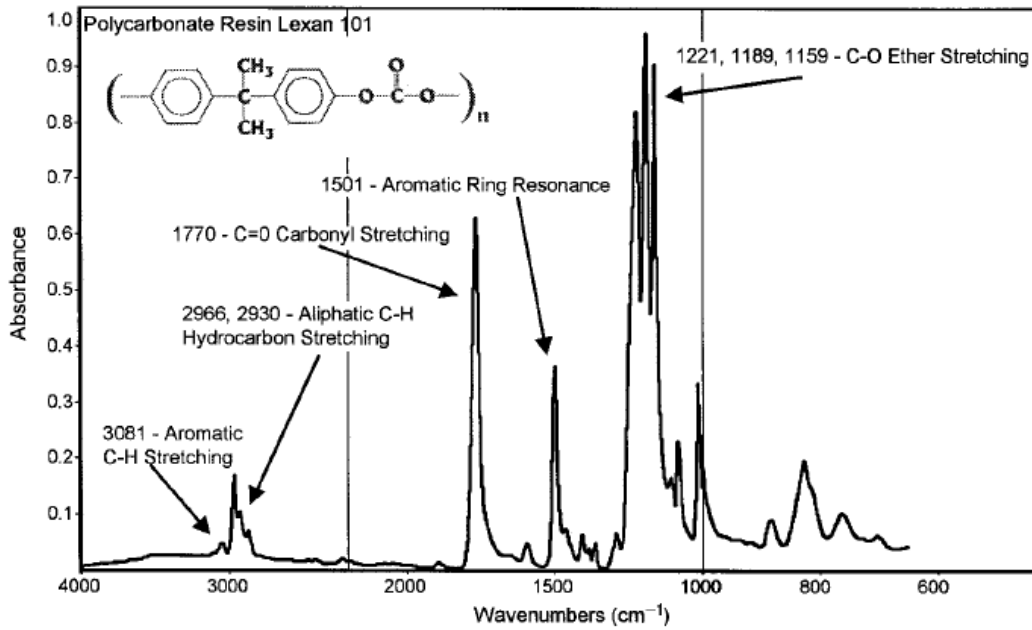


Figure-3.6 FTIR spectrum showing correlation between structure and absorption bands (Jansen, 2001).

Spectra had been obtained over ATR technique with the HP samples. The instrument used for studies was Thermo Nicolet 550 Series FTIR.

3.2.1.4 SEM analysis

A scanning electron microscope (SEM) is a type of electron microscope that produces images of a sample by scanning it with a focused beam of electrons. The electrons interact with atoms in the sample, producing various signals that can be detected and that contain information about the sample's surface topography and composition when integrated with energy dispersive spectroscopy (EDS). It generates and accelerates electrons to an energy range 0.1-30 keV. There are different types of electron emitters and electron lenses. Basic components of a SEM microscope can be seen in Figure-3.7 (Radetic, 2011).

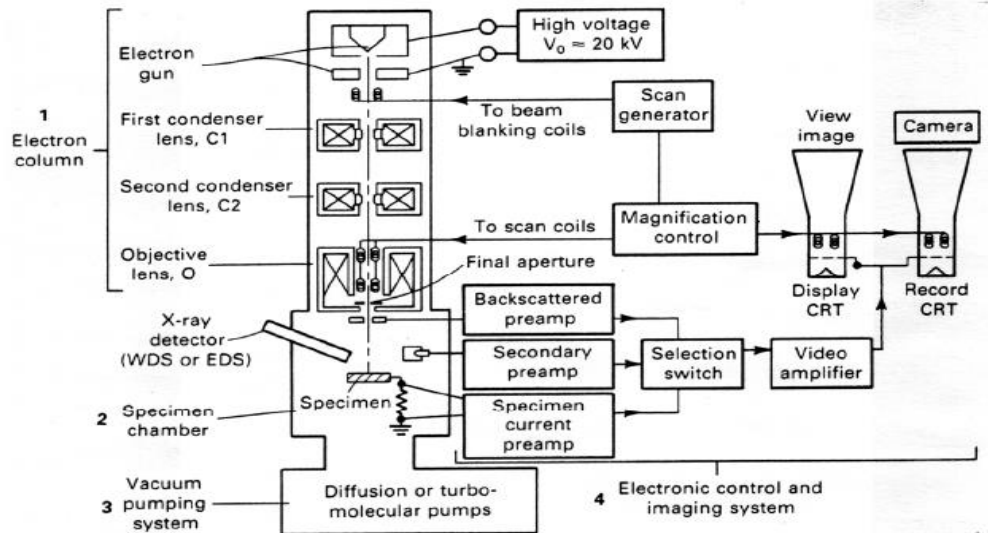


Figure-3.7 Basic components of a SEM microscope.

Some important definitions regarding microscope system can be listed as:

Filament heating current: It is the current used to resistively heat a thermionic filament to the temperature at which it emits electrons.

Emission current: It is the flow of electrons emitted by the filament.

Beam current: It is the portion of the electron current that goes through the hole in the anode.

Electron Column: It consists of an electron gun and two or more electron lenses, operating in a vacuum.

Electron Gun: It produces a source of electrons and accelerates these electrons to an energy in the range of 1-40 keV. The beam diameter produced directly by the conventional electron gun is too large to generate a sharp image at high magnification.

Electron Lenses: They are used to reduce the diameter of this source of electrons and place a small, focused electron beam on the specimen. Most SEMs can generate an electron beam at the specimen surface with a spot size of less than 10 nm while still carrying sufficient current to form an acceptable image.

Working Distance (WD): The distance between the lower surface of the objective lens and the surface of the specimen is called the working distance.

Depth-of-Focus: The capability of focusing features at different depths within the same image.

Secondary Electron: They are electrons of the specimen ejected during inelastic scattering of the energetic beam electrons. Secondary electrons are defined purely on the basis of their kinetic energy; that is, all electrons emitted from the specimen with an energy less than 50 eV.

The inspection studies on HP samples were done with Philips brand XL-30S FEG model microscope.

3.2.1.5 Relative viscosity

The relative viscosity is basically a measure of the size or extension in space of polymer molecules. It is empirically related to molecular weight for linear polymers. Since the measurement and usefulness of viscosity-molecular weight correlation are so great, it constitutes a very valuable tool for characterization of polymers (Billmeyer, 1962).

The relative viscosities were measured by Schott brand AVS PRO II viscosimeter with dissolution of polymer in m-cresol via capillary method. The measurement was performed according to ISO 307.

3.2.1.6 Burst strength

The burst strength of a part is the maximum pressure that it can withstand without giving any leakage. So it gives an idea about the material's maximum limits for strength.

Burst strength tests on samples were employed as per internal standards of Bosch company.

The pieces were filled with water under a certain pressure for 30 seconds and after, the pressure was increased by a rate of 1 bar/min until the part gives leakage. The time at which the part bursted and leakage started, this pressure was recorded for sample as burst strength value. At least 3 samples used for averaging of test results.

3.2.2 Tests with tensile test specimens (TTS)

Standard tensile test specimens were used to investigate the mechanical property changes as tensile properties and impact properties over time. Specimens both with and without weld-line were looked through to see weld-line effect on strength of the material. Five samples were used for each data point to obtain average value. Tensile tests (ASTM D 638 and ISO 527) were conducted by Zwick Z100 machine. Charpy impact tests (ASTM D 256 and ISO 179) were employed on samples by Instron Ceast 7100 machine.

Tests with tensile bars have been employed and they clearly show that weld-lines create critical weakening effect on strength of the material.

The first set of experiments was conducted at a very high concentration of chlorine as 1000 ppm and at a temperature of 95 °C.

Another set of experiments was conducted at temperatures of 60, 90 and 120 °C to see the strength retention and obtain comparison data for TTS ww and TTS wow. Figure-3.8 shows sample shapes and test set-up.



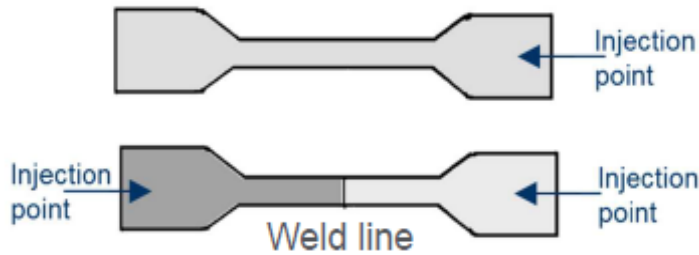


Figure-3.8 Test set-up and TTS samples.

Medium:

Aqueous solution of sodium dichloroisocyanurate (which is a N-chloramine compound and carrier substance for hypochlorite OCl^- , or “free chlorine”) with a concentration of OCl^- as 1000 ppm was used. pH value was kept at neutral value 7 by refreshment water weekly.

Test specimens:

ISO-tensile bars as $60 \times 10 \times 3 \text{ mm}^3$, DIN- tensile impact bars as $80 \times 15 \times 1 \text{ mm}^3$ and ISO-Charpy-impact tensile bars as $80 \times 10 \times 4 \text{ mm}^3$ were prepared.

Test procedure:

The test bars were immersed in 500 mL bottles at 95°C and the mechanical properties were measured after 5000 h (tensile strength, impact strength) in comparison to conditioned (acc. to ISO 1110, 70°C , 62% R.H.) original values and comparison of absolute values.

3.2.2.1 Tensile properties

The short-term tensile test is one of the most widely used mechanical tests of plastics for determining mechanical properties such as tensile strength, yield strength, yield point, and elongation. The stress-strain curve from tension testing is also a convenient way to classify plastics. While a hard and brittle material such as general-purpose phenolic is characterized by high modulus and low elongation, a hard and tough material is characterized by high modulus, high yield stress, high elongation at break, and high ultimate strength.

The chemical composition and the long-chain nature of polymers lead to some important differences with metals. These differences include significantly lower stiffnesses, much higher elastic limits or recoverable strains, a wider range of Poisson's ratios and time-dependent deformation from viscoelasticity.

At the yield point, the average axis of molecular orientation in thermoplastics may begin to conform increasingly with the direction of the stress. The term draw is sometimes used to describe this behavior. There is usually a break in the stress-strain curve as it begins to flatten out, and more strain is observed with a given increased stress. The result is that the giant molecules begin to align and team up in their resistance to the implied stress. Frequently, there is a final increase in the slope of the curve just before ultimate failure as given in Figure-3.9. Even the smallest amount of the teaming-up effect imparts greatly improved impact resistance and damage tolerance. In thermoplastics, there is much more area under the stress-strain curve than in conventional thermosets, which are more rigid networks with much less area under the stress-strain curve.

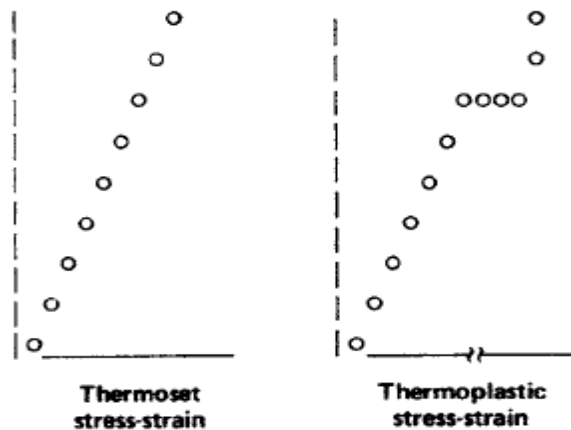


Figure-3.9 Thermoset versus thermoplastic stress-strain behavior.

Yield stresses of plastics depend on a variety of molecular mechanisms, which vary among polymer classes and may not be strictly comparable. However, regardless of the underlying mechanisms, yield stress data have a low coefficient of variation, typically 0.03. Brittle fracture strengths are much more variable, reflecting the distributions of defects that one might expect.

3.2.2.2 Impact strength

The Charpy geometry consists of a simply supported beam with a centrally applied load on the reverse side of the beam from the notches given in Figure-3.10. The notch serves to create a stress concentration and to produce a constrained multiaxial state of tension in a small distance below the bottom of the notch. The load is applied dynamically by a free-falling pendulum of known initial potential energy. The important dimensions of interest for these tests include the notch angle, the notch depth, the notch tip radius, the depth of the beam, and the width of the beam.

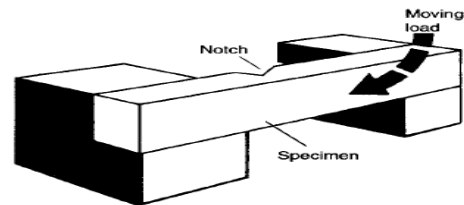


Figure-3.10 Charpy test specimen types and test configuration.

4. RESULTS AND DISCUSSION

All test results obtained for HP, TTS ww and TTS wow are given in this section.

4.1 DSC Analysis of HP Samples

DSC analyses were performed to investigate the crystallization kinetics, degree of crystallinity and melting point of HP PPA GF40 samples. Nonisothermal crystallization kinetics were conducted since during the extrusion process for manufacturing parts, cooling rates were effective on crystallinity of the samples and the intention was also to understand this effect.

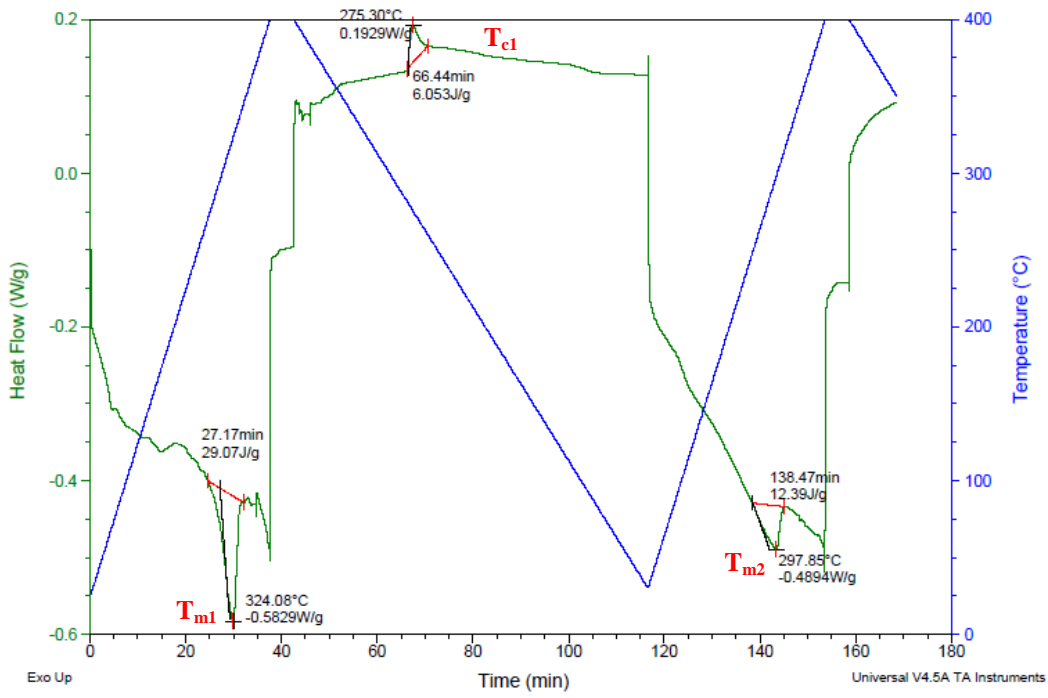
The results obtained for the first and second melting temperatures and nonisothermal crystallization kinetics parameters are given in this section.

4.1.1 Melting point measurements of HP PPA GF40 samples

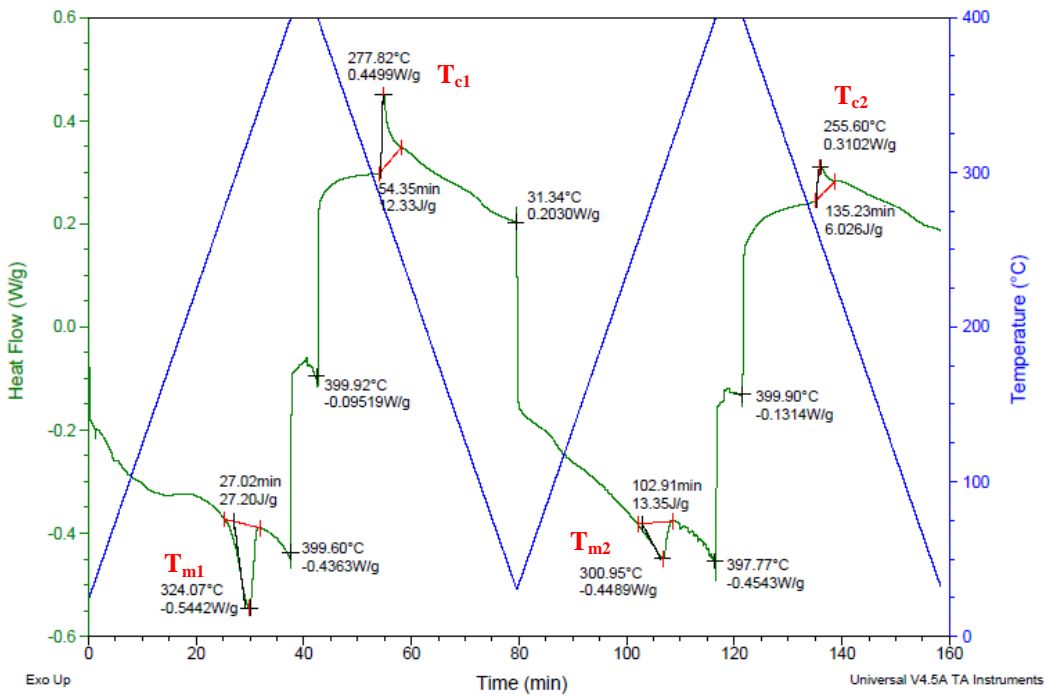
Nonisothermal experimental results with cooling rates of 5, 10 and 20 °C/min are shown with DSC thermograms in Figure 4.1. DSC thermograms of all HP sample experiments can be found in Appendix B, Figure B1. Melting points of the composite films are obtained from the minimum points of the first and second endotherms in the thermograms which are shown as T_{m1} and T_{m2} . Crystallization points obtained from the maximum peak points of the first and second exotherms are shown on the thermograms as T_{c1} and T_{c2} .

The melting temperature, T_m is mainly related to the degree of hydrogen bonding between the chains, which depends on the density of the amide groups (Garbassi and Po, 2003). So the radical changes in T_m gives also an idea about the change in molecular structure.

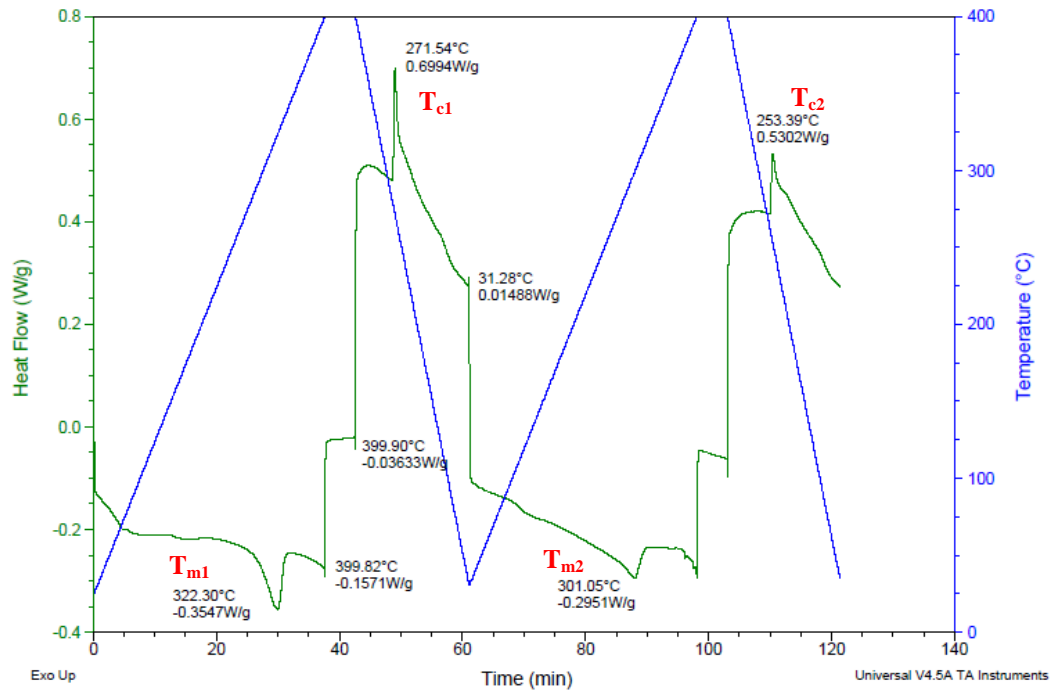
While some of the experiments with samples conducted with twice coolings over time, some were just conducted with once cooling. The idea was also to see the second cooling effect on some representative samples.



(a)



(b)



(c)

Figure-4.1 Thermograms of PPA GF40 HP samples, a) 0-hr. CH with a cooling rate of 5 °C/min, b) 0-hr. CH with a cooling rate of 10 °C/min, c) 0-hr. CH with a cooling rate of 20 °C/min.

Melting and crystallization temperatures of samples for the nonisothermal crystallization are given in Tables-4.1 and 4.2. The table clearly shows that, after first disappearing of crystals during melting, the structure of the crystals in the matrix loses their integrity. This is observed by drop in melting temperature and also crystallization degree during second melting during rearrangement of crystals.

Table-4.1 T_m values of HP PPA GF40 samples obtained from nonisothermal DSC thermograms.

SAMPLE NAMES	COOLING RATES					
	5 °C/min		10 °C/min		20 °C/min	
	T_{m1}	T_{m2}	T_{m1}	T_{m2}	T_{m1}	T_{m2}
0-hr CH	324	298	324	301	322	300
1700-hr CH	321	288	321	295	325	298
2500-hr CH	325	296	323	299	324	300
6061-hr CH	328	300	325	302	325	304
7400-hr CH	320	296	323	302	322	301
0-hr DHW	324	292	312	NA	325	NA
1700-hr DHW	323	290	320	NA	323	NA
2500-hr DHW	325	289	323	NA	326	301
6061-hr DHW	323	293	323	298	325	302
7400-hr DHW	326	294	326	296	327	300

 T_{m1} : 1st melting temperature T_{m2} : 2nd melting temperatureTable-4.2 T_c values of HP PPA GF40 samples obtained from nonisothermal DSC thermograms.

SAMPLE NAMES	COOLING RATES					
	5 °C/min		5 °C/min		5 °C/min	
	T_{c1}	T_{c2}	T_{c1}	T_{c2}	T_{c1}	T_{c2}
0-hr CH	275	NA	278	256	272	251
1700-hr CH	270	241	275	253	270	253
2500-hr CH	275	252	274	253	270	249
6061-hr CH	279	258	276	256	275	254
7400-hr CH	275	249	277	255	271	249
0-hr DHW	274	251	276	NA	270	NA
1700-hr DHW	268	237	268	NA	270	NA
2500-hr DHW	265	233	270	NA	270	248
6061-hr DHW	270	238	275	253	274	251
7400-hr DHW	274	251	269	244	270	252

 T_{c1} : 1st crystallization temperature T_{c2} : 2nd crystallization temperature

T_{m2} values of tested samples change considerably after cooling down and melting again as can be seen in Figure-4.2. The magnitude of T_{m1} and T_{m2}

changes for different cooling rates generally lies between 20-35 and these can be seen in Figure-4.3. T_m changes for DHW samples were higher. This can be attributed to more aggressive media for DHW samples under the additional effect of oxygen in the hot water. $(T_{c1} - T_{c2})$ values also show a reduction as CR increases. However, there is no significant difference with respect to ageing durations.

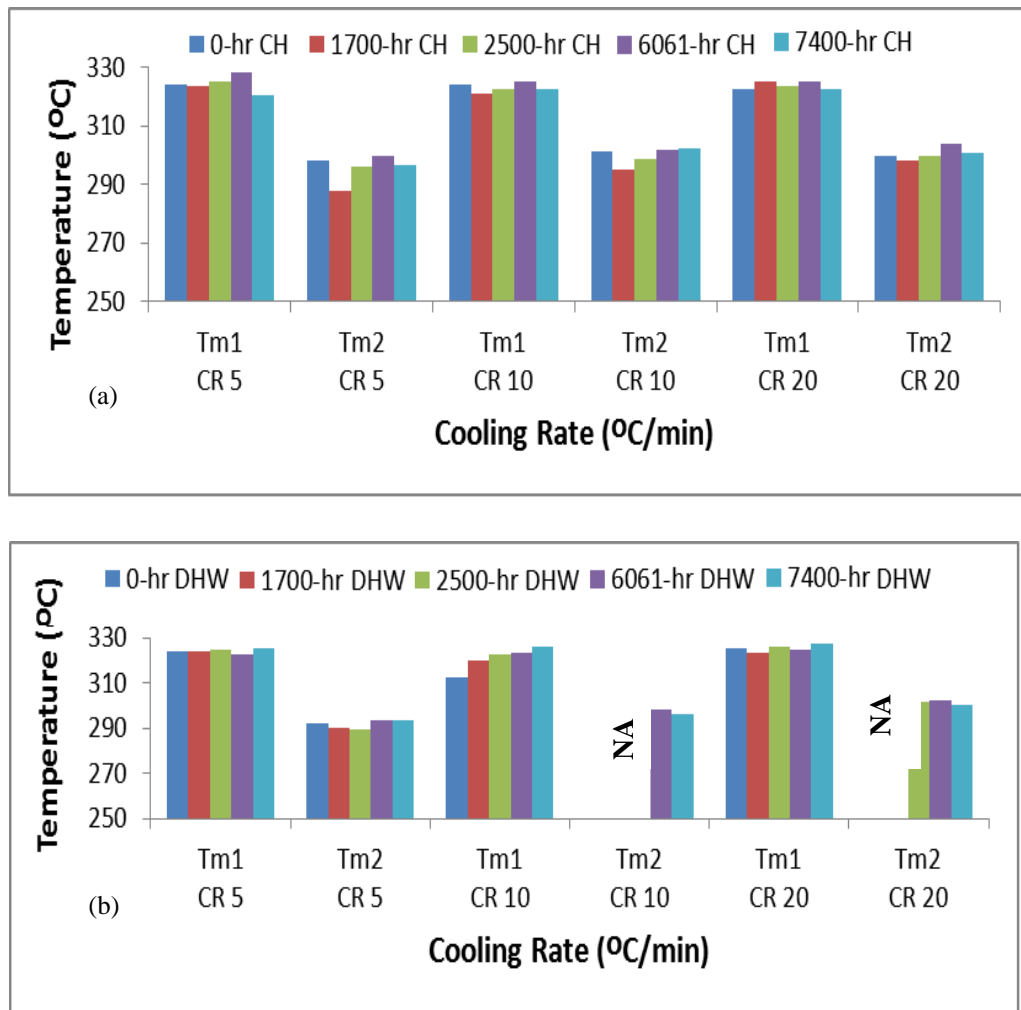


Figure-4.2 T_{m1} and T_{m2} values for HP samples at various cooling rates (a) CH, (b) DHW.

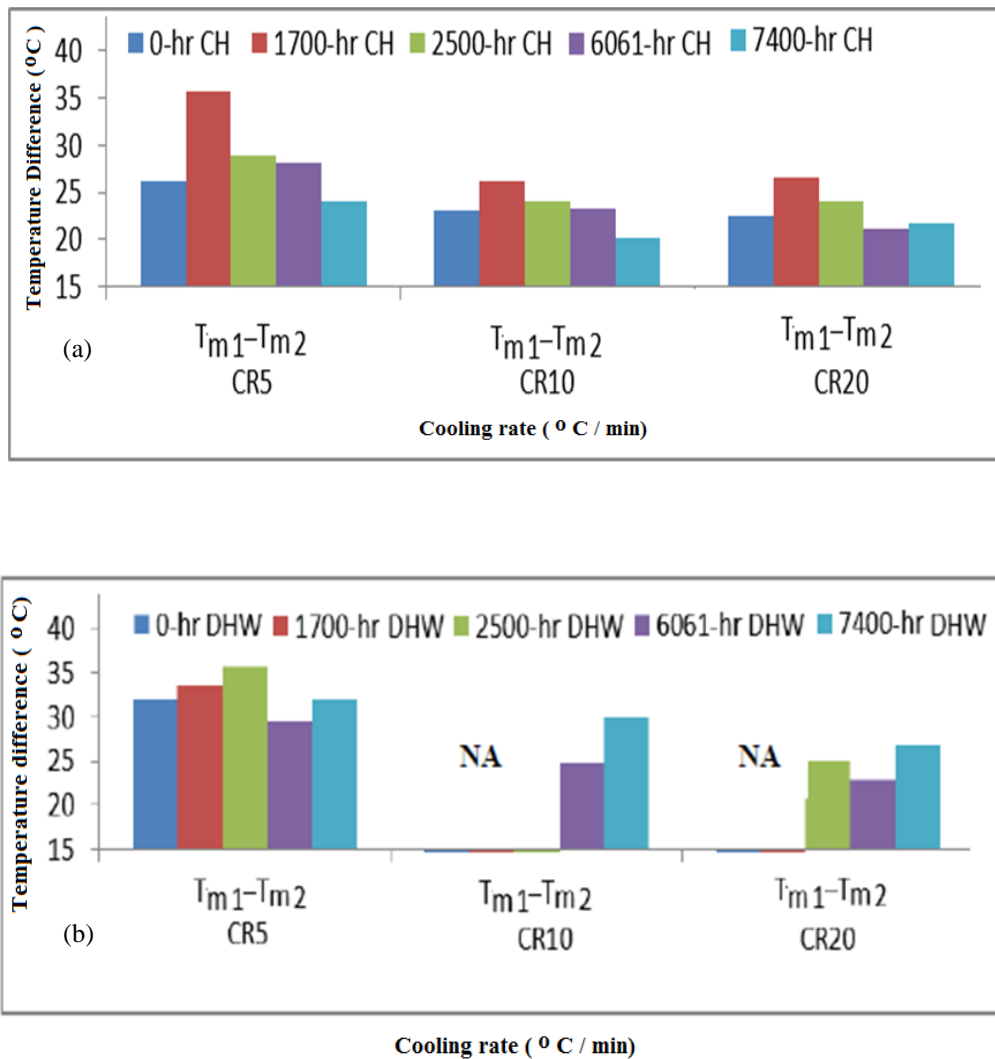


Figure-4.3 $T_{m1} - T_{m2}$ value changes for HP samples at various cooling rates (a) CH, (b) DHW.

For 1700-hr CH sample under cooling rate of 5 °C exhibited a high temperature difference between T_{m1} and T_{m2} . This might be attributed to more damage in crystalline structure.

1700-hr DHW sample was analyzed twice because at first attempt the result was 54 °C for ($T_{m1} - T_{m2}$) difference. This same sample shows a remarkable difference over DSC thermogram curve with having two distinct separate melting peaks as given in Figure-4.4. These peaks show depolymerization in the structure.

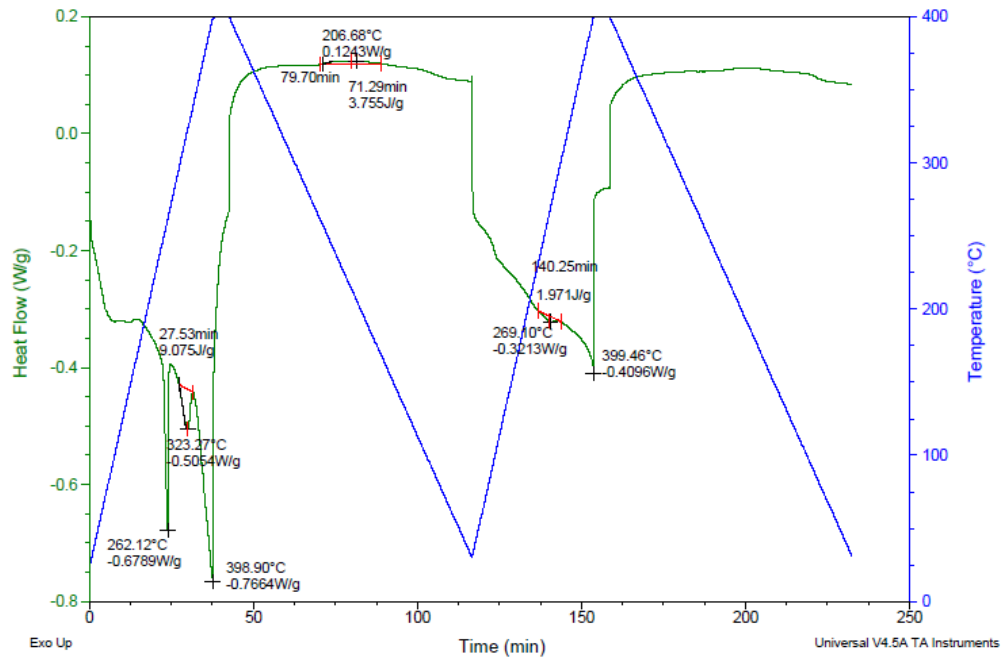
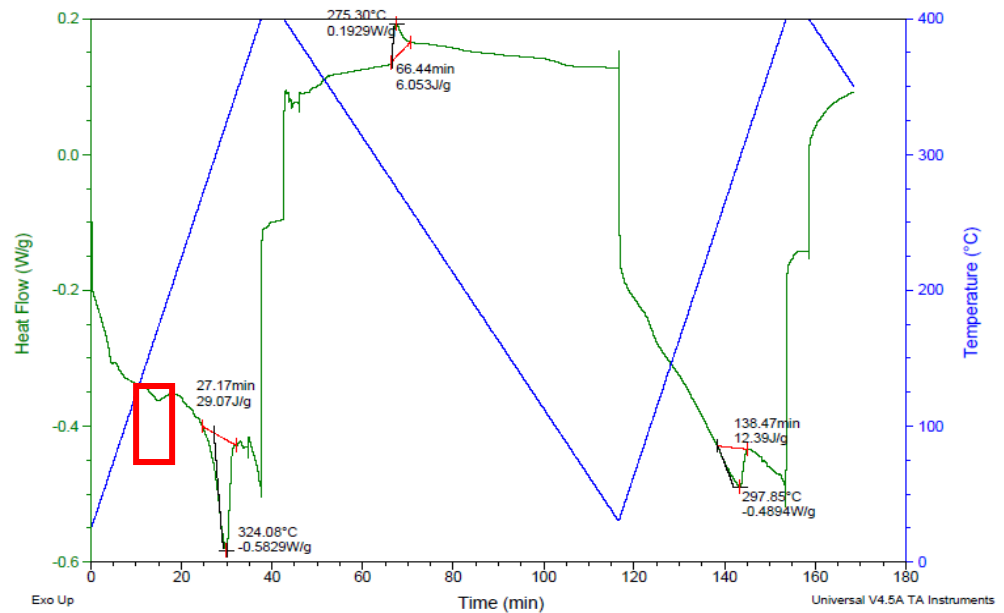
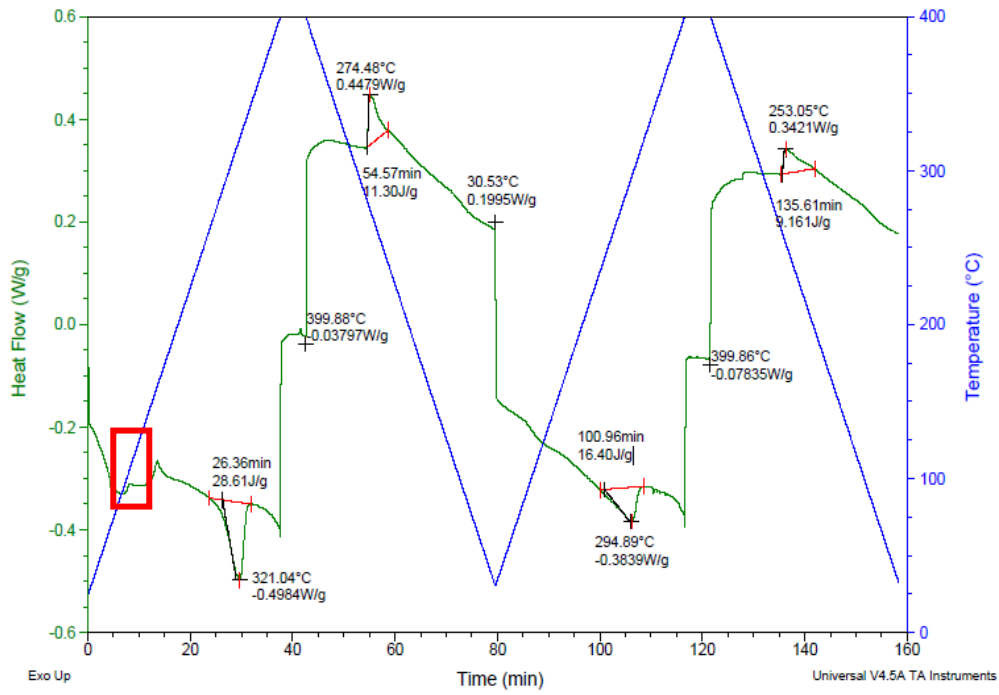


Figure-4.4 1700-hr. DHW with a cooling rate of 5 °C/min.

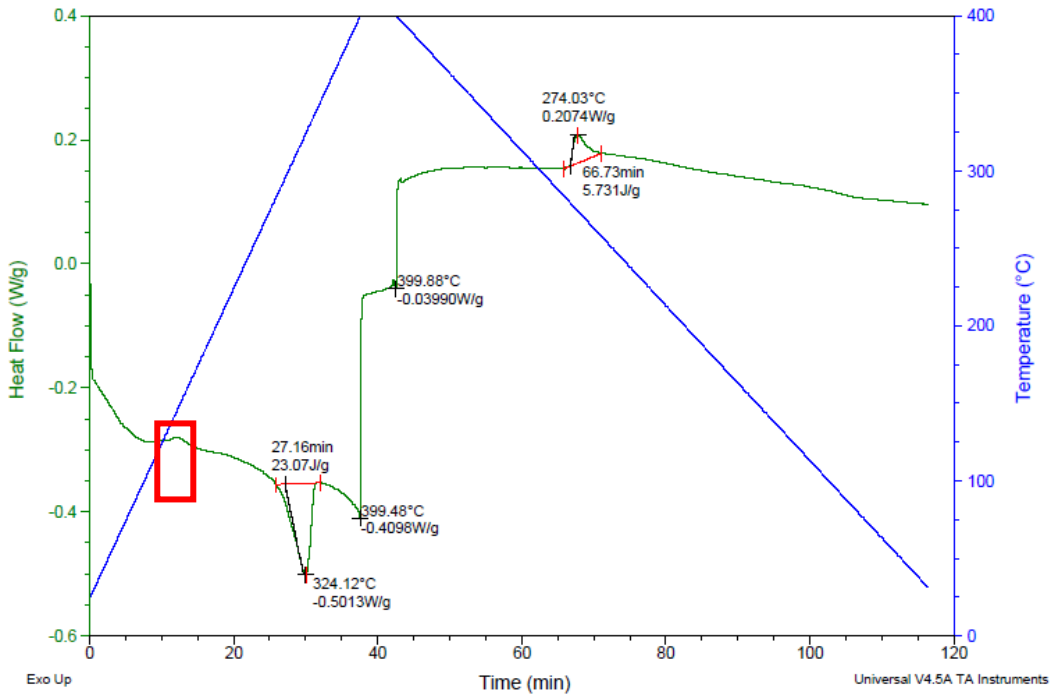
Polyphthalamide as being a slow-crystallizing material may undergo low-temperature crystallization, representing the spontaneous rearrangement of amorphous segments within the polymer structure into a more orderly crystalline structure. Such exothermic transitions indicate that the as-molded material had been cooled relatively rapidly. This is observable with some of the samples which can be seen with Figure-4.5.



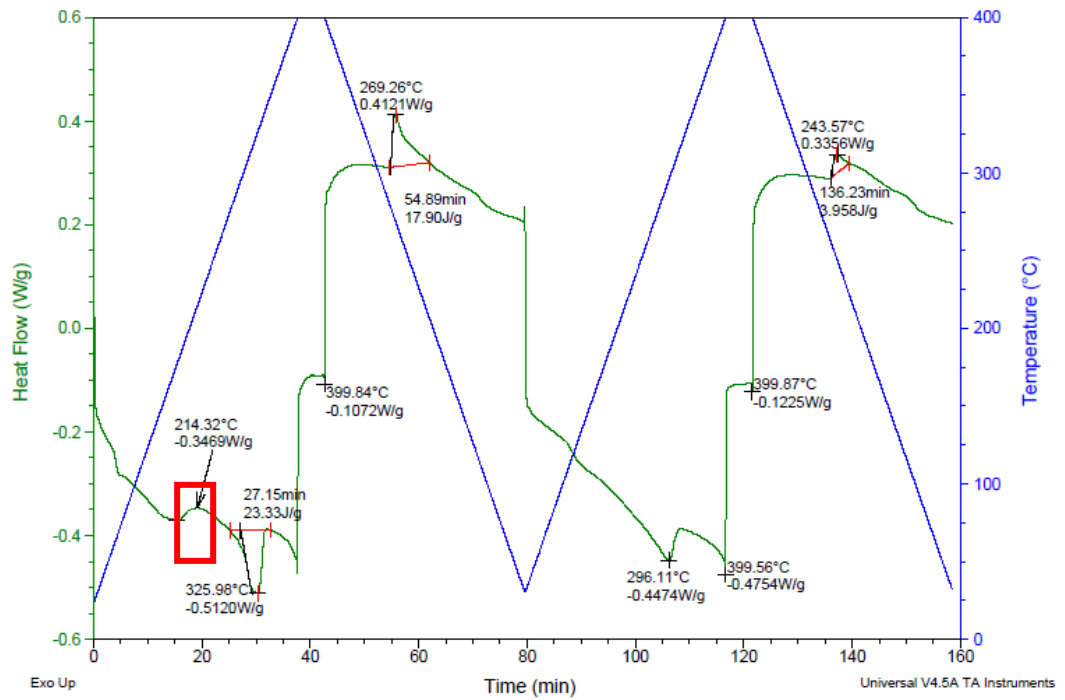
0-hr CH



1700-hr CH



0-hr DHW

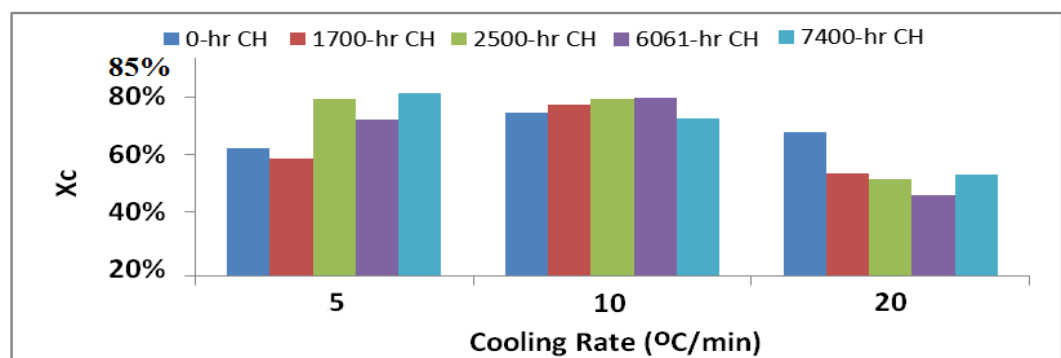


7400-hr DHW

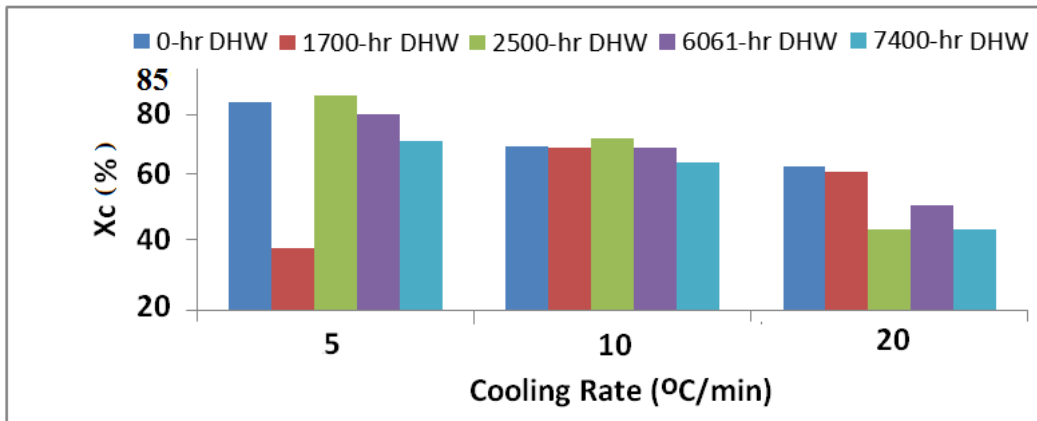
Figure-4.5 Thermograms of HP PPA GF40 samples that show exothermic peak before T_m .

4.1.2 Degree of crystallinity

The Degree of Crystallinity values of HP samples by nonisothermal DSC analysis are given in Figure-4.6 and Table 4.3. Degree of crystallinity (X_c) values for HP samples decrease at higher cooling rates. This is due to shorter time interval for the reordering of crystals in the structure at faster cooling rates. So after cooling down they are rearranged and but gives a lower enthalpy of fusion saying that degree of crystallinity values were much lowered after first melting and imperfect crystal rearrangement occurred.



(a)



(b)

Figure-4.6 X_c changes for HP samples at various cooling rates (a) CH, (b) DHW.

It is also clear with the samples that, over ageing under environmental stresses, the X_c values tend to reduce meaning that structural integrity is getting worse over time.

When ageing duration results are investigated, until 2500 hr aged samples, there is no big difference between CH and DHW samples. So addition of O_2 to the media for DHW samples shows its adverse effects over lifetime after certain time. This means, while both sides continue their lifetime without any trouble, after a break-even point there is a possibility that DHW parts might cause failure since drop percentage reduces below 25%.

Table-4.3 ΔH_m , ΔH_c and X_c values of HP PPA GF40 samples.

SAMPLE NAMES	CR 5 °C/min					
	ΔH_{m1} (J/g)	ΔH_{m2} (J/g)	ΔH_{c1} (J/g)	X_c (%)	$X_{c,2}$ (%)	ΔH_m (%)
0-hr CH	24	10	6	76	40	59
1700-hr CH	23	16	10	59	38	33
2500-hr CH	27	9	6	79	33	66
6061-hr CH	30	17	9	72	47	46
7400-hr CH	26	12	5	81	58	54
0-hr DHW	23	15	4	82	73	36
1700-hr DHW	5	2	4	25	NA	60
2500-hr DHW	21	7	4	83	43	69
6061-hr DHW	22	11	5	78	55	50
7400-hr DHW	18	13	6	70	54	30
SAMPLE NAMES	CR 10 °C/min					
	ΔH_{m1} (J/g)	ΔH_{m2} (J/g)	ΔH_{c1} (J/g)	X_c (%)	$X_{c,2}$ (%)	ΔH_m (%)
0-hr CH	27	13	7	74	46	51
1700-hr CH	29	16	7	77	56	43
2500-hr CH	24	13	5	79	62	46
6061-hr CH	30	13	6	80	54	57
7400-hr CH	25	10	7	72	30	61
0-hr DHW	17	NA	6	68	NA	NA
1700-hr DHW	26	NA	8	68	NA	NA
2500-hr DHW	21	NA	6	71	NA	NA
6061-hr DHW	20	13	6	68	54	34
7400-hr DHW	23	10	9	63	10	55
SAMPLE NAMES	CR 20 °C/min					
	ΔH_{m1} (J/g)	ΔH_{m2} (J/g)	ΔH_{c1} (J/g)	X_c (%)	$X_{c,2}$ (%)	ΔH_m (%)
0-hr CH	17	9	6	68	33	46
1700-hr CH	24	16	11	53	31	32
2500-hr CH	24	11	12	51	NA	55
6061-hr CH	26	14	14	46	NA	46
7400-hr CH	26	10	12	53	NA	63
0-hr DHW	18	NA	7	62	NA	NA
1700-hr DHW	21	NA	8	61	NA	NA
2500-hr DHW	14	5	8	43	NA	66
6061-hr DHW	23	NA	11	50	NA	NA
7400-hr DHW	20	12	12	43	NA	40

ΔH_{m1} : Enthalpy of 1st melting, ΔH_{m2} : Enthalpy of 2nd melting ΔH_{c1} : Enthalpy of 1st crystallization.

4.1.3 Crystallization kinetics

4.1.3.1 Avrami model for nonisothermal crystallization kinetics and statistical analysis

Avrami crystallization model is evaluated from nonisothermal DSC first exotherms Figure-4.7. DSC crystallization exotherms of all polymeric samples could be found in Appendix B, Figures B2 and B3. From the first exotherms, time dependent relative crystallinity is calculated and given in Figure-4.8. Other relative crystallinity graphs of the samples can be found in Appendix B, Figures B3 and B4. All relative crystallinity (X_r) versus time curves have the same characteristic sigmoidal shape and crystallization half time, $t_{1/2}$, is defined from this curve. Initial part of the S-shaped curves is generally considered as nucleation step of the crystallization process. Each curve showed a linear part considered as primary crystallization; subsequently, a second non-linear part deviated off slightly and considered to be due to secondary crystallization, which was caused by rod shaped geometric growth.

Linear part of the curve is fitted by Avrami model and successfully applied for the all aged HP samples, see Figure-4.9. The Avrami plots of all samples can be found in Appendix C, Figures C1 and C2. Avrami exponent, n , and growth rate constant, K , and crystallization half time, $t_{1/2}$, values are calculated from the Avrami plots and are given in Table-4.4. The Avrami exponent n values scatter around 2, suggesting rod-shaped crystals also as seen by microscopic analysis. Furthermore, the crystallization half time values either tend to remain stable or decrease especially until 6061-hr for both CH and DHW samples.

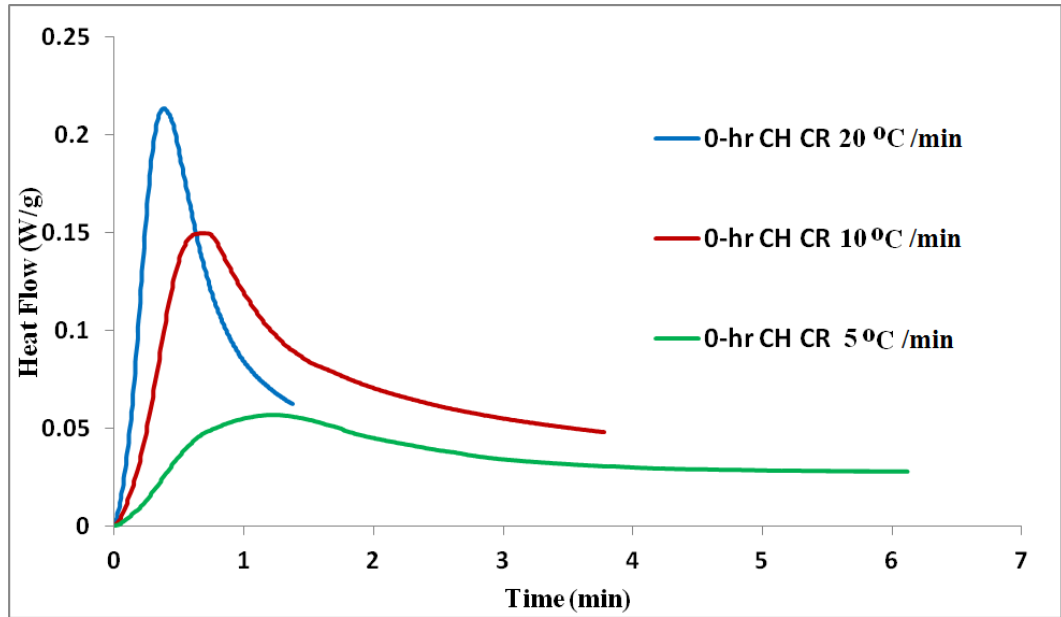


Figure-4.7 DSC exotherms of 0-hr CH HP samples at various cooling rates (CR).

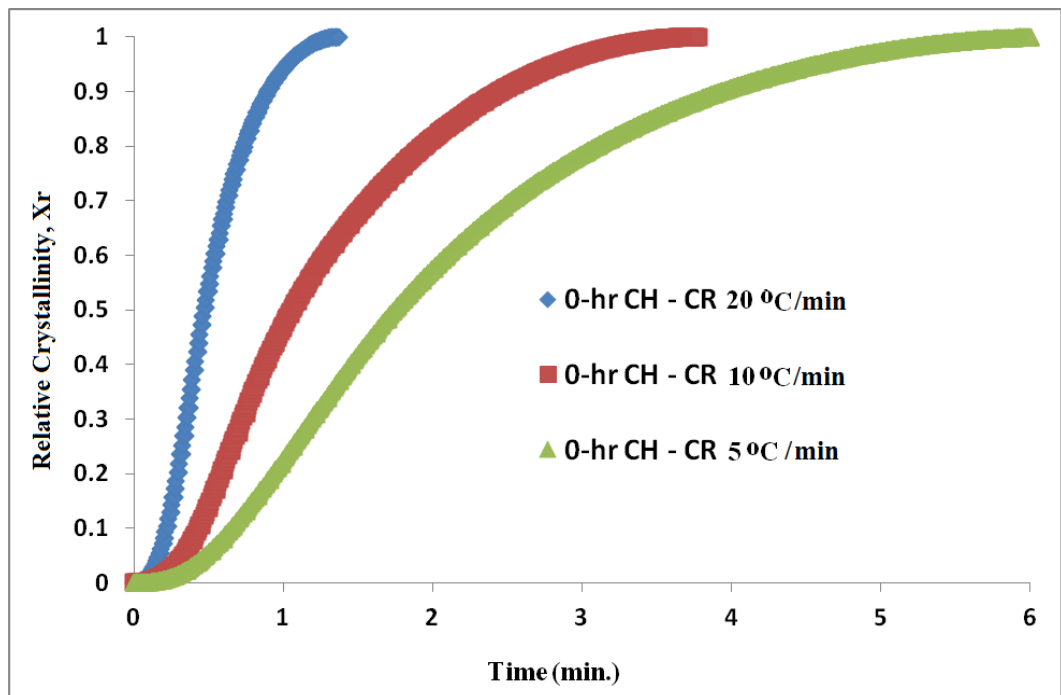


Figure-4.8 Time dependent relative crystallinity of 0-hr CH HP samples at various cooling rates (CR).

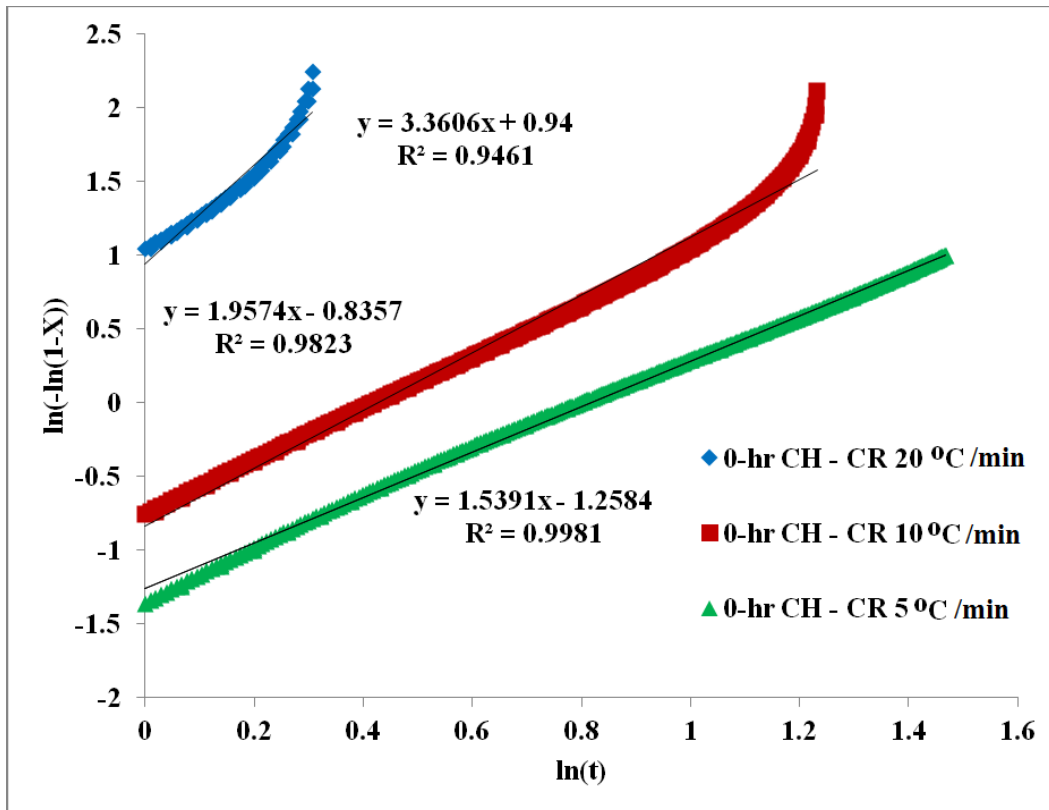


Figure-4.9 Avrami plot of 0-hr CH HP samples at various cooling rates (CR).

Table-4.4 Avrami exponent (n), growth rate constant (K), crystallization half time ($t_{1/2}$) values.

SAMPLE NAMES	COOLING RATES								
	5 °C/min			10 °C/min			20 °C/min		
	n	$K_{\text{intercept}} * 10^2$	$t_{1/2}$ (min)	n	Growth Rate $K_{\text{intercept}} * 10^2$	$t_{1/2}$ (min)	n	$K_{\text{intercept}} * 10^2$	$t_{1/2}$ (min)
0-hr CH	1.5	28.4	3.1	2.0	43.4	1.9	3.4	256.0	0.7
1700-hr CH	2.3	16.1	2.5	2.0	263.8	2.0	1.8	78.8	1.5
2500-hr CH	2.2	34.6	1.8	2.1	60.7	1.5	1.8	86.9	1.4
6061-hr CH	2.0	59.7	1.5	2.1	79.6	1.3	1.8	90.2	1.4
7400-hr CH	1.9	59.7	2.2	1.7	63.1	1.8	1.7	78.4	1.5
0-hr DHW	1.9	27.8	2.3	1.3	103.0	1.3	1.6	92.5	1.5
1700-hr DHW	no crystallization occurred			1.9	26.7	2.4	2.0	95.4	1.5
2500-hr DHW	2.4	21.0	1.9	1.8	56.5	1.8	2.2	117.8	1.1
6061-hr DHW	2.8	65.1	1.0	2.2	68.9	2.0	1.5	61.9	1.0
7400-hr DHW	1.9	25.4	2.5	1.7	30.1	2.6	1.9	81.2	1.4

4.1.3.2 Ozawa model for nonisothermal crystallization kinetics

The Ozawa model is applied and successfully fits the nonisothermal crystallization behavior of the samples.

The relative crystallinity, X_r , as a function of the crystallization temperature is obtained from the crystallization exotherms of samples by partial integration of the crystallization exotherms as seen in Figure-4.10 X_r versus temperature plot of selected PPA GF40 samples are given in Appendix C, Figures C1 and C2. Ozawa plots for all samples can be found in Appendix D, Figures D1 and D2.

Ozawa plot of HP samples at various temperatures is given in Figure-4.11. Slopes of these straight lines give Ozawa constant m , and intercepts are $K(T)$ and these results are given in Table-4.5. It can be seen with the values that as temperature increases, Ozawa constant m increases, but Ozawa rate constant $K(T)$ decreases.

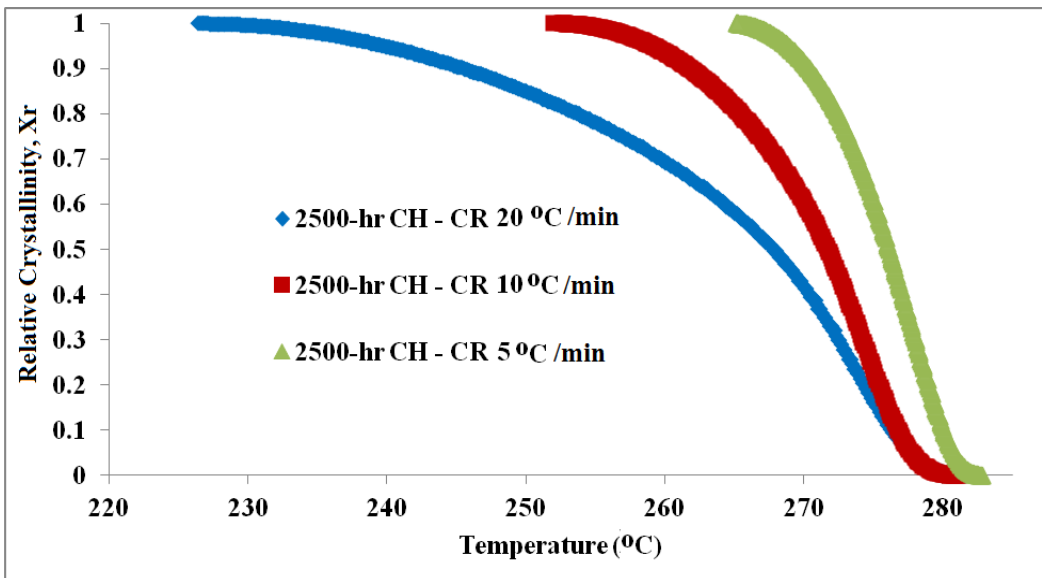


Figure-4.10 Relative crystallinity of 2500-hr HP CH samples vs. T various cooling rates (CR).

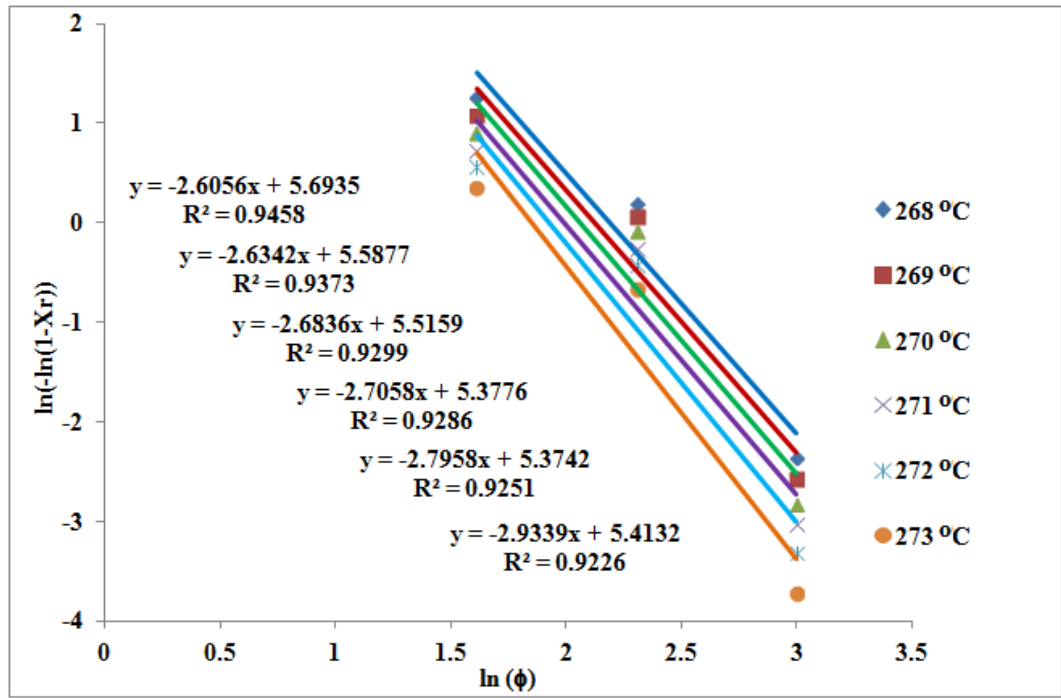


Figure-4.11 Ozawa plot of 2500-hr HP CH samples.

4.1.4 Activation energy of crystallization

Kissinger and Augis–Bennett plots of the samples are given in Figure 4.12 and Figure 4.13. ΔE_A values obtained from slopes of the lines are listed in Table 4.6. ΔE_A is negative because of exothermic nature of the transition from melt to crystalline state and the negative activation energy values also imply that crystallization mechanisms are accelerated by decreasing temperatures.

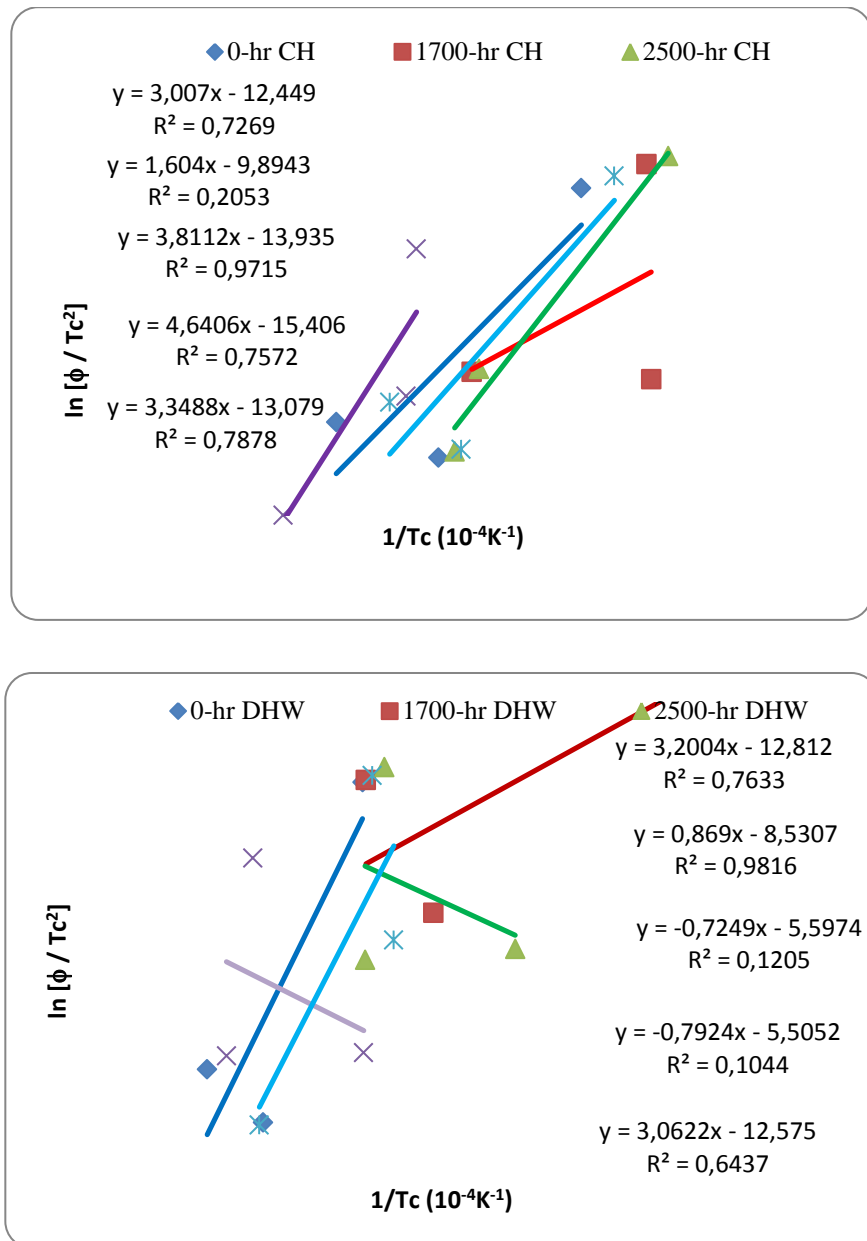


Figure-4.12 Kissinger plots of nonisothermally crystallized selected samples.

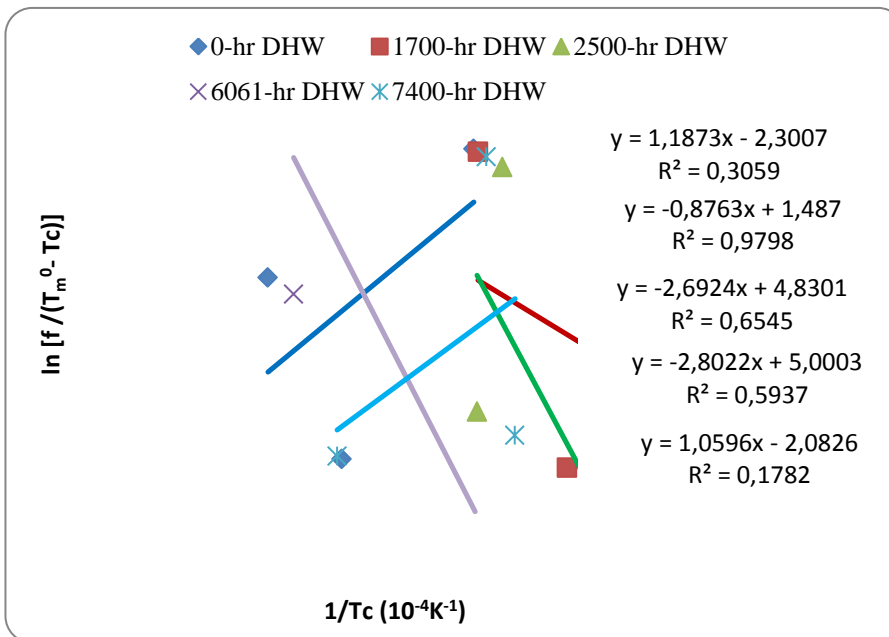
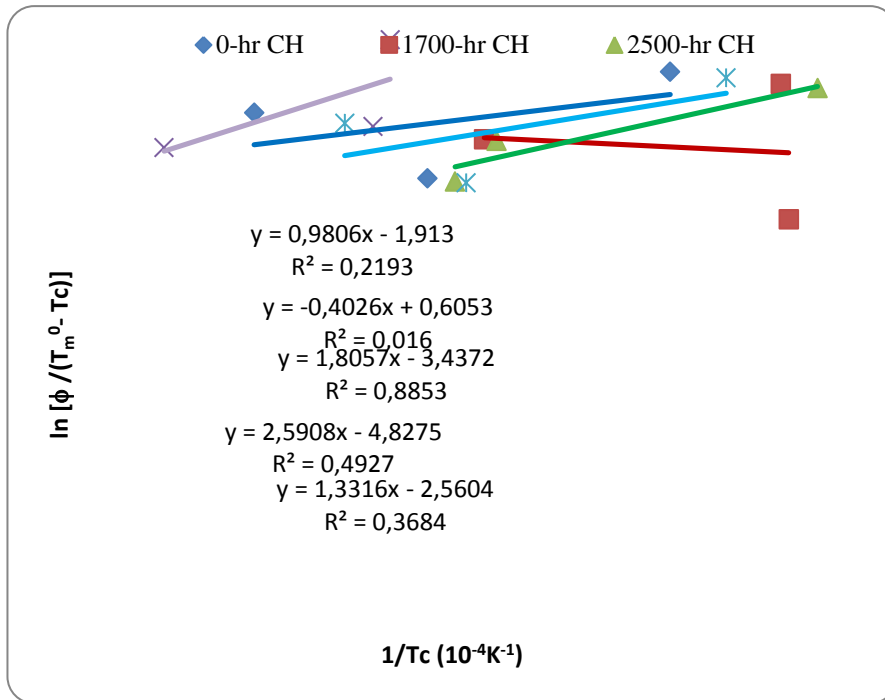


Figure-4.13 Augis-Bennett plots of nonisothermally crystallized selected samples.

Table-4.6 Activation energy values of crystallization obtained from Kissinger and Augis-Bennett models for nonisothermally crystallized selected PPA GF40 HP samples.

Sample Names	Kissenger Slope	R ²	Augis-Bennett Slope	R ²	Kissenger ΔE_A (kJ mol ⁻¹)	Augis-Bennett ΔE_A (kJ mol ⁻¹)
0-hr CH	3.0070	0.73	0.9806	0.22	-25.00	-8.15
1700-hr CH	1.6040	0.20	-0.4026	0.02	-13.34	3.35
2500-hr CH	3.8112	0.97	1.8057	0.89	-31.70	-15.01
6061-hr CH	4.6406	0.76	2.5908	0.49	-38.58	-21.54
7400-hr CH	3.3488	0.79	1.3316	0.37	-27.84	-11.07
0-hr DHW	3.2004	0.76	1.1873	0.31	-26.61	-9.87
1700-hr DHW	0.8690	0.98	0.8763	0.98	-7.22	-7.28
2500-hr DHW	-0.7249	0.12	2.6924	0.65	6.03	-22.38
6061-hr DHW	-0.7924	0.10	2.8022	0.59	6.59	-23.30
7400-hr DHW	3.0622	0.64	1.0596	0.18	-25.46	-8.81

Coefficient of determination (R²) results given in Table-4.6 show that, Augis-Bennett model generally is not valid for this material and results are not acceptable. However, Kissenger model is mostly applicable as seen with higher R² values and can be used to study the crystallization kinetics of glass fiber reinforced polyphthalamide material.

4.2 TGA Analysis of HP Samples

TGA analysis were performed on aged HP PPA GF40 samples and all TGA thermograms of the samples are shown in Appendix E, Figures E1 and E2 separately.

The amide structures lose their 2-3 % of weight up to 200 °C due to loss of moisture stacked in hydrophilic amide groups. Between 400 and 500 °C, they almost decompose completely as also predicted and can be seen in Figures-4.14 and 4.15 (Benzler, 2001).

First drop after high weight loss starts at 520 °C and ends around 550 °C. The initial two steps starting from 520 °C seen with TGA analysis show that the fibers are aramid fibers. Aramid fibers undergo decomposition at lower temperature when compared to the glass fibers. The aramid fiber loses around 3.12 % its weight from room temperature up to 300 °C and after 300 °C up to 520°C, it tends to lose its weight around 1.31% (Benzler, 2001). On other hand, aramid fibers are more susceptible to be attacked by oxidizing elements like oxygen and chlorine as found in water media. The second step temperature interval is between 550 and 600 °C.

The remaining percentage after 600 °C represents inorganic glass fiber found in the polymer structure. Because it is not affected with the heat employed on samples, it shows the value of around 40% as it was in the original state.

As can be seen with the Table-4.7, CH side of PPA material stabilization temperatures are mostly higher and equal when compared with the DHW side of PPA material. This situation is attributable to more aggressive environment in DHW side of components.

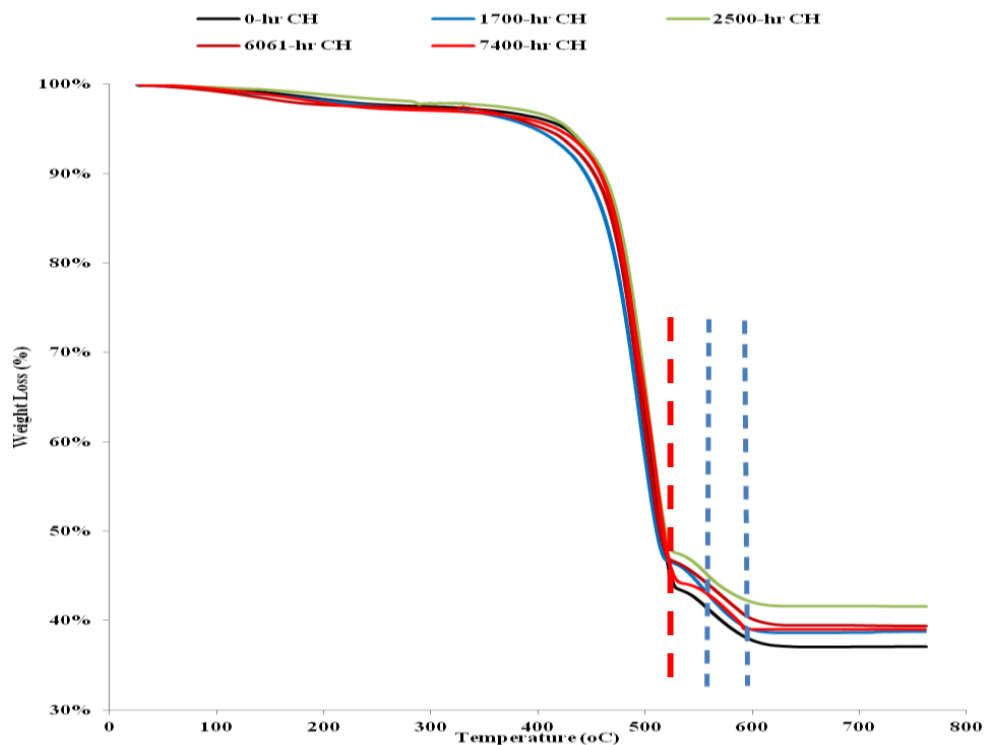


Figure-4.14 TGA graphs for HP PPA GF40 CH samples.

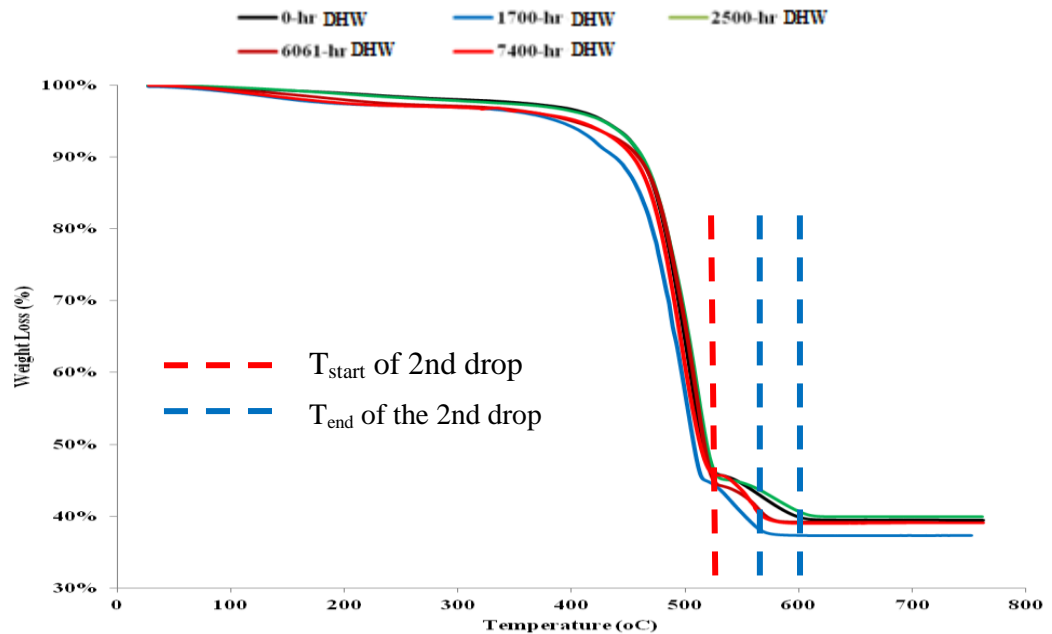


Figure-4.15 TGA graphs for HP PPA GF40 DHW samples.

It is a common practice to consider 50% weight loss as an indicator for structural destabilisation (Chisholm et al., 2005). Table-4.7 shows the half life time and temperature values obtained for the parts to come to 50% of their initial weight. The temperature at which 50% weight loss observed is indicated as $T_{1/2}$ and the time at which 50% weight loss observed is indicated as $t_{1/2}$. There is not noticeable difference with these values for CH and DHW samples, so it is apparent that in terms of thermal stability values of the samples for both application conditions, the performances were similar. Also we can say the results are satisfactory since there is no significant reduction when compared to 0-hr value. Furthermore when we look at the stabilization temperatures, DHW parts show a value drop of 5 °C more due to more aggressive environment they are exposed to.

On the other hand, it is meaningful to say, because the parts are cut from complicated structures, the extruded samples differ so much with their interior matrix and crystallinity to explain small deviations in $T_{1/2}$ and $t_{1/2}$ values. The very clear statement can be told for 1700-hr DHW sample, which shows the lowest T value at which it loses its 50% of initial weight, that is 507 °C. This sample was also observed for its poor crystalline structure (almost 0 X_c value %) with DSC

experiments. So as the integrity lost over time, its temperature value to come to 50% of its initial weight reduced significantly.

Table-4.7 Half life times and T transitions for HP PPA GF40 samples via TGA experiments.

Ageing Duration (hours)	PPA GF40 HP Samples				
	T _{1/2} (°C)	t _{1/2} (min.)	T _{start} of 2nd drop (°C)	T _{end} of the 2nd drop (stabilization T in °C)	Remaining % at 750 °C
0-hr CH	516	23.4	528 (44 %)	620 (37 %)	37.0
1700-hr CH	510	24.2	519 (47 %)	609 (39 %)	38.8
2500-hr CH	517	24.3	525 (48 %)	610 (42 %)	41.6
6061-hr CH	514	24.2	523 (47 %)	604 (40 %)	39.4
7400-hr CH	516	24.5	529 (45 %)	593 (39 %)	39.0
0-hr DHW	515	24.3	527 (46 %)	615 (40 %)	39.4
1700-hr DHW	507	24.0	515 (45 %)	580 (37 %)	37.0
2500-hr DHW	518	24.5	528 (46 %)	620 (40 %)	40.0
6061-hr DHW	517	24.4	529 (44 %)	590 (39 %)	39.0
7400-hr DHW	513	24.2	525 (46 %)	583 (39 %)	39.0

4.3 FTIR Analysis of HP Samples

The molecular formula of the compound is as previously given in Figure-1.2. It has different intensities of fragments as given in Table-4.8. The table summarizes main groups defined with FTIR analyses. Figures-4.16 and 4.17 show functional groups seen for 0-hr and aged HP PPA GF40 samples. All the rest FTIR spectra of the samples are shown in Appendix F, Figures F1 and F2.

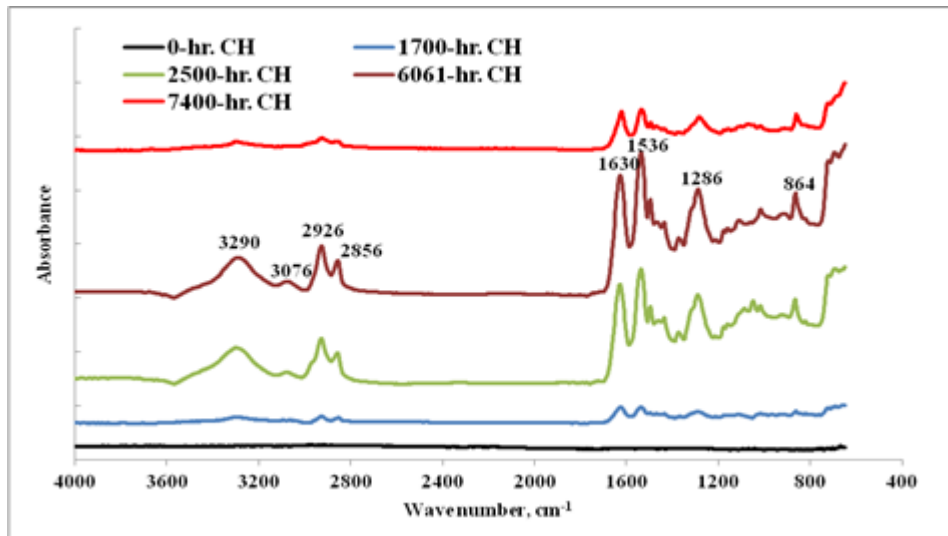


Figure-4.16 Functional groups of CH HP PPA GF40 samples by FTIR.

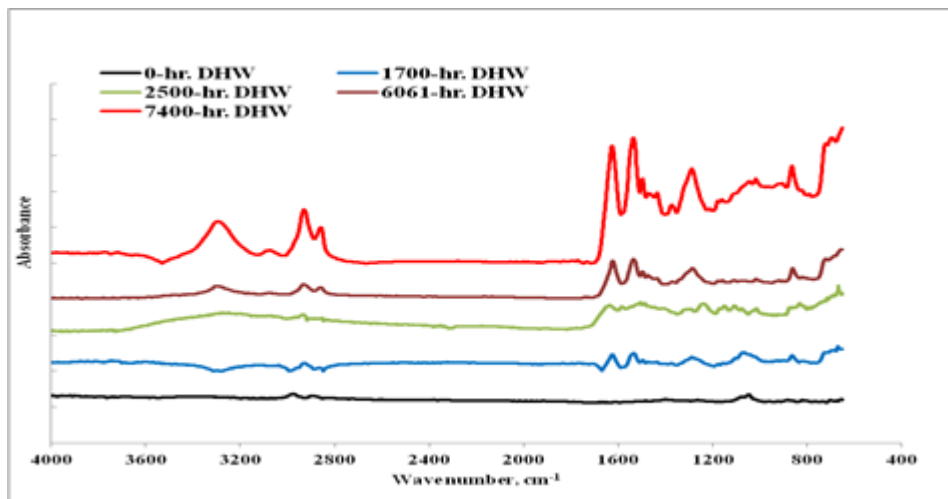


Figure-4.17 Functional groups of DHW HP PPA GF40 samples by FTIR.

Table-4.8 Groups of HP PPA samples defined by FTIR (Coates, 2000; Skoog and Leary, 1991).

Bond	Type of Compound	Frequency Range cm ⁻¹	Intensity
C-H	Alkanes	2850-2970	Strong
		1340-1470	Strong
Asymmetric CH stretching	Alkanes	2925-2950	Strong
Symmetric CH stretching	Alkanes	2860-2880	Strong
C-H	Alkenes C=C	3010-3095	Medium
		675-995	Strong
C-H	Alkynes C≡C	3200-3300	Strong
C=C	Alkenes	1610-1680	Variable
C=C	Aromatic Rings	1500-1600	Variable
C-N	Amines, amides	1180-1360	Strong

In Figures-4.18 – 4.21, the carbon bands were taken as reference and the change for amide/amine and aromatic groups were tracked. For all CH samples both aromatic and amide bonds found in the structure tend to increase very slowly due to hydrophilic structure and cleavage of amide bonds with hydrolysis. However, it is fair to say the material structure did not differ significantly since y-axis was kept at very low values to observe the minor changes.

DHW samples show quite similar behaviour when compared with CH side of the samples. It is important to say 1700-hr sample is an exclusion. Because 1700-hr samples also showed higher degradation when compared to all other samples with other analyses as well which maybe attributed to a local non-heterogenous ageing. Furthermore, carbonyl bond (1700 cm⁻¹) is not observed with any samples. So we can say that the material was not oxidized by strong oxidizing agents significantly.

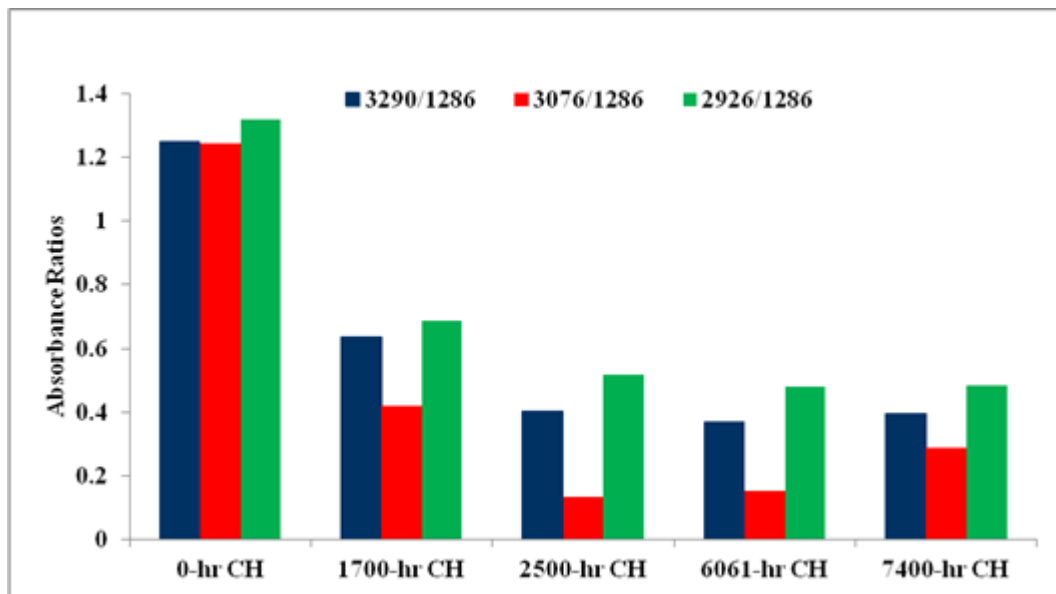


Figure-4.18 Amide (1286) to carbon bonds (3290 and 2926) ratio for HP CH samples.

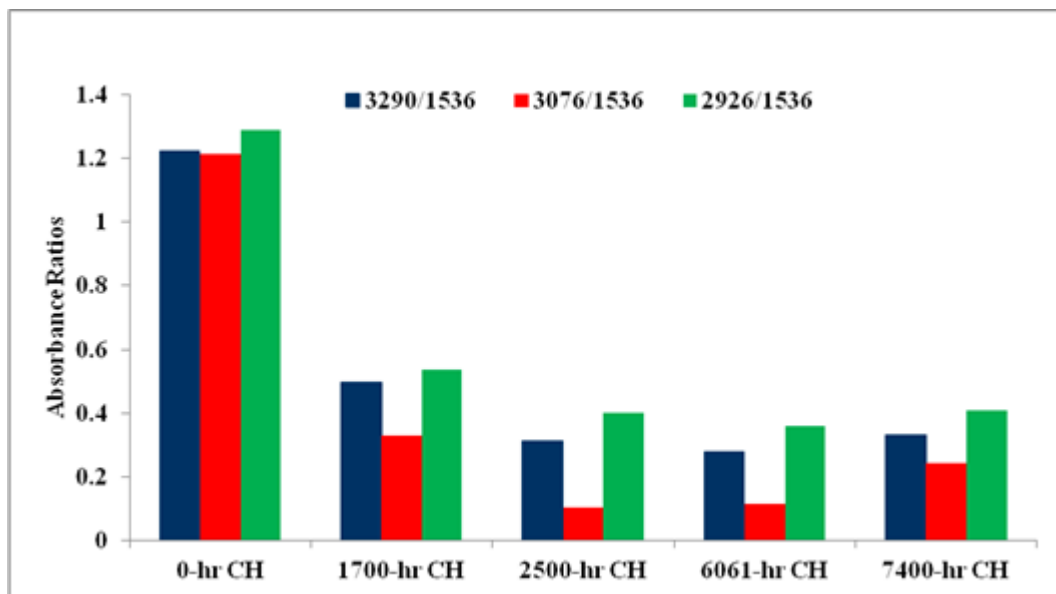


Figure-4.19 Aromatic rings (1536) to carbon bonds (3290 and 2926) ratio for HP CH samples.

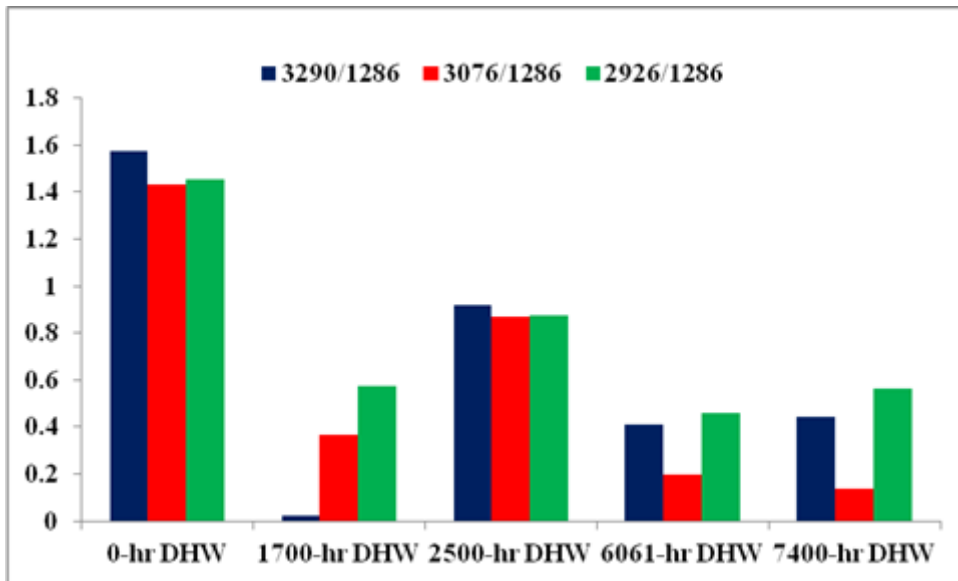


Figure-4.20 Amide (1286) to carbon bonds (3290 and 2926) ratio for HP DHW samples.

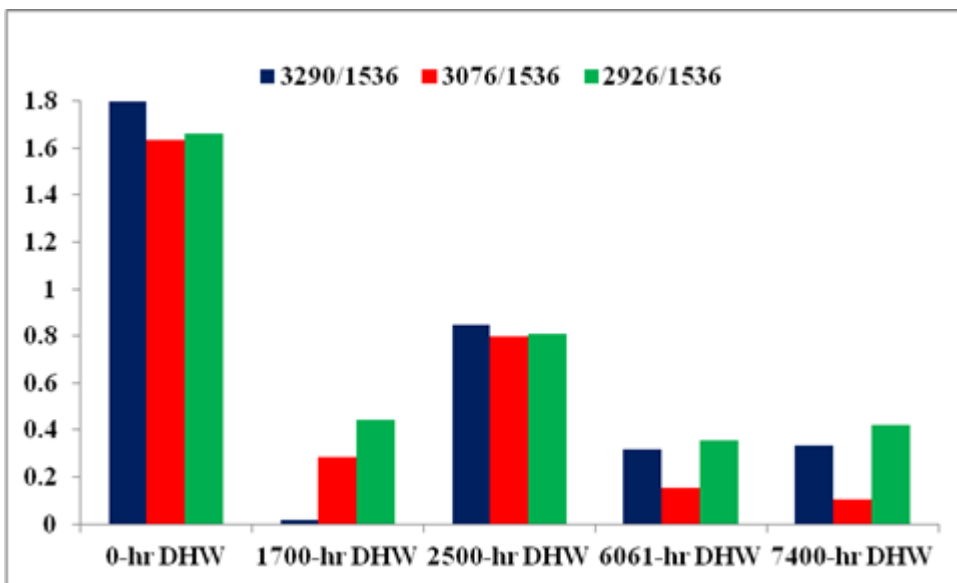


Figure-4.21 Aromatic rings (1536) to carbon bonds (3290 and 2926) ratio for HP DHW samples.

4.4 SEM Analysis of HP Samples

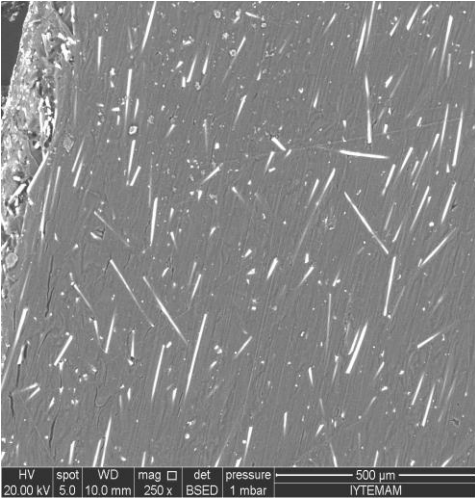
SEM analyses of PPA samples were employed in a magnification mood of 250x and 1000x respectively for each component. See Figures-4.22 and 4.23 for sample images of CH and DHW HP PPA GF40 respectively.

The images show that cracks are visible since 1700 hours of aged samples for both CH and DHW sides of components. On CH and DHW samples marked with red circle for 1700-hr aged sample, it can be seen that the crack emerged from the polymer matrix-glass fiber interface. So for some regions, the polymer matrix-glass fiber interaction was not good enough to stand for ageing conditions. However, mostly the interaction at polymer-glass fiber interface seems like there is a good bonding.

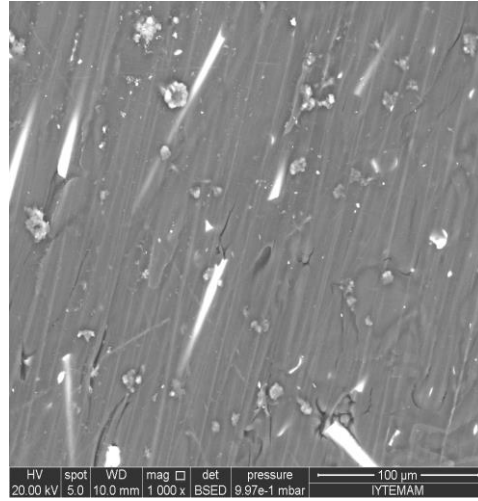
CH samples aged for 2500-hr marked with blue circle show that in the polymer there are also regions without glass fiber with defects which can be attributed to non-homogeneous production from injection molding machine with air bubbles and/or contaminants during the process. So there are multiple crack initiation sites within the structure.

When samples aged for 2500 hours are examined both for CH and DHW samples, it is seen that the glass fibers are more visible with DHW components meaning that the polymer was dissolved in water media more leaving the region more naked with glass fibers. This complies with greater attack by oxygen in the water media for DHW samples.

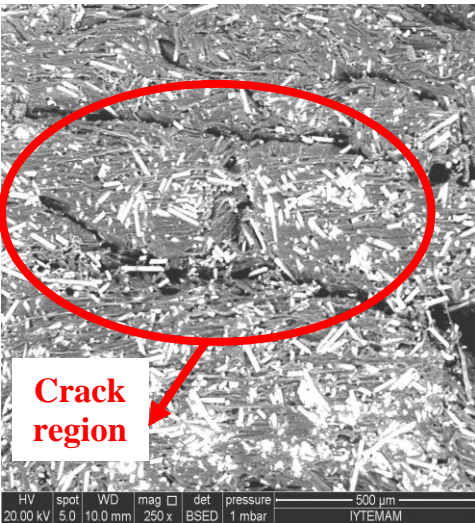
The samples show similar state for 6061 hours. But it is investigated for 7400 hours that, while for CH side the polymer-glass fiber interface is still there, it seems like for the specific region that was observed for DHW side lost this bonding which will for sure lead to weakening of the structure. It also seems with the images that the types of fractures are mostly of brittle type.



0-hr. CH 250X magnification



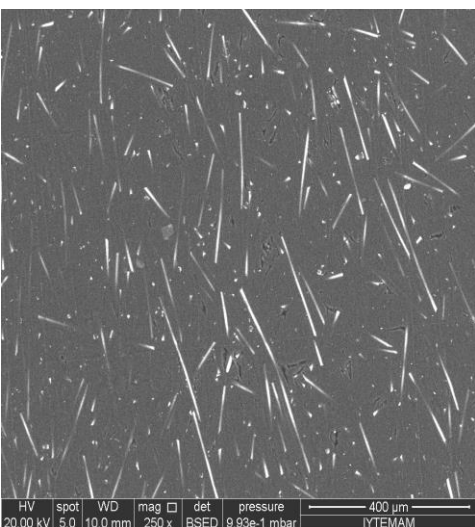
0-hr. CH 1000X magnification



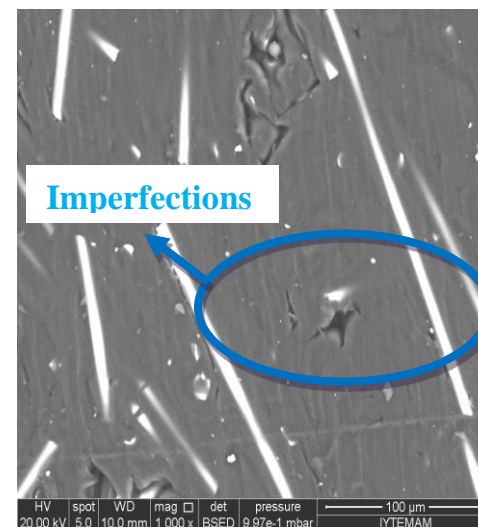
1700-hr. CH 250X magnification



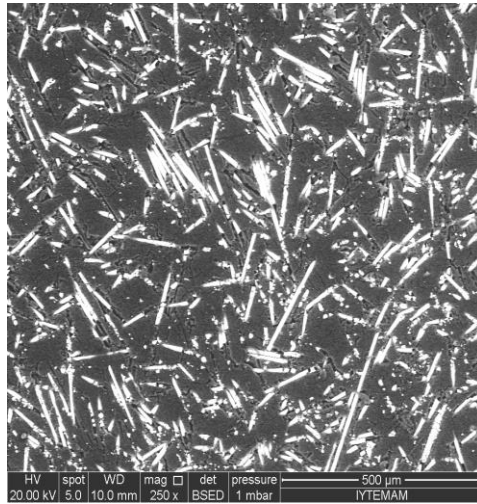
1700-hr. CH 1000X magnification



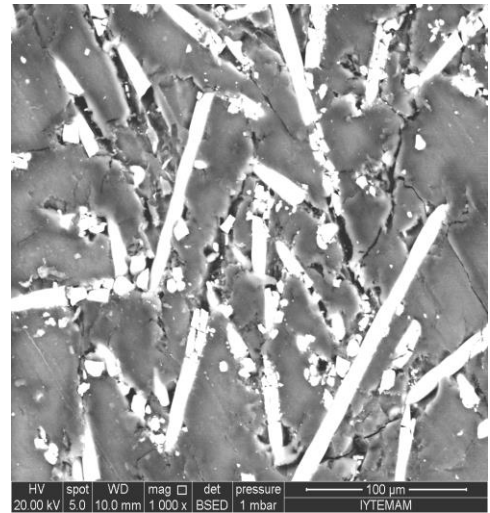
2500-hr. CH 250X



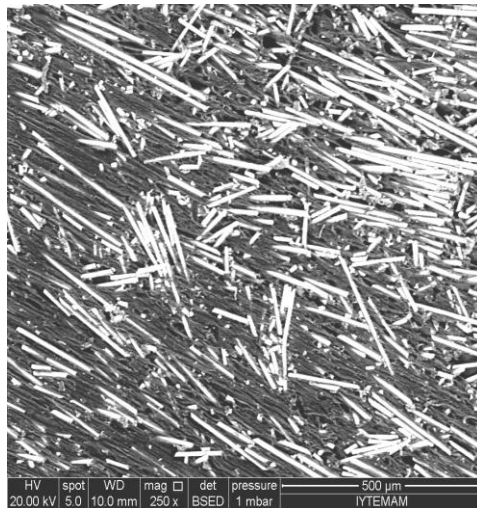
2500-hr. CH 1000X



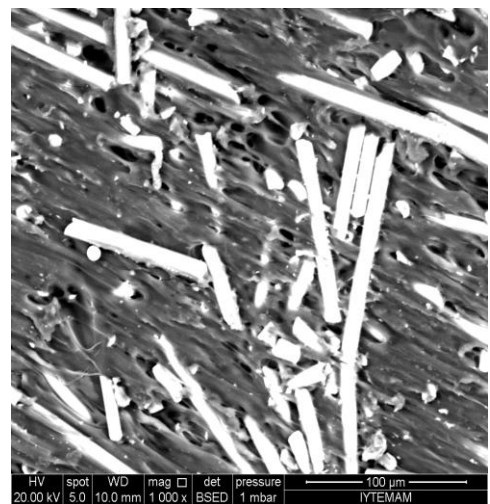
6061-hr. CH 250X



6061-hr. CH 1000X

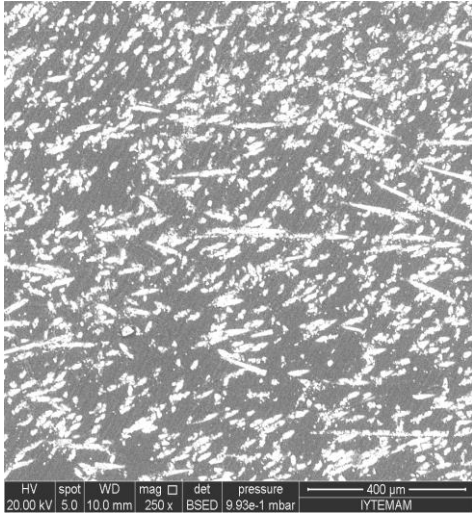


7400-hr. CH 250X

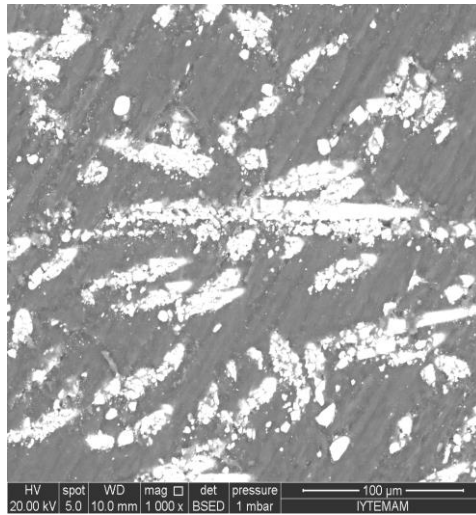


7400-hr. CH 1000X

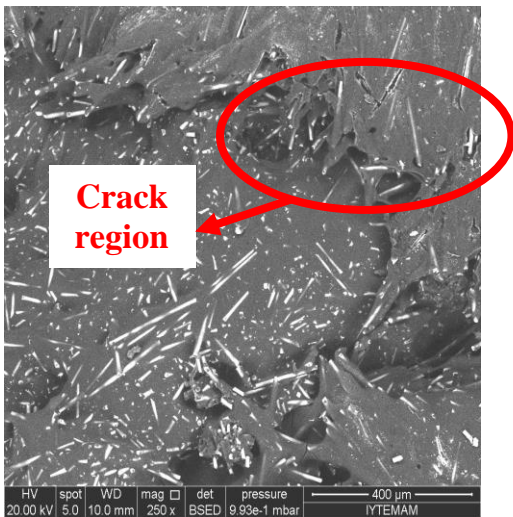
Figure-4.22 SEM images of HP PPA GF40 components' CH side.



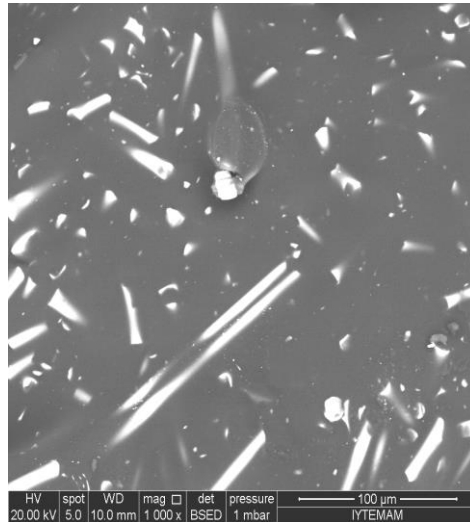
0-hr. DHW 250X



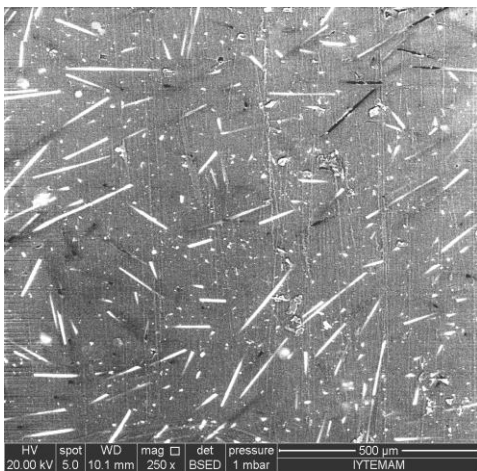
0-hr. DHW 1000X



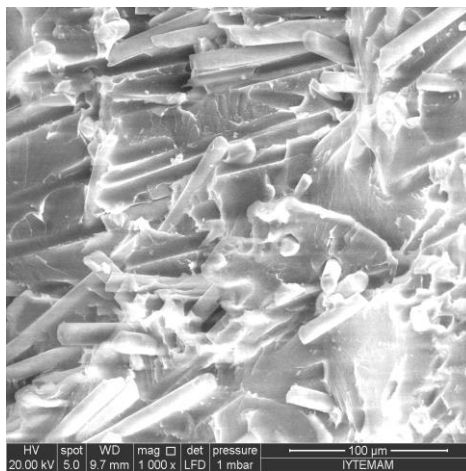
1700-hr. DHW 250X



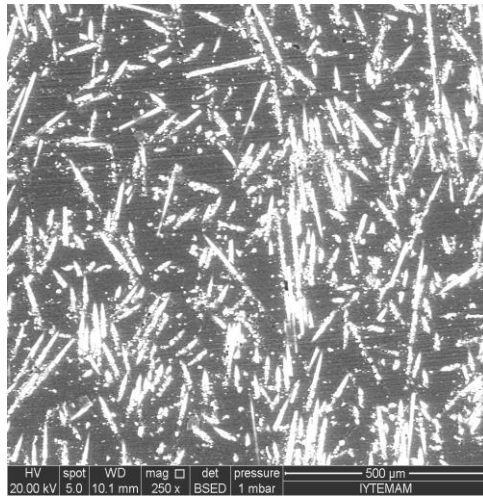
1700-hr. DHW 1000X



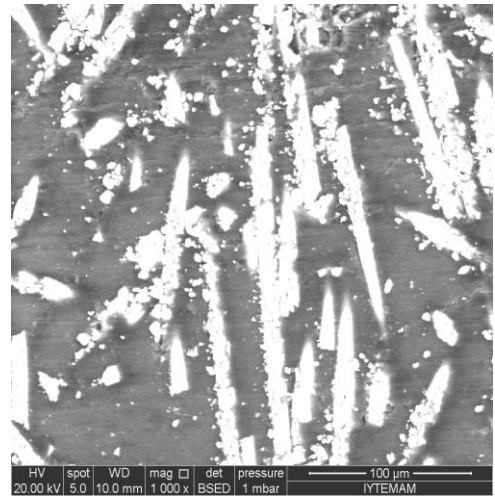
2500-hr. DHW 250X



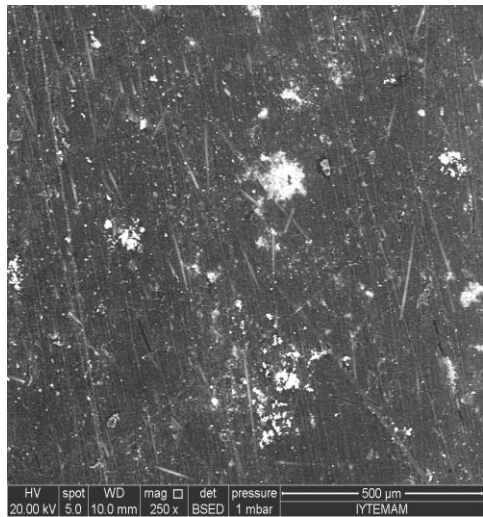
2500-hr. DHW 1000X



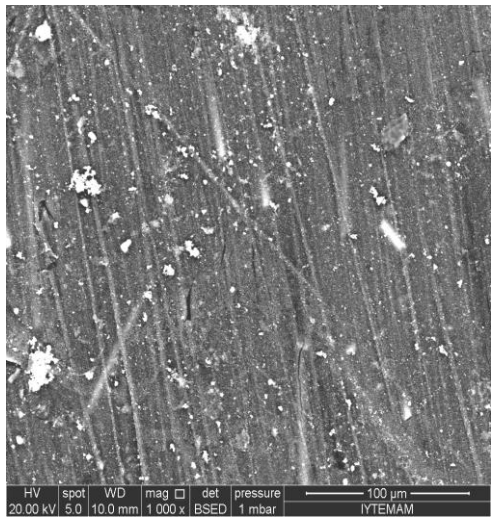
6061-hr. DHW 250X



6061-hr. DHW 1000X



7400-hr. DHW 250X



7400-hr. DHW 1000X

Figure-4.23 SEM images of HP PPA GF40 components' DHW side.

4.5 Relative Viscosity Analysis of HP Samples

Relative viscosity measurements are given in Table-4.9. The table gives the relative viscosity value changes in percentage over time for 2500-hr and 6061 hr CH and DHW PPA GF40 samples.

Sample subscripts referred to as 1 and 2 seen in Table-4.9 belong to different positions on the hydraulic part. Inner-layer is the 1 mm part of the thickness that is contact with running water. Outer layer is the next ~ 1 mm of the thickness coming after inner layer. The results clearly show that the main structure has different properties within different regions of the part, since they are extruded from machine and cannot be homogeneous in everywhere due to differences in design and various glass fiber alignments in the design. When a comparison made between CH and DHW samples, DHW samples were destructed around 1.5 times more at inner sides of the parts in line with more aggressive media they are exposed to.

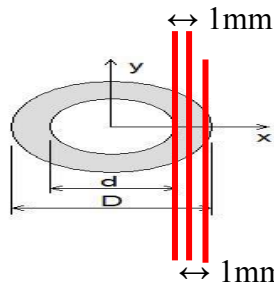


Table-4.9 Relative viscosity changes over time.

O ₂ level (ppm)	Samples	Water at 95 °C			
		2500 hr. of ageing		6061 hr. of ageing	
0	CH ₁	outer-layer	0	outer-layer	19%
0		inner-layer	0	inner-layer	17%
0	CH ₂	outer-layer	0	outer-layer	17%
0		inner-layer	0	inner-layer	15%
10	DHW ₁	outer-layer	8%	outer-layer	19%
10		inner-layer	12%	inner-layer	28%
10	DHW ₂	outer-layer	7%	outer-layer	15%
10		inner-layer	12%	inner-layer	26%

4.6 Tensile Properties of TTS ww and TTS wow

Tensile properties were measured to see the mechanical strength change over time due to increase of defects after exposure to highly aggressive environment with chlorine for various potential strong glass fiber reinforced polymeric materials. The standard deviations were below 5 MPa.

4.6.1 Tests with 1000 ppm chlorinated water at 95 °C for various GF content polymers

The tests were carried out with exaggerated high chlorine levels with 1000 ppm to see quick comparison effect of glass fiber reinforced PPA samples with glass fiber reinforced PA 66 and PP samples. PPA GF40 materials showed around 20% reduction in tensile strength after 3000 hours. Since the reduction of performance in polymeric matrix composites is usually associated with loss in mechanical load carrying capability of the polymer matrix, it is meaningful to see the changes over time with tensile tests, see Figures 4.24 - 4.32. Early experiments done on atactic polystyrene have shown that below the glass transition temperature (T_g), the relative effect of molecular weight on mechanical properties increases as the experimental regimen moves from elastic to viscoelastic region (Nicholson et al., 1999). In all of the graphs, “cond. ISO 1110” stands for conditioned parts with respect to ISO 1110. The samples aged in water were compared with conditioned samples but not with dry samples. Because hydrophilic materials as amide structures are found in polyphalamides, moisture is found to reduce stiffness and increase creep, presumably through plasticisation effect in a very short time is a quite well-known fact (Hassan et al., 2011). The absorption of moisture leads to the degradation of fiber matrix interfacial region and creating poor stress transfer efficiencies resulting in a reduction of mechanical and dimensional properties (Dhakal et al., 2007; Yang et al., 1986).

Increasing the amount of glass fiber leads to higher stiffness of composite thus more energy is required to break the specimens. As the volume fraction of fiber reinforcement in composites increases, more fiber-matrix interfacial area is created and the more applied load is transferred to the fiber by the interface

(Mohd Ishak et al., 2001). That's why, it is more difficult to break the specimen and hence results in greater tensile strength and tensile modulus. Figure-4.24 confirms that as glass fiber content increases, tensile strength at break values also increase. All results prove that, all reinforced PPA's shows much better performance when compared with reinforced PA66 and PP's.

However, if the fiber-matrix adhesion is weak, cracks tend to form at the interface and link up quickly through highly stressed sections of the matrix, resulting in premature failure of the composite. Nevertheless, it can be seen that the composite strength and composite modulus increase with an increase in the fiber loading. This shows that fiber-matrix adhesion for these composites is strong (Hassan et al., 2011).

In the order of increasing fiber loading, the tensile strength and tensile modulus increase. These results confirm that the fibers act as an effective reinforcing agent for PPA giving rise to a more rigid material (Manchado et al., 2002) for 0-hr condition.

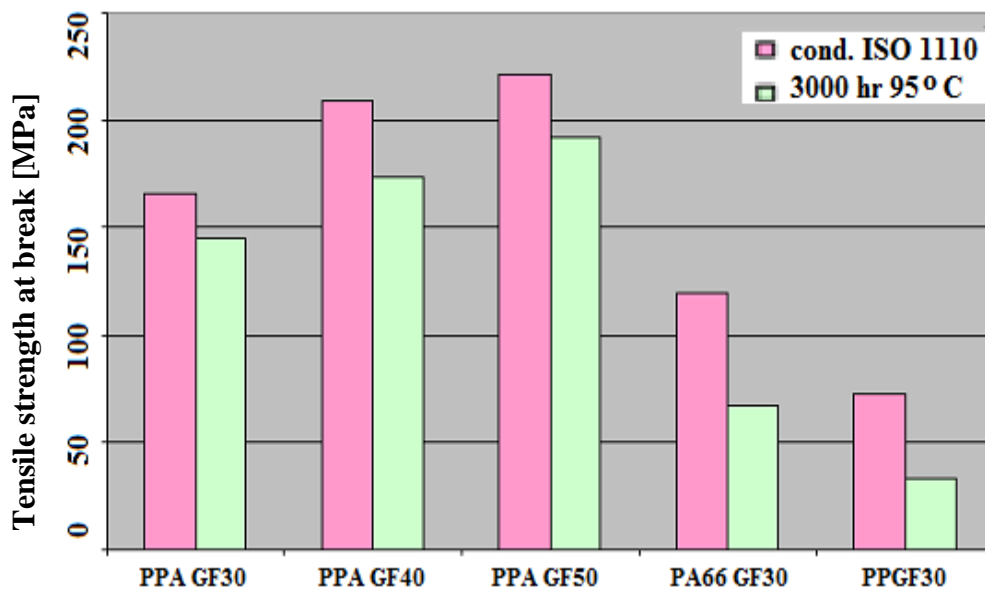


Figure-4.24 Absolute values of tensile strength for DIN-impact tensile bars ($80 \times 15 \times 1 \text{ mm}^3$) related to original conditioned values at 1000 ppm chlorinated 95°C water after 3000 hr.

When aged samples are investigated in Figures-4.25 – 4.28, after 3000 hr of ageing, even though absolute tensile strength value of PPA GF40 stays higher

than PPA GF30, the drop ratio compared to 0-hr conditioned values for PPA GF40 is worse than PPA GF30. However, in the long term, as seen in Figures-4.29 - 4.31, both absolute tensile strength and the drop ratio compared to 0-hr conditioned values have better results meaning that the higher the glass fiber content, the stronger the part gets. Since the parts still keep more than 50% of their initial tensile strength values even at such a highly concentrated chlorinated media, the material can be used confidently at defined temperature (AMODEL® Polyphthalamide Design Guide, 2003).

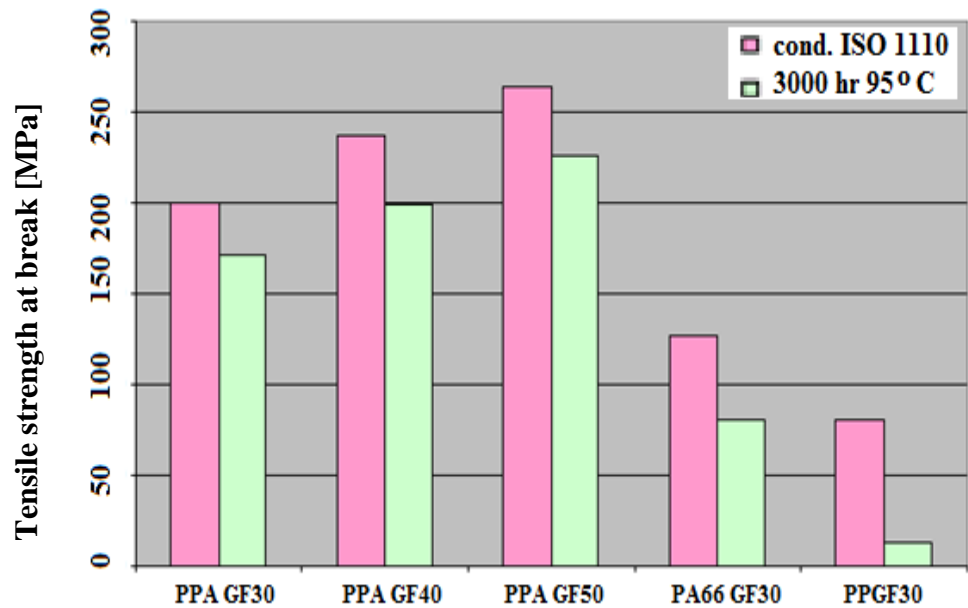


Figure-4.25 Absolute values of tensile strength for ISO-tensile bars ($60 \times 10 \times 3 \text{ mm}^3$) related to original conditioned values at 1000 ppm chlorinated water after 3000 hr at 95 °C.

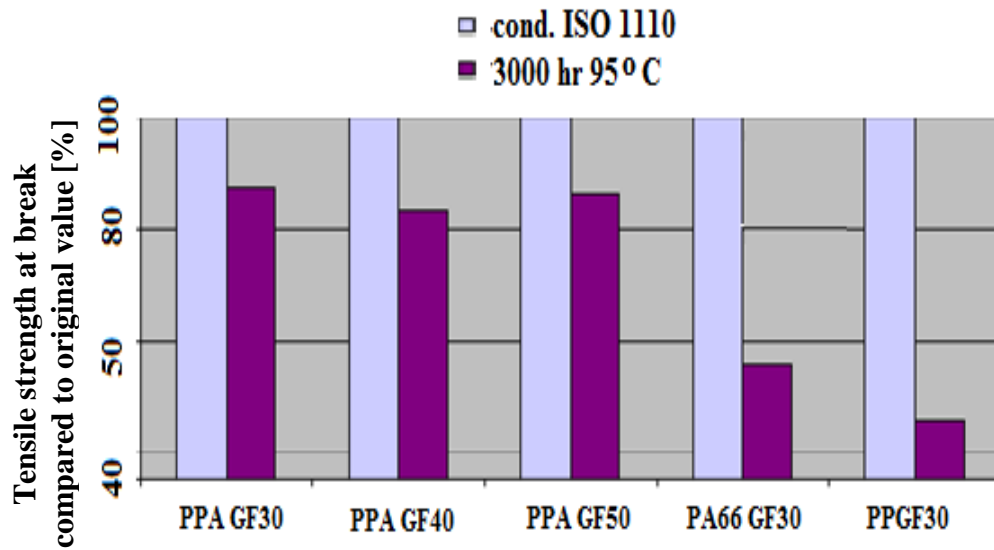


Figure-4.26 Relative decrease of tensile strength for DIN-impact tensile bars ($80 \times 15 \times 1 \text{ mm}^3$) related to original conditioned values at 1000 ppm chlorinated water after 3000 hr at 95 °C.

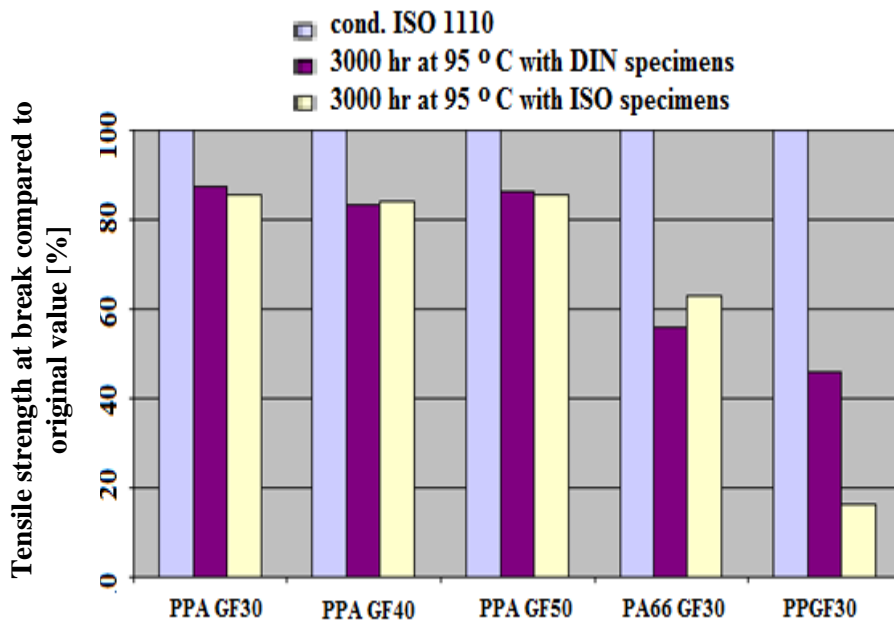


Figure-4.27 Relative decrease of tensile strength - thick ISO-bars compared to thin DIN-bars at 1000 ppm chlorinated water at 95 °C.

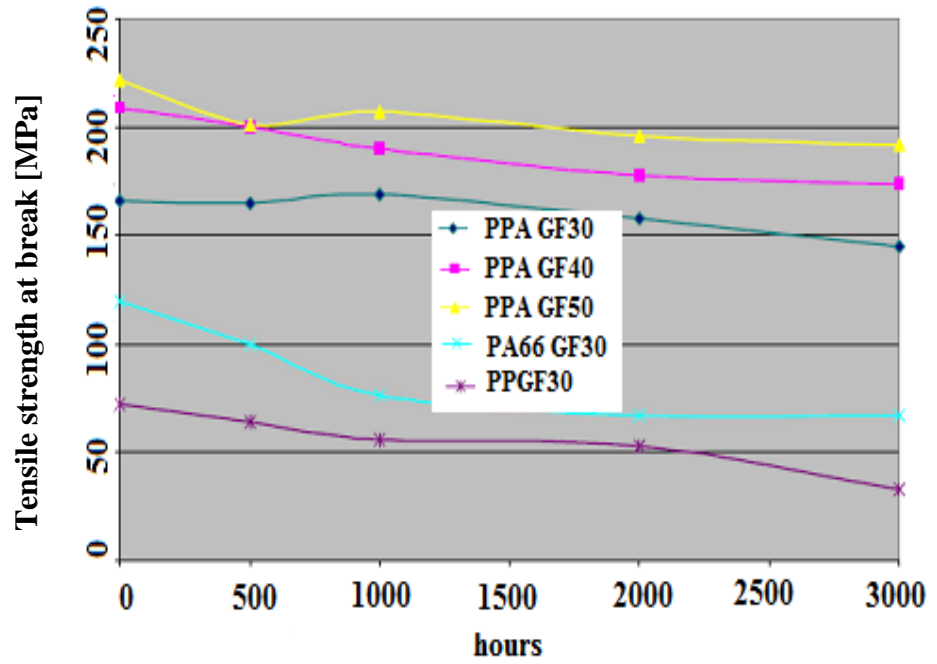


Figure-4.28 Tensile strength versus time for DIN-impact tensile bars (80x15x1 mm³) at 1000 ppm chlorinated water at 95 °C.

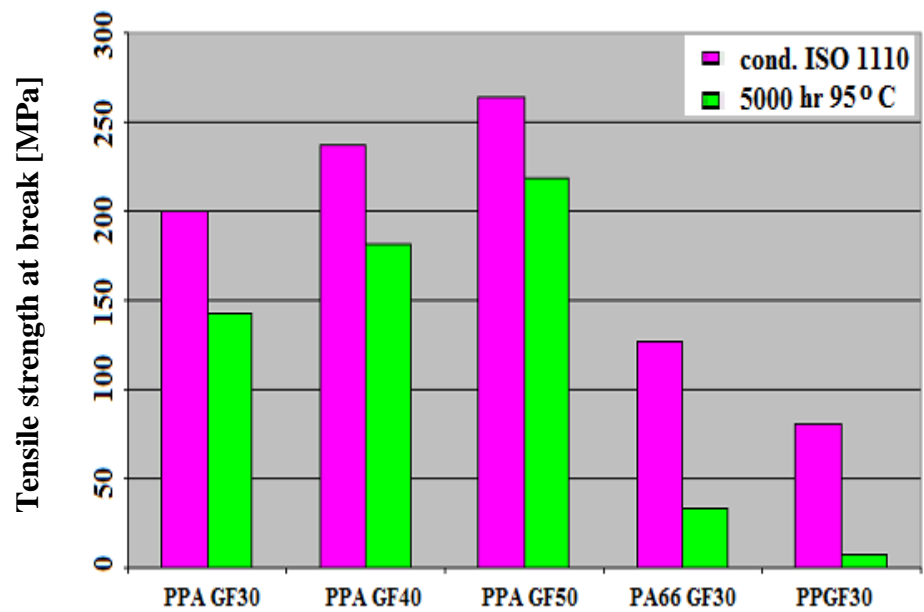


Figure-4.29 Absolute values of tensile strength for ISO-tensile bars (60x10x3 mm³) related to original conditioned values at 1000 ppm chlorinated water after 5000 hr at 95 °C.

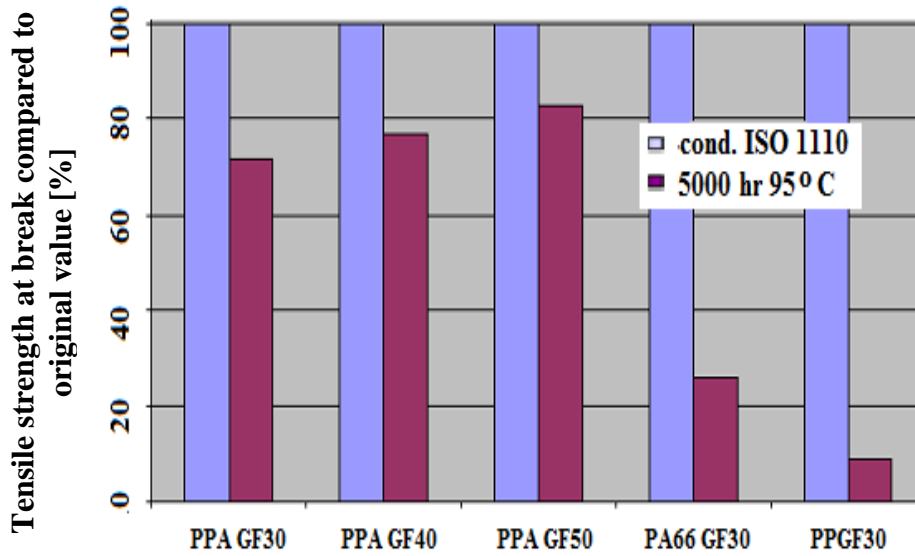


Figure-4.30 Relative decrease of tensile strength for ISO-tensile bars (60x10x3 mm³) related to original conditioned values at 1000 ppm chlorinated water after 5000 hr at 95 °C.

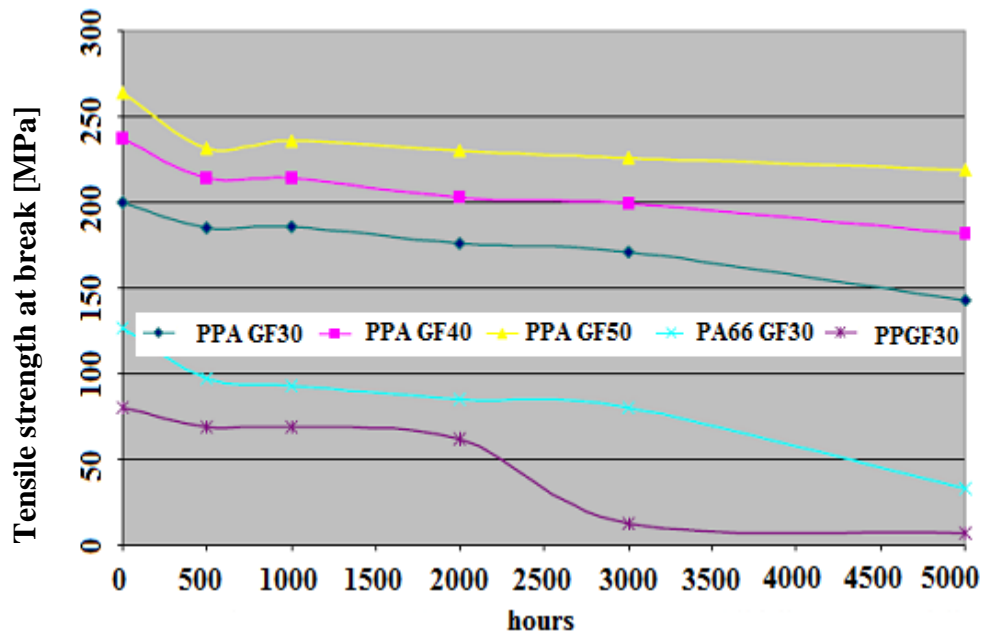


Figure-4.31 Tensile strength versus time for ISO-tensile bars (60x10x3 mm³) at 1000 ppm chlorinated water at 95 °C.

Curves in Figure-4.32 are obtained to see knitline (weldline) effect on tensile strength change of part to predict knitlines found in real parts. Two strongest materials seen as PPA GF40 and PA66 GF30 were compared at an average combi running water temperature that is 60 °C. At initial stages, while PPA GF40 tends to drop sharply, PA66 GF30 seems more stable. However after

10000 hours, the drop becomes much more for PA66 GF30 while PPA GF40 drops more smoothly. So when extrapolation is made, in the long term, it is evident that PA66 GF30 usage is critical and not as reliable as PPA GF40 since it loses around 80% when compared with initial tensile strength value with knitline.

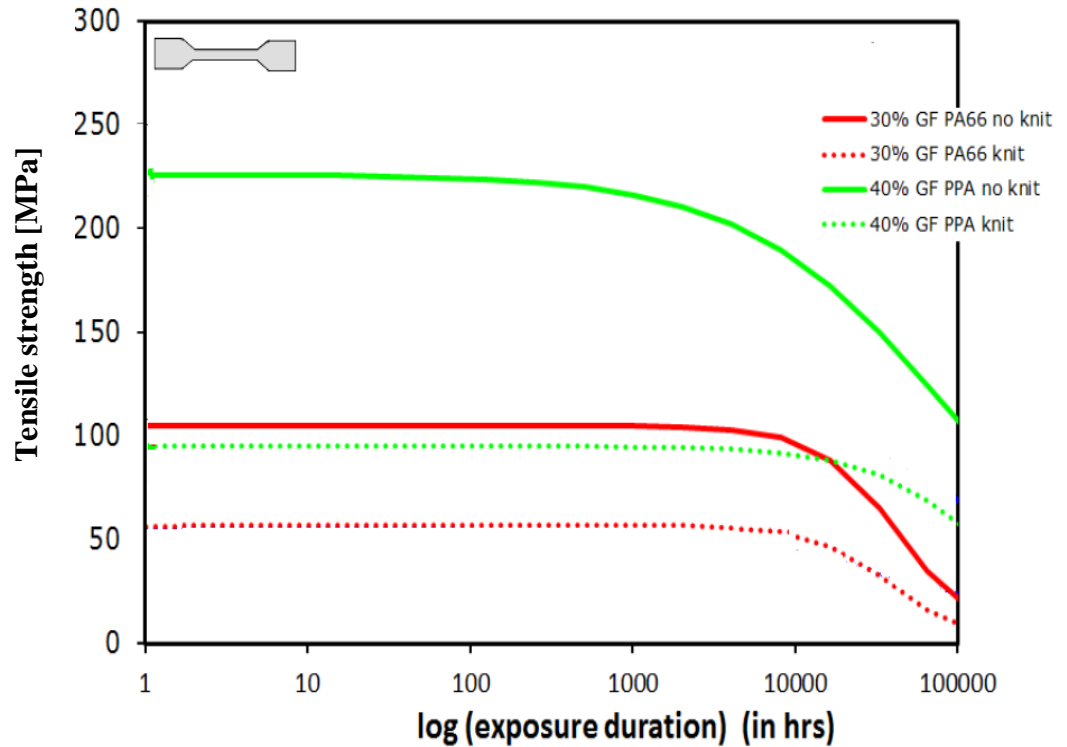


Figure-4.32 Tensile strength retention mastercurves
water with TTS and TTS wow at 60 °C.

4.7 Impact Strength of TTS

Impact strength of HP PPA GF40 samples measured and compared with glass fiber reinforced PA 66 and PP samples which can be seen with Figures 4.33-4.35.

Figures-4.33 – 4.35 clearly show that, as the glass fiber content increases, the impact strength value also increases. It was also seen with previously made study and told as composite notched impact is highly dependent on fiber content and exhibited a sharp linear increase over especially 10-30 % range. After this limit, increase rate is slower (Thomason, 2009). Also in line with tensile tests,

even though in the short term PA66 GF30 seems to have better performance, at the long term, its performance drops drastically when compared with PPA GF40. So still, PPA GF40 has the best performance among all alternative studied polymers. Since the PPA parts still keep around 50 % of their initial impact strength values even at such a highly concentrated chlorinated media, the material can be used confidently at defined temperature (AMODEL® Polyphthalamide Design Guide, 2003).

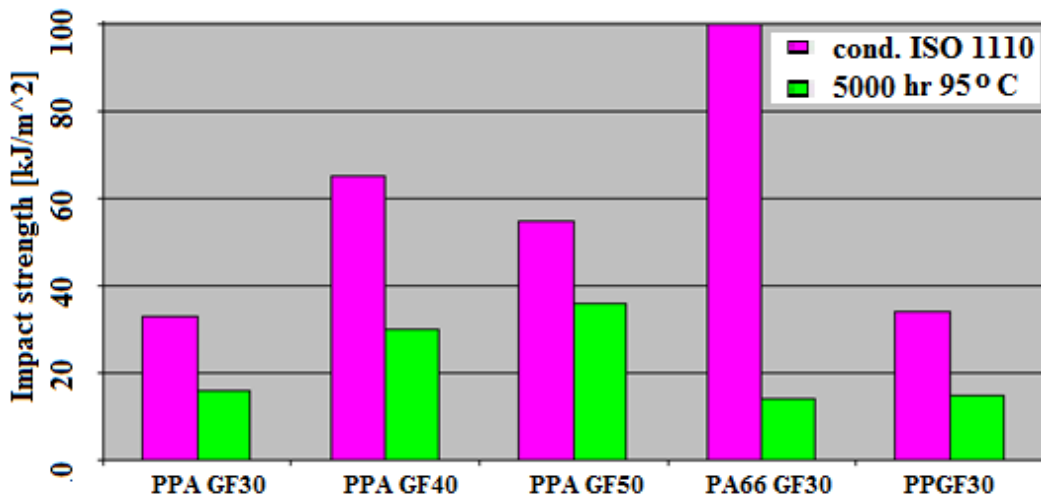


Figure-4.33 Absolute values of impact strength for charpy impact tensile bars (80x10x4 mm³) related to original conditioned values at 1000 ppm chlorinated 95 °C water after 5000 hr.

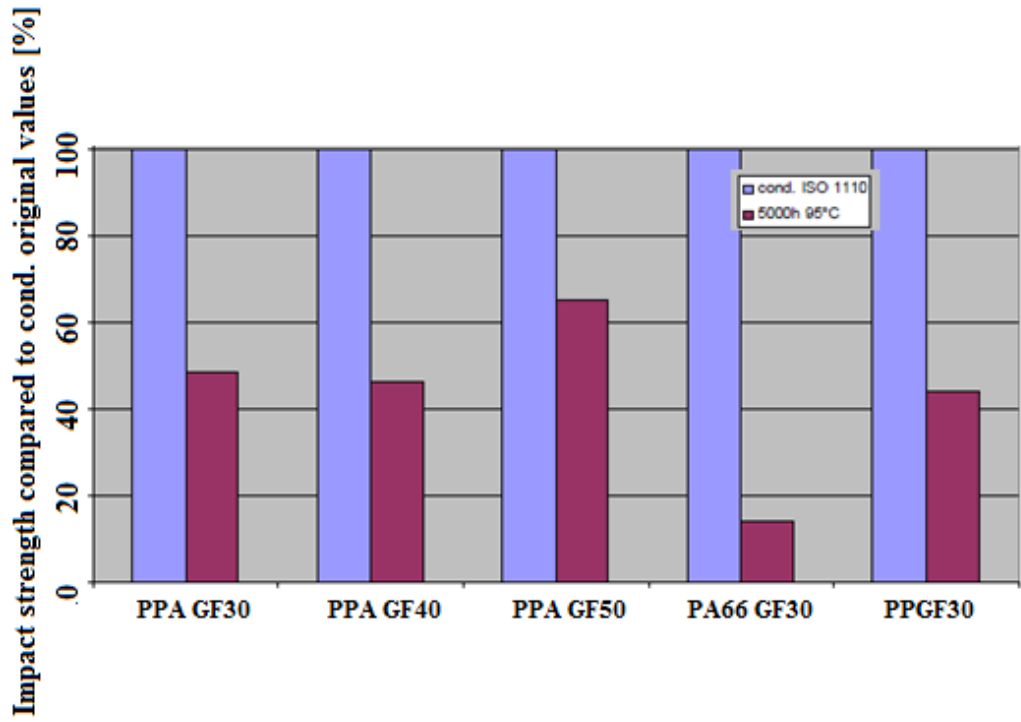


Figure-4.34 Relative decrease of impact strength for Charpy impact tensile bars (80x10x4 mm³) related to original conditioned values at 1000 ppm chlorinated 95 °C water after 5000 hr.

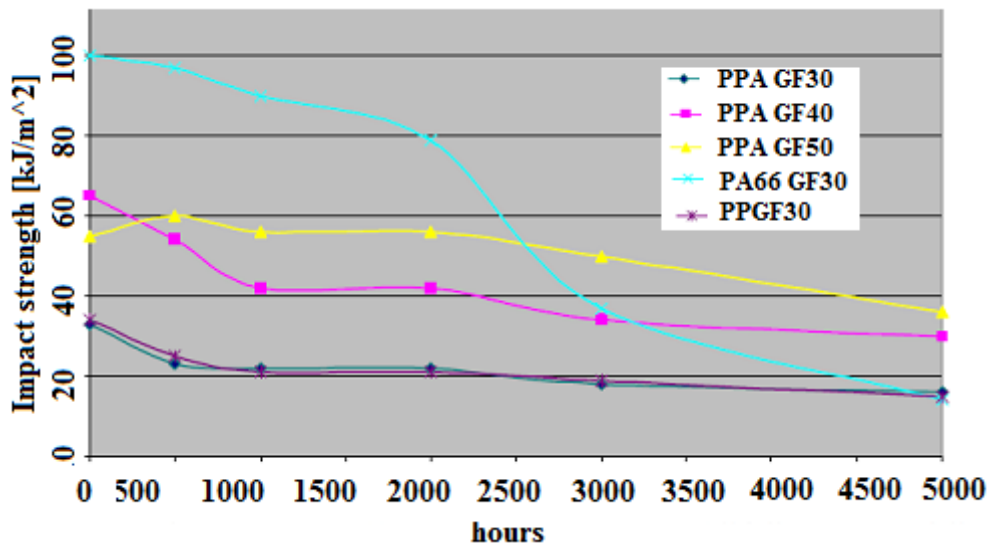


Figure-4.35 Impact strength versus time.

5. CONCLUSION

Nonisothermal experimental results with cooling rates of 5 °C/min, 10°C/min and 20 °C/min were obtained by DSC thermograms show that two step melting affects the melting point by reducing from T_{m1} to T_{m2} with an average value of 25 °C. T_{m2} values of tested samples change considerably after cooling down and melting again. For most of the samples, T_m and T_c reductions were higher for DHW parts which are attributable to more aggressive water media with oxygen. Melting temperature drop suggests that whenever material is used at high temperature media, the structure will lose its properties adversely. Changes in the degree of crystallinity values with cooling rates of 5 and 10 °C/min did not show a remarkable difference between CH and DHW parts. So to see changes in degree of crystallinity values, 20 °C/min is preferable.

Degree of crystallinity (X_c) values give a noticeable drop especially until 2500-hr for both CH and DHW samples at a cooling rate of 20 °C/min. This expresses loss of interfacial adhesion between the glass fibers and the resin matrix by faster hydrolysis at initial stage. After 2500-hr of ageing, the drop is not that noticeable due to slower rate of hydrolytic attack (AMODEL® Polyphthalamide Design Guide, 2003).

Polyphthalamide as being a slow-crystallizing material may undergo low-temperature crystallization, representing the spontaneous rearrangement of amorphous segments within the polymer structure into a more orderly crystalline structure. Such exothermic transitions indicate that the as-molded material had been cooled relatively rapidly. This was observable with some of the samples that shows manufacturing might had been done at high extrusion rates than it should have been.

The Ozawa model was applied and it was predicted that this model successfully fits the nonisothermal crystallization behavior of the PPA GF40 samples. Ozawa plot of HP samples at various temperatures was calculated and it was seen with a general trend as temperature increases, Ozawa constant m increases, but Ozawa rate constant $K(T)$ decreases.

Related with activation energy of crystallization results, Kissinger and Augis–Bennett plots of the samples were obtained. Coefficient of determination (R^2) results show that Augis-Bennett model is mostly not valid for this material. However, Kissinger model is mostly applicable as seen with higher R^2 values.

The temperature at which 50% weight loss observed is indicated as $T_{1/2}$ and the time at which 50% weight loss observed is indicated as $t_{1/2}$ by TGA experiments. There is not noticeable difference for these values for both CH and DHW samples, so it is apparent that in terms of thermal stability values of the samples for both application conditions, the performances are similar. Also we can say the results are satisfactory since there is no significant reduction when compared to 0-hr value. For minor deviations of these values, it is meaningful to say, because the parts are cut from complicated structures, the extruded samples differ so much with their interior matrix and crystalline structure.

The FTIR analyses conducted for all CH samples show that both aromatic and amide bonds found in the structure tend to increase relative to carbon bonds over ageing till 6061-hr for CH parts significantly due to hydrophilic structure and cleavage of amide bonds with hydrolysis. However, it is fair to say the traced functional groups of material structure did not differ significantly. The results were also similar for DHW parts, so the effects of different experimental parameters weren't significantly observed for functional groups. Carbonyl bond (1700 cm^{-1}) was not observed with any samples. So it can be told as the material was not oxidized by strong oxidizing agents significantly.

The SEM images show that cracks are visible since 1700 hours of aged samples for both CH and DHW parts of components. So for some exceptional regions, the polymer-matrix interaction was not good enough to stand for ageing conditions. However, mostly the interaction at polymer matrix-glass fiber interface seems like there is a good bonding. The polymer images also show that there are defect regions without glass fibers which can be attributed to non-homogeneous production from injection molding machine with air bubbles and/or contaminants during the process. So there are multiple crack initiation sites within the structure.

Relative viscosity results show that, in the long term, DHW samples were destructed around 1.5 times more after 6061-hr at inner sides of the parts when compared with CH samples. This result is in line with more aggressive media they are exposed to. So relative viscosity is an important property to follow to understand the degradation effect on the material and correlate with formation of cracks.

Tensile and impact strength properties were measured to see the mechanical strength change over time upon increase of defects after exposure to highly aggressive water environment with 1000 ppm chlorine for various potential strong glass fiber reinforced polymeric materials. All results prove that, all reinforced PPA's shows much better performance when compared with reinforced PA66 and PP's. When extrapolation is made, it is evident that PA66 GF30 usage is critical and is not as reliable as PPA GF40 in the long term, since it loses around 80% when compared with initial tensile strength value with weldline.

6. RECOMMENDATIONS

The long-term service temperature is defined as the maximum temperature at which a plastic has changed no more than 50% of its initial properties after 20,000 hours of storage in hot air (EN 60216-1:2001 Electrical insulating materials -Properties of thermal endurance-, 2001). Since the total data do not represent the whole lifetime but just around 30 % ageing, so it seems there is a development potential with the structure due to all above defined experimental results. All experiments and investigations prove that there is an improvement potential to produce more durable polyphthalamide structure. One possible future study could be trying different types of fibers with different ratio additions to strengthen the matrix. It is also reasonable to study with fibers having different aspect ratios (length/diameter). The studies even might result with lower price since some glass fiber types are lower in price.

Some optimized standard specimens can be prepared which reflect real part design over some simulation programs by experts. These specimens should be more homogenous and easy to be cut. Isothermal experiments can be held to see nominal use temperature effect on crystallinity of the material on such specimens. In case some fractographic techniques may also be studied together with further statistical evaluations, then it could be possible to define the relations between crystallization and real life product properties of the polymeric structure.

All experiments suggest that, the PPA GF40 material can be used confidentially if some non-homogeneity is prevented and better quality products are produced in the manufacturing side.

REFERENCES

- Akay, M. O., O'Regan, D. F. , Bailey, R. S.,** 1995, Fracture Toughness and Impact Behaviour of Glass-Fibre-Reinforced Polyamide 6,6 Injection Mouldings, *Composites Science and Technology*, 55, 109-118p.
- AMODEL® Polyphthalamide Design Guide,** 2003, Solvay Advanced Polymers.
- Backman, A.,** 2010, Effects of Chlorinated Water on Polymeric Water Distribution Systems.
- Benzler, B.,** 2001, Application Laboratory, Giessen, Germany, Mettler Toledo.
- Bernstein R., Derzon, D.K., Gillen, K.T.,** 2010, Nylon 6.6 accelerating aging studies: II. Long-term thermal-oxidative and hydrolysis results, *Polymer Degradation and Stability*, 95, 1471-1479p.
- Bernstein, R. D., Bernstein, R., Derzon, D.K., Gillen, K.T.,** 2005, Nylon 6.6 Accelerated Aging Studies: Thermal-Oxidative Degradation and Its Interaction with Hydrolysis, *Polymer Degradation and Stability*, 88, 480-488p.
- Billmeyer, F.W.,** 1962, Textbook of Polymer Science, Interscience Publishers, Wilmington, Delaware, 1962, 79-80p.
- Brooks, G.,** 1990, Patent No. EP0395414B1-Crystalline Polyphthalamide Composition Having Improved Heat Resistance Properties.
- Celina, M.G., Gillen, K.T. and Assink, R.A.,** 2005, Accelerated Aging and Lifetime Prediction: Review of Non-Arrhenius Behaviour due to Two Competing Processes, *Polymer Degradation and Stability*, 90, 395-404p.
- Chisholm, N., Mahfuz, H., Rangari, V.K., Ashfaq, A. and Jeelani, S.,** 2005, Fabrication and mechanical characterization of carbon/SiC-epoxy nanocomposites, *Composite Structures*, Vol. 67. No. 1, 115-124p.
- Coates, J.,** 2000, Interpretation of Infrared Spectra, A Practical Approach in *Encyclopedia of Analytical Chemistry* R.A. Meyers, Chichester: Ó John Wiley & Sons Ltd.

REFERENCES (continued)

- Crawford, R.**, 2005, *Plastics Engineering*, Elsevier.
- Dhakal, H.N., Zhang, Z.Y., Richardson, M.O.W.**, 2007, Effect of water absorption on the mechanical properties of hemp fibre reinforced unsaturated polyester composites, *Composite Science Technology*, Vol. 67. 1674-1683p.
- Durmus A., Ercan N., Soyubol G., Deligöz and Kaşgöz A.**, 2005, Nonisothermal Crystallization Kinetics of Poly(ethylene terephthalate)/Clay Nanocomposites Prepared by Melt Processing.
- EMS Material Database**, Grivory HT1V-4 FWA Black 9225, Technical Data Sheet, <http://www.emsgrivory.com/en/ems-material-database/> (Last access: 10.07.2013).
- EN 60216–1:2001 Electrical insulating materials -Properties of thermal endurance-**, 2001.
- Farjas, J. and Roura, P.**, 2006, Modification of the Kolmogorov–Johnson–Mehl–Avrami Rate Equation for Non-Isothermal Experiments and Its Analytical Solution, Department of Physics, University of Girona.
- Garbassi, F., Po, R.**, 2003, Engineering Thermoplastics-Overview, *Encyclopedia of Polymer Science and Technology*, John Wiley and Sons, Vol. 2. No. 3, New York.
- Gates, T.S. and Grayson, M.A.**, 1998, On The Use of Accelerated Aging Methods for Screening High Temperature Polymeric Composite Materials, *American Institute of Aeronautics and Astronautics (AIAA)*, 99-1296, 2, 925-935p.
- Gates, T.**, 2003, On the Use of Accelerated Test Methods for Characterization of Advanced Composite Materials.
- Harper, C. A.**, 2002, *Handbook of Plastics, Elastomers, and Composites*, McGraw Hill Professional.

REFERENCES (continued)

- Hassan, A., Rahman, N.M.M.A., Yahya, R.,** 2011, Plasticisation effect on thermal, dynamic mechanical and tensile properties of injection-moulded glass-fibre/polyamide 6,6, *Journal of Science and Technology, Department of Chemistry, Polymer and Composite Materials Research Laboratory, University of Malaya, 50603 Kuala Lumpur.*
- Hiemenz, P.,** 1984, *Polymer Chemistry: The Basic Concepts*, New York.
- Janeschitz, H.,** 2010, *Crystallization Modalities in Polymer Melt Processing*, 228p.
- Jansen, J.,** 2001, *Characterization of Plastics in Failure Analysis*.
- Kahraman, T.,** 2013, *Crystallization Kinetics of Polycaprolactone (PCL)-Clay Composite Films With Oleic Acid and Glycerol Mono Oleate Additives and Product Properties*. Bornova, İzmir: Ege University Graduate School of Applied Science, Chem. Eng. Dept., MSc Thesis.
- Lampman, S.,** 2003, *Characterization and Failure Analysis of Plastics*, ASM International, The Materials Information Society.
- Manchado, M.A.L., Biagiotti, J., Kenny, J.M.,** 2002, Comparative study of the effects of different fibres on the processing and properties of polypropylene matrix composites, *Journal of Thermoplastic Composite Materials*, Vol. 15, 337-353p.
- Mandell, J.F., Smith, K.L., and Huang, D.D.,** 1981, *Polym. Eng. Sci.*, Vol 21, p 1173.
- Martin, R.,** 2008, *Ageing of composites*, The Institute of Materials, Minerals and Mining.
- Moalli, J.,** 2001, *Plastics failure, analysis and prevention*, *Plastics Design Library*.
- Mohd Ishak, Z.A., Ariffin, A., Senawi, R.,** 2001, Effects of hygrothermal aging and a silane coupling agent on the tensile properties of injection moulded short glass fibre reinforced poly(butylenes terephthalate) composites, *European Polymer Journal*, Vol. 37. 1635-1647p.

REFERENCES (continued)

- Nicholson, Lee M., Whitley, Karen S., Gates, Thomas S. and Hinkley, Jeffrey A.**, 1999, How molecular structure affects mechanical properties of advanced polymers, Hampton: National Research Council Resident Research Associate, NASA Langley Research Center.
- Poppe, W., Chen, Y., and Paschke, E.**, 1986, Crystalline copolyamide from terephthalic acid, isophthalic acid and C6 diamines, Amoco Corporation, US Patent 4863991.
- Radetic, T.**, 2011, Fundamentals of scanning electron microscopy and Energy dispersive X-ray analysis in SEM and TEM, Beograd, Serbia: Faculty of Technology and Metallurgy, University of Belgrade.
- Rattaa, V. A.**, 2000, Thermal stability, crystallization kinetics and morphology of a new semicrystalline polyimide polymer, 8121-8138p.
- Saxena, N.S., Mousa, M.A. and Bhandari, I.D.**, 1999, Determination of Avrami exponent from non-isothermal differential scanning calorimetry of Se₇₀Te₂₄Cd₆ chalcogenide glass, Department of Physics, University of Rajasthan.
- Scheirs, J.**, 2000, Compositional and failure analysis of polymers, John Wiley and Sons.
- Skoog, D. A. and Leary, J.J.**, 1991, Principles of instrumental analysis, 4th Edition, Saunders College Publishing, 278p.
- Solvay**, 2011, Effects of chlorinated water on plastic-based water delivery systems, Solvay Advanced Polymers Technical Bulletin.
- Solvay**, 2002, Effects of chlorinated water on thermoplastics, Solvay Advanced Polymers Technical Bulletin.
- Thomason, J.L.**, 2009, The influence of fibre length, diameter and concentration on the impact performance of long glass-fibre reinforced polyamide 6,6, Composites: Part A 40, Elsevier, 114–124p.

REFERENCES (continued)

- Vyazovkin, S. and Dranca, I.**, 2006, 2006, Isoconversional analysis of combined melt and glass crystallization data, *Macromol. Chem. Phys.*, 207, 20–25p.
- Vyazovkin, S., Stone, J. and Sbirrazzuoli, N.**, 2005, Hoffman–Lauritzen parameters for non-isothermal crystallization of poly(Ethylene Terephthalate) and Poly(Ethylene Oxide) melts, *Journal of Thermal Analysis and Calorimetry*, 80, 177-180p.
- Yang, G.C., Zheng, H.M., Li, J.J., Jian, N.B., Zhang, W.B.**, 1996, Relation of modification and tensile properties of sisal fibre, *Acta Scientiarum Naturalium Universitatis Sunyatseni*, Vol. 35, 53-57p.
- Wallenberger, Frederick T., Watson, James C., and Li, H.**, 2001, Glass fibers. *ASM Handbook*, 21: Composites.
- United States Environmental Protection Agency**, Water: monitoring & assessment, <http://water.epa.gov/type/rsl/monitoring/vms52.cfm> (Last access: 04.06.2013).

CURRICULUM VITAE**Nur (İSLAM) KARAŞAHİN**

+ 90 533 240 02 42

islamnur@gmail.com**PERSONAL INFORMATION**

Date and Place of Birth: 07/12/1982 – İzmir / TÜRKİYE**Marital Status:** Married**Driving License:** Present / B - Active Driver**T.C. No:** 17639813468**Fields of Interest:** Watching movie/documentary, driving car, playing tennis, reading book/publications on psychology, doing pilates**EDUCATIONAL BACKGROUND**

2008-2013 **Aegean University İzmir, Türkiye**
Engineering Faculty / Chemical Eng., MSc**Thesis Period, Subject:** Investigation of Oxygen and Chlorine Effect on Lifetime of PPA (Polyphthalamide) Components Under Pressurized and Hot Water Conditions**2001-2006** **Middle East Technical University Ankara, Türkiye**
Engineering Faculty / Chemical Eng., BSc**2000-2001** **Çakabey College, Türkiye****1998-2000** **Turgutlu Halil Kale Science High School, Türkiye****1994-1998** **Karşıyaka Anatolian High School İzmir, Türkiye**

WORK EXPERIENCE

10/2011-ongoing

Robert Bosch GmbH, Bosch Thermotechnology

Material Expert

Assuring reliability of polymeric and elastomeric materials' service life by accelerated lifetime tests

Development of test procedures related with lifetime estimation of materials

Contribution for guideline development studies on polymeric and elastomeric materials

Supporting quality development studies and conducting root cause analysis within frame of tests, 8D documentation tools

Establishment of cooperation for new future development projects

International active leadership/membership role for completion of issues explained above

04/2007 – 10/2011

Petkim Petrokimya Holding A.Ş.

Research and Development (R&D) Senior Engineer (Main Area: Polymer)

Offering solutions to the problems throughout the process and doing modifications in the process accordingly,

For producing high value-added products, developing new projects,

Doing studies with HPLC-ToF/MS, FT-IR, DSC, Tensile Test Machine, Rheometer, Gas Chromatography laboratory equipments and analytical methods for characterization, formulation and deformulation of polymer and other types of materials to serve for the value of Petkim related with customer satisfaction,

Following technical issues and new trends over various channels, preparing reports and presenting important studies in events like congresses, conferences, etc...

Participating in Plant Cost Reduction Meetings (HDPE, LDPE, LDPE-T, PP Plants) and realizing related projects, doing bottleneck analysis.

Projects Involved:

The Scientific and Technological Research Council of Turkey (TÜBİTAK) Technology and Innovation Funding Programs Directorate (TEYDEB) Funded Projects:

- ✓ **Project Manager;** Developing High Corona Stable PP Product for Metallized BOPP Film Applications (November 2009-ongoing)

- ✓ **60-70% working project engineer:** Research for Production of Cross-Linkable Polyethylene (XLPE) Used in Cable Sector (April 2007-August 2008)

** Project was completed successfully and production of XLPE was decided as being one of the 2011 investment projects of Petkim. Now, the phase is about evaluation of offers about building XLPE plant obtained from different companies and I am in charge of analyzing offers on technical side in the evaluation team.

Some Other Technical Projects Involved:

- ✓ Obtaining high value added DCPD Product from Bottom Product of Ethylene Plant C-405D Column
- ✓ Enhancing Heptane Recovery Efficiency of PP Plant C-403 Column
- ✓ LDPE Plant E201 Inter-Cooler Modification
- ✓ LDPE Plant E202 After-Cooler Modification
- ✓ Investigation an Alternative for Inhibitor Solution Used in ACN Plant

Other Project Groups and Studies Involved in Petkim

- ✓ LIMS (Laboratory Information Management System)
- ✓ Integrated Management System (Environmental, Occupational Health and Safety, Quality Management Systems) (1 year)
Assignment for internal inspection studies in Petkim departments before Turkish Standards Institution inspection for self-evaluation.
- ✓ REACH (Registration, Evaluation, Authorisation and Restriction of Chemicals) (1 year)
- ✓ EFQM (European Foundation for Quality Management) (3 months)
Related with “Intellectual Property Management” criterion, constituting patent application procedure.
- ✓ Studies for making up a financial model of Petkim future plans and investments with the consultancy of PricewaterhouseCoopers Company (8 months)

02/2007 – 04/2007

Gür-Pet Petroleum Products Co. Ltd.

Quality Assurance Responsible

ISO 9001:2000 Quality Management System training,

For application of “Environmental Impact Statement” pre-license and license, preparing and sending the necessary files to Ministry of Environment and Forestry.

2005 – 2006 (10 ay)

Güçlü Machine Textile and Foreign Trade

Co. Ltd. Ankara, Türkiye

University Period Part Time Job – Executive Assistant

Translation of documents and reports, conducting abroad phone contacts, searching for tenders, establishing business contacts.

Internships**2005 (1 month)****Aliğa TÜPRAŞ Refinery İzmir, Türkiye****Production Plant**

Performing mass balance calculations over tank system and preparing the report.

2003 (1 month)**DYO Paint Factories Inc. İzmir, Türkiye****Production Plant**

Doing process control studies of an equipment on flow chart and preparing the report.

FOREIGN LANGUAGES AND COMPUTER SKILLS

Foreign Languages

English – Advance Level

German – Beginner Level (4th Level)

French – Beginner Level (3rd Level)

Computer Skills

Microsoft Office Programs

AspenTech/Unisim Simulation Programs

Weibull Analysis

CERTIFICATES AND ATTENDED EVENTS

Contributions in Events

- ✓ **10. International Chemical Engineering Congress**, “Investigation of Ageing Behaviours of PA6,6 (Polyamide 6,6) Under Pressurized and Hot Water Media” presentation, UKMK10, İstanbul (3-6/09/2012)
- ✓ **1. Aegean R&D and Technology Days – AreGE**”, “Development of a High Corona Stable Polypropylene (PP) Product for Metalized BOPP Film Applications and Investigation of the Crystallization Kinetics Effect on Corona Stability” poster, Ege Üniversitesi, TÜBİTAK ve Elginkan Vakfı, İzmir AKM (1-3/12/2010)
- ✓ **“IV. Chemistry Industrial Development Council”**, active role in workshop (07-08/05/2009)

Trainings and Events

- ✓ **“TA Instruments Roadshow”**, Likrom Analitik Çözümler Paz. San. ve Tic. Ltd. Şti., İstanbul (12/04/2013)
- ✓ **“Yalın 6σ Proje Fırsatları Belirleme Çalıştayı”**, SPAC Danışmanlık, Bosch Termoteknik San. ve Tic. A.Ş., Manisa (01.05.2013-04.06.2012)
- ✓ **“Plastik Malzemeler ve Üretim Teknikleri”**, İmes Eğitim Ltd. Şti., İstanbul (14-15/04/2013)
- ✓ **“Risk Değerlendirmesi”**, MOSB-MED, Bosch Termoteknik San. ve Tic. A.Ş., Manisa (28/03/2012)
- ✓ **“Process Integration and Thermal Pinch”**, Assoc. Prof. Dr. Serap Cesur, Asst. Prof. Dr. Zehra Özçelik, Ege University, (01-03/08/2011)
- ✓ **“Laboratory Type Twin Screw Extruder Training”**, Coperion – Stuttgart / Germany, (10-13/05/2011)
- ✓ **“Advance Level Microsoft Excel 2010 Training”**, İ. Akademi, (06-08/05/2011)
- ✓ **“Upscaling in Batch Processes”**, R&D Center in-house training, (12/01/2011)
- ✓ **“EFQM Referee Training”**, Fatin Yücel, (04-04/01/2011)
- ✓ **“EFQM 2010 Revision Training”**, Fatin Yücel, (26/10/2010-26/11/2010, 21 hours)
- Case study over Akasya Lojistik Company example
- ✓ **“Business Plan Model Training”**, PwC (PricewaterhouseCoopers), (19-20/07/2010)
- ✓ **“Customer Oriented and Leadership Seminar”**, Günsu Başar, (21-23/05/2010)
- ✓ **“Polymer Days” event, participation as speaker**, KMO Students İstanbul Branch (08/04/2010)
- ✓ **“EU 7th Framework Programme and Project Application Training”**, İstanbul Chamber of Industry, (20-21/01/2010)
- ✓ **“Türkiye Petrochemical and Chemistry Industry – Strategic Importance, Current & Future Situation” Workshop**, Turkish Chemicals Manufacturers Association, (22/12/2009)
- ✓ **International Chemistry Industry Congress**, (17-18/12/2009)
- ✓ **“Petkim Integrated Management System In-house Inspection Training”**, Artı Consultancy, (23-27/10/2009)
- ✓ **“Comparison Training”**, Tuğrul Çelebi, (28/07/2009)
- ✓ **“Integrated Management System Training (Environmental, Occupational Health and Safety, Quality Management Systems)”**, Artı Consultancy, (21-23/07/2009)
- ✓ **“Environmental Regulations Training”**, Artı Consultancy, (16/07/2009)
- ✓ **“IV. Chemistry Industry Development Council”**, Active role in workshop (07-08/05/2009)

- ✓ **“Exergy and Applications Summer Course”**, TÜBİTAK MAM, Energy Institute, (16-17/06/08)
- ✓ **“Basic Principles of Extrusion and Rheology & Applications in Polymer Technology Seminar”**, Hacettepe University Radiation and Polymer Science Laboratories (28-29/11/07)
- ✓ **“V. International Packaging Congress and Exhibition”**, TMMOB Chamber of Chemical Engineers, İzmir (22-24/11/07)
- ✓ **“HPLC-MS/Tof (High Pressure Liquid Chromatograph-Mass Spectrometer/Time of Flight) Training”**, Bruker Daltonics - Bremen / Germany (29/10/07-01/11/07)
- ✓ **“TS-EN-ISO/IEC 17025:2005 Accreditation of Experiment and Calibration Basics”** and **“Introduction to Uncertainty of Measurement”**, TMMOB Chamber of Chemical Engineers, Ankara (16-18/05/07)
- ✓ **“Training Workshop for Preparation of *Technology and Innovation Funding Programs Directorate (TEYDEB) Funded Projects*”**, Aegean Region Chamber of Industry (17/03/07)

ACTIVITIES AND MEMBERSHIPS

- ✓ **“Petkim Innovation Club”** (2010-2011 Term)
Participation as technical jury in event named as FIRST® (For Inspiration and Recognition of Science and Technology) LEGO® League (FLL) or named as “Science Heroes” in Türkiye.
- ✓ **“Petkim Human Resources Commision”**, On the way to EFQM, related with “Employees” criterion, discussing subjects with multidisciplinary group members.
- ✓ **“Chamber of Chemical Engineers”**
- ✓ **“Sports International”**
- ✓ **“GAIA International Packaging Congress ”**, Bosphorus University Management and Economics Club (18-23/06/06)
- ✓ **“METU Alumni Association”**
- ✓ **“AEGEE-Ankara (Association des Etats Généraux des Etudiants de l'Europe)/METU”**, Youth Council Working Group Secretary (2002-2003 Term)
- ✓ **“NLP (Neuro Linguistic Programming) Training”**, Turgay Biçer, (2000-2001)